

---

Theses and Dissertations

---

2010

# Virtual pre-operative reconstruction planning for comminuted articular fractures

Thaddeus Paul Thomas  
*University of Iowa*

Copyright 2010 Thaddeus Paul Thomas

This dissertation is available at Iowa Research Online: <http://ir.uiowa.edu/etd/2778>

---

## Recommended Citation

Thomas, Thaddeus Paul. "Virtual pre-operative reconstruction planning for comminuted articular fractures." PhD (Doctor of Philosophy) thesis, University of Iowa, 2010.  
<http://ir.uiowa.edu/etd/2778>.

---

Follow this and additional works at: <http://ir.uiowa.edu/etd>



Part of the [Biomedical Engineering and Bioengineering Commons](#)

VIRTUAL PRE-OPERATIVE RECONSTRUCTION PLANNING FOR  
COMMUNUTED ARTICULAR FRACTURES

by

Thaddeus Paul Thomas

An Abstract

Of a thesis submitted in partial fulfillment  
of the requirements for the Doctor of  
Philosophy degree in Biomedical Engineering  
in the Graduate College of  
The University of Iowa

December 2010

Thesis Supervisor: Associate Professor Donald D. Anderson

## ABSTRACT

Highly comminuted intra-articular fractures are complex and difficult injuries to treat. Once emergent care is rendered, the definitive treatment objective is to restore the original anatomy while minimizing surgically induced trauma. Operations that use limited or percutaneous approaches help preserve tissue vitality, but reduced visibility makes reconstruction more difficult. A pre-operative plan of how comminuted fragments would best be re-positioned to restore anatomy helps in executing a successful reduction. The objective of this work was to create new virtual fracture reconstruction technologies that would deliver that information for a clinical series of severe intra-articular fractures.

As a step toward clinical application, algorithmic development benefits from the availability of more precise and controlled data. Therefore, this work first developed 3D puzzle solving methods in a surrogate platform not confounded by various *in vivo* complexities. Typical tibial plafond fracture fragmentation/dispersal patterns were generated with five identical replicas of human distal tibia anatomy that were machined from blocks of high-density polyetherurethane foam (bone fragmentation surrogate). Replicas were fractured using an instrumented drop tower and pre- and post-fracture geometries were obtained using laser scans and CT. A semi-automatic virtual reconstruction computer program aligned fragment native surfaces to a pre-fracture template.

After effective reconstruction algorithms were created for the surrogate tibias, the next aim was to develop new algorithms that would accommodate confounding biologic factors and puzzle solve clinical fracture cases. First, a novel image analysis technique was developed to segment bone geometries from pre- and post-surgical reduction CT scans using a modified 3D watershed segmentation algorithm. Next, 3D puzzle solving algorithms were advanced to obtain fracture reconstructions in a series of highly comminuted tibial plafond fracture cases. Each tibia was methodically reconstructed by

matching fragment native (periosteal and articular) surfaces to an intact template that was created from a mirror image of the healthy contralateral limb. Virtual reconstructions obtained for ten tibial plafond fracture cases had average alignment errors of  $0.39 \pm 0.5$  mm. These novel 3D puzzle solving methods are a significant advancement toward improving treatment by providing a powerful new tool for planning the surgical reconstruction of comminuted articular fractures.

Abstract Approved: \_\_\_\_\_  
Thesis Supervisor  
\_\_\_\_\_  
Title and Department  
\_\_\_\_\_  
Date

VIRTUAL PRE-OPERATIVE RECONSTRUCTION PLANNING FOR  
COMMINUTED ARTICULAR FRACTURES

by

Thaddeus Paul Thomas

A thesis submitted in partial fulfillment  
of the requirements for the Doctor of  
Philosophy degree in Biomedical Engineering  
in the Graduate College of  
The University of Iowa

December 2010

Thesis Supervisor: Associate Professor Donald D. Anderson

Copyright by  
THADDEUS PAUL THOMAS  
2010  
All Rights Reserved

Graduate College  
The University of Iowa  
Iowa City, Iowa

CERTIFICATE OF APPROVAL

---

PH.D. THESIS

---

This is to certify that the Ph.D. thesis of

Thaddeus Paul Thomas

has been approved by the Examining Committee  
for the thesis requirement for the Doctor of Philosophy  
degree in Biomedical Engineering at the December 2010 graduation.

Thesis Committee: \_\_\_\_\_  
Donald D. Anderson, Thesis Supervisor

\_\_\_\_\_  
Thomas D. Brown

\_\_\_\_\_  
Nichole M. Grosland

\_\_\_\_\_  
J. Lawrence Marsh

\_\_\_\_\_  
Joseph M. Reinhardt

\_\_\_\_\_  
Andrew R. Willis

## ACKNOWLEDGMENTS

Many individuals from the Dept. of Orthopaedics have made my research possible. I would like to thank Dr. J. Lawrence Marsh, Andrew R. Willis, Doug Pedersen, Jim Rudert, Tom Baer, Julie Mock and Jessica Goetz for their support, and Dr. Matthew Frank from the Iowa State University for manufacturing the surrogate tibias. Also, I acknowledge the other members of my committee, Drs. Nicole M. Grosland and Joseph M. Reinhardt for their constructive advice. I would like to sincerely thank my advisors Drs. Thomas D. Brown and Donald D. Anderson for their outstanding mentoring and training that they have provided.

## ABSTRACT

Highly comminuted intra-articular fractures are complex and difficult injuries to treat. Once emergent care is rendered, the definitive treatment objective is to restore the original anatomy while minimizing surgically induced trauma. Operations that use limited or percutaneous approaches help preserve tissue vitality, but reduced visibility makes reconstruction more difficult. A pre-operative plan of how comminuted fragments would best be re-positioned to restore anatomy helps in executing a successful reduction. The objective of this work was to create new virtual fracture reconstruction technologies that would deliver that information for a clinical series of severe intra-articular fractures.

As a step toward clinical application, algorithmic development benefits from the availability of more precise and controlled data. Therefore, this work first developed 3D puzzle solving methods in a surrogate platform not confounded by various *in vivo* complexities. Typical tibial plafond fracture fragmentation/dispersal patterns were generated with five identical replicas of human distal tibia anatomy that were machined from blocks of high-density polyetherurethane foam (bone fragmentation surrogate). Replicas were fractured using an instrumented drop tower and pre- and post-fracture geometries were obtained using laser scans and CT. A semi-automatic virtual reconstruction computer program aligned fragment native surfaces to a pre-fracture template.

After effective reconstruction algorithms were created for the surrogate tibias, the next aim was to develop new algorithms that would accommodate confounding biologic factors and puzzle solve clinical fracture cases. First, a novel image analysis technique was developed to segment bone geometries from pre- and post-surgical reduction CT scans using a modified 3D watershed segmentation algorithm. Next, 3D puzzle solving algorithms were advanced to obtain fracture reconstructions in a series of highly comminuted tibial plafond fracture cases. Each tibia was methodically reconstructed by

matching fragment native (periosteal and articular) surfaces to an intact template that was created from a mirror image of the healthy contralateral limb. Virtual reconstructions obtained for ten tibial plafond fracture cases had average alignment errors of  $0.39 \pm 0.5$  mm. These novel 3D puzzle solving methods are a significant advancement toward improving treatment by providing a powerful new tool for planning the surgical reconstruction of comminuted articular fractures.

## TABLE OF CONTENTS

|  |      |
|--|------|
| LIST OF TABLES .....                                       | vii  |
| LIST OF FIGURES .....                                      | viii |
| CHAPTER 1 - INTRODUCTION.....                              | 1    |
| CHAPTER 2 - LITERATURE REVIEW.....                         | 7    |
| Comminuted Intra-Articular Fractures .....                 | 7    |
| Tibial Plafond Fracture.....                               | 7    |
| Soft Tissue Injury .....                                   | 9    |
| Computed Tomography (CT).....                              | 10   |
| Acute Fracture Severity and its CT-Based Assessment .....  | 11   |
| Fracture Reduction and Treatment Techniques.....           | 13   |
| Post-Traumatic Osteoarthritis.....                         | 16   |
| Computer Vision and Assistance in Orthopaedics .....       | 18   |
| Bone Segmentation from CT Data .....                       | 18   |
| Computational Reconstruction Methods .....                 | 20   |
| Computer Assisted Orthopaedic Surgery .....                | 21   |
| Summary.....   | 27   |
| CHAPTER 3 - MATERIALS AND METHODS .....                    | 28   |
| A Development Platform for 3D Puzzle Solving .....         | 28   |
| Surrogate Fabrication .....                                | 28   |
| Fracture Generation .....                                  | 29   |
| Native Surface Identification.....                         | 31   |
| 3D Puzzle Solving Method.....                              | 35   |
| In vitro Cadaver Testing .....                             | 37   |
| Cadaver Specimen Preparation.....                          | 38   |
| Development and Application to Clinical Cases.....         | 43   |
| Patient Management .....                                   | 43   |
| CT Segmentation .....                                      | 44   |
| CT Derived Fragment Geometry Validation .....              | 51   |
| Fragment Mesh Segmentation and Classification .....        | 52   |
| Fragment Position Initialization .....                     | 56   |
| Finalizing Fracture Reduction .....                        | 59   |
| Accuracy Assessment.....                                   | 60   |
| CT-Based Fracture Severity Assessment.....                 | 60   |
| Quantifying the Clinical Utility of 3D Puzzle Solving..... | 63   |
| Specimen Preparation.....                                  | 64   |
| Study Design .....   | 68   |
| Performance Assessment.....                                | 71   |
| CHAPTER 4 - RESULTS.....                                   | 74   |
| Surrogate Fracture Reconstruction .....                    | 74   |
| CT Segmentation .....                                      | 77   |
| Surface Classification.....                                | 79   |
| Fragment Position Initialization .....                     | 82   |

|  |     |
|--|-----|
| Injury Severity Assessment .....                     | 87  |
| Surgical Simulation .....                            | 89  |
| CHAPTER 5 - DISCUSSION .....                         | 94  |
| Surrogate Developmental Work .....                   | 95  |
| Image Analysis Technique .....                       | 96  |
| Pre-Operative Utility .....                          | 99  |
| Clinical Translation .....                           | 103 |
| Fracture Energy and Injury Severity Assessment ..... | 108 |
| Surgical Simulation .....                            | 113 |
| CHAPTER 6 - LIMITATIONS .....                        | 117 |
| CHAPTER 7 - CONCLUSION .....                         | 120 |
| APPENDIX   |     |
| A.    CLASSIFICATION RESULTS .....                   | 122 |
| B.    OSTATS .....                                   | 123 |
| C.    SURGICAL SKILLS RUBRIC .....                   | 124 |
| REFERENCES .....                                     | 125 |

## LIST OF TABLES

|          |   |     |
|----------|---|-----|
| Table 1  | Ten tibial plafond fracture patients were retrospectively analyzed in this study.....   | 44  |
| Table 2  | In order to improve speed and stability, a series of algorithms grossly reduced each fracture prior ICP. The average distance between fragments in their displaced versus reduced positions, are compared to the average distance between fragments in their initialized versus reduced positions. .... | 83  |
| Table 3  | Alignment error for overall native (periosteal and articular combined) and periosteal/articular surfaces individually are shown. The periosteal surfaces aligned better to the intact template than the articular surface. ....   | 84  |
| Table 4  | Results from the first five surgical simulation sessions are reported. ....   | 90  |
| Table A1 | Classification results with patient-specific vs. compiled training models are provided. ....  | 122 |
| Table B1 | Detailed global 5 point rating scale and pass/failure score for Objective Structured Assessment of Technical Skill. ....  | 123 |
| Table C1 | Grading for surgeon performance. ....   | 124 |

## LIST OF FIGURES

|           |   |    |
|-----------|---|----|
| Figure 1  | Radiographs and volumetric rendering from a high-energy tibial plafond fracture with severe comminution (~15 fragments).....  | 8  |
| Figure 2  | A closed tibial plafond fracture with white and red fracture blisters presents evidence of severe soft tissue damage. In order to prevent complications, an external fixator is applied to stabilize the joint while the soft tissues are allowed to recover. After one to three weeks, the soft tissues are more tolerant to the surgical insult of definitive surgery. .... | 9  |
| Figure 3  | Conventional pre-operative planning method for reconstructing fractures.....  | 14 |
| Figure 4  | Open reduction internal fixation (left) and percutaneous/limited (right) surgical approaches illustrate the tradeoff between joint visualization and iatrogenic trauma.....   | 15 |
| Figure 5  | Virtual reduction and fixation for pre-operative pelvic and acetabular surgery.....   | 22 |
| Figure 6  | Suero et al. present segmentation results for an example C1 tibial plateau fracture. Although the authors state that the total planning time was 167mins for this case, no virtual reconstruction results are put forth.....  | 23 |
| Figure 7  | CT images of an example mandibular fracture case are presented. ....  | 23 |
| Figure 8  | Initial, intermediate and final mandibular reconstruction stages are shown. ....  | 24 |
| Figure 9  | A virtual mandibular osteotomy is compared to what was surgically achieved. The virtual plan (green surface) is superimposed on the post-operative isosurface. ....   | 25 |
| Figure 10 | A tibial plafond fracture is segmented (a). Bone fragment fracture surfaces are identified (b) and interactively matched to corresponding fragments (c). Fracture surfaces are then aligned with a modified iterative closest point algorithm.....  | 26 |
| Figure 11 | Process for surrogate tibia creation. From a CT isosurface, the endosteal and native surfaces of the tibia were modeled for generating NURBs surfaces. Surrogate material was then machined from the CAD model with rapid prototyping.....  | 29 |
| Figure 12 | The polyetherurethane distal tibia was encased in a soft tissue simulant (candle gel) (a) and an instrumented droptower was used to create comminuted fractures (b), similar to those clinically observed such that fragment displacement would replicate in vivo patterns (c).....   | 30 |
| Figure 13 | Distal tibia replicas were 3D laser scanned before and after fracturing (a, c). Post-fracture CTs provided visual confirmation of comminution and a data set for investigating segmentation techniques (b). ....  | 31 |

|           |  |    |
|-----------|--|----|
| Figure 14 | Fragment surface classification according to color (hue). Using the precise color information that was obtained during laser scanning, fracture surfaces (color blue) were automatically and accurately separated from the endosteal (green) and the periosteal and articular (red) surfaces with thresholding.....  | 32 |
| Figure 15 | Fragment surface classification was performed with a region growing algorithm. ....  | 33 |
| Figure 16 | A random facet seeded the region growing algorithm (a). A patch's 1-ring neighbors (yellow facets) were annexed into the patch if their surface normal vectors deviated less than a defined threshold (b, green facet). Otherwise, facets were marked as visited and passed over (b, yellow). Patches iteratively propagated up to borders of high curvature (c). .... | 34 |
| Figure 17 | Surface classification results from the region growing algorithm are shown. After the surface normal analysis (a), the classification is refined (b), and the patch with the largest surface area was determined to be native surface (c). ....  | 35 |
| Figure 18 | A surrogate fracture puzzle solution is shown. Anatomic geometry is restored using a semi-automatic virtual bone fragment reconstruction system. ....  | 36 |
| Figure 19 | The process of preparing the cadaveric specimen is shown. With the joint capsule intact, the proximal shaft of the tibia and the inferior talar surface were potted in PMMA. A steel platen for impaction was attached to the talar side. ....   | 38 |
| Figure 20 | A drop tower delivered 50-75J of kinetic energy to cadaver ankle joints in order to produce a clinically relevant tibial plafond fracture. ....  | 39 |
| Figure 21 | Since the cadaveric CT (a) could not be reliably segmented from intensity information (b), image texture (c) was analyzed to yield discrete fragment segmentations (d). ....   | 40 |
| Figure 22 | Virtual and physical reconstruction results for the cadaveric tibia are shown. ....  | 42 |
| Figure 23 | Illustrative CT data for a comminuted tibial plafond fracture. ....  | 45 |
| Figure 24 | A flowchart of the image analysis technique for extracting bone fragment geometries from clinical CT data. ....  | 46 |
| Figure 25 | In a watershed segmentation, the intensity of a CT slice (left) can be conceptualized topographically in 2D (right) where fragments correspond to basins, and ridgelines to fragment boundaries. ....  | 46 |
| Figure 26 | Very dense volumes within the gross bony structure are identified from thresholding (a) and used as markers for a subsequent watershed implementation (b). All objects connected to the most distal plane (talus), and the second smallest object connected to the proximal plane (fibula) were removed from the volume for tibial analysis. ....                      | 47 |

|           |  |    |
|-----------|--|----|
| Figure 27 | The cortical mask (a) was analyzed and new markers were identified from an extended maximum transform (b). After imposing minimum at those sites, a watershed operation propagated boundaries up to cortical edges (c, d).....   | 48 |
| Figure 28 | Over-segmented fragments (a) are analyzed (b) and automatically fused (c).....   | 49 |
| Figure 29 | Convex hulls are fit to a 2.5x2.5x2.5 sub volume of the tibia's mask, centered at a voxel that intersects two or more fragments and the outer tibial surface. The difference in volume between the convex hull and sub volume was quantified. Concave locations (a) had volumes > 0.75mm <sup>3</sup> , convex locations were <0.3mm <sup>3</sup> .....  | 50 |
| Figure 30 | Clinical CT data of a comminuted tibial plafond fracture are shown (a). Novel image segmentation techniques were developed for generating discrete fragment models that could be spatially manipulated and reduced (b, c). .....   | 50 |
| Figure 31 | Example fragment comparing the watershed segmented fragment (a), to the manually segmented fragment (b). Accuracy was assessed by the distance deviation between the two registered fragments (c). .....   | 52 |
| Figure 32 | CT appearance of the distal tibia anatomy. Relative to the tibia's outer surface, the CT intensities vary with characteristic profiles along the inward surface normals for each anatomic region (diaphysis, metaphysis and articular). .....  | 53 |
| Figure 33 | Different bone structures of the distal tibia display characteristic CT intensity profiles.....  | 54 |
| Figure 34 | For assessment, a trained user manually segmented the tibia by anatomy. Tibia's mesh was classified by maximum probability. Then surface patches (groups of facets) received the one label that was most frequently detected. Computer and human classification results were in excellent agreement. ....  | 56 |
| Figure 35 | Displaced fragments (a) are grossly reduced with a series of algorithms that computationally mimic the surgeon's intra-operative actions. First, axial alignment is restored by shifting the constellation of fragments toward the template's primary axis (b). Next, limb length is restored by longitudinally translating fragments such that articular patches are at the same level as the template's (c). In the final step in gross reduction, fragments are translated and rotated radially such that the overlap between periosteal patches and the template is maximized..... | 57 |
| Figure 36 | Displaced (a) and initialized (b) fragments are shown for an illustrative case. Alignment processing time was reduced. For an example fragment, the ICP computational time was reduced from 10s in its original position (c), to 7s after initialization.....  | 58 |

|            |  |    |
|------------|--|----|
| Figure 37  | A flowchart of the puzzle solving process. Intact template and fragment geometries are generated by analyzing pre-operative CT data. Native surfaces (periosteal and subchondral) are then segmented and classified from geometric and bone density information. The fracture is then reduced by first registering the template to the fracture's base fragment, then grossly positioning fragments in a series of initialization steps, and finally precisely aligning fragment-template surfaces with an iterative closest point (ICP) algorithm. .... | 59 |
| Figure 38  | Residual incongruities (Case ID 2) were visible after the intact template was registered to the surgically reconstructed plafond. Quality of reduction was quantified by measuring the distance deviation between the physically reconstructed articular surface and the template. The average articular deviation for this case was 1.1mm. ....   | 60 |
| Figure 39  | Fracture surface CT intensities queried from the intact CT volume provide for reliable measured and subsequently improved fracture energy analyses. ....   | 61 |
| Figure 40  | High curvature areas were identified on the intact template (a) and the fractured bone (c). The ridgeline along the malleoli (b, silver curve), and the fracture surfaces (d, green curve) were extracted. Articular insult was quantified by the fracture curve's length, normalized to the intact's. ....  | 62 |
| Figure 41  | In limited approach fracture reduction, bone fragments are percutaneously manipulated under fluoroscopic guidance. ....  | 64 |
| Figure 42  | A surrogate distal tibia is impacted with a drop-tower to produce a three segment fracture. ....   | 65 |
| Figure 43  | Fractured surrogate fragments were virtually apposed to replicate a moderately displaced pattern that was physically configured by an orthopaedist. ....   | 66 |
| Figure 44  | Foot and ankle model obtained from Sawbones. Muscle and soft tissues are simulated with homogenous foam that encased in a outer skin-like material. There is normal anatomy (fibula, talus, etc.) adjacent to the tibial cavity where the fracture surrogate tibia resided. ....   | 67 |
| Figure 45  | The protocol for surgical simulation and post-reduction evaluation is shown. ....  | 68 |
| Figure 46  | A surgical simulation trial is depicted where fragments are percutaneously manipulated under fluoroscopic guidance, and fixed with k-wires. ....   | 69 |
| Figure 47  | Custom puzzle solving software provides comprehensive visualization capabilities. The user could hide and/or change the transparency of all individual models. Animations also demonstrated the trajectories for precisely reducing fracture fragments. ....   | 70 |
| Figure 48. | Hand motions were tracked with a Qualysis motion capture system. Fiducial markers attached to the back of the hand are located in space and registered to pre-simulation models. ....  | 71 |

|            |   |    |
|------------|---|----|
| Figure 49  | A sample plot of a surgeon’s hand velocity during the simulation. Red dots represent instances of discrete actions. From the synchronized video data, time periods when the surgeon’s hands were not touching the model were excluded from analysis (e.g. time period encapsulating $1.3 \times 10^4$ s).....                                       | 72 |
| Figure 50  | Although some dusting was observed at the most proximal segment of the tibia, the articular and metaphyseal bone volume was preserved during impact. Subsequently, the 5 replica tibias were accurately reconstructed by matching native surfaces to the pre-fractured template.....  | 74 |
| Figure 51  | Reconstruction of the whole bone (top row) and the articular surface (bottom row) is shown for a typical surrogate tibia (a). Individual segmented fragments are shown color-coded (b). The pre- and post-fracture periosteal surface distance deviation calculations (c) verified that the original anatomy was accurately restored.....           | 75 |
| Figure 52  | Histograms comparing native (i.e., periosteal) (a) and fracture (i.e. interfragmentary) surface (b) alignment errors for both articular, and non-articular fragments, for the five surrogates.....  | 76 |
| Figure 53  | Novel image analysis techniques were developed for generating discrete fragment models that could be spatially manipulated and reduced. The process started with extracting the whole tibia (a), then non-cortical tissues were masked out (b). Individual cortical fragments (c) were used as seeds from which bone boundaries propagated (d)..... | 78 |
| Figure 54  | The deviation between watershed and manual segmentation results is shown for each case. There was better agreement on the location of the native boundaries than there was for the fracture boundaries.....   | 79 |
| Figure 55  | The accuracy of patient-specific vs. compiled classifications for total articular and periosteal areas is reported. Whole patches were given a single label if 50% of their surface area matched a model with 90% probability.....  | 80 |
| Figure 56. | Five cases display surface density classification results using patient-specific and compiled population models. The majority of diaphysis (blue), metadiaphysis (cyan), metaphysis (green) and articular (dark red) surfaces were recovered. Regions that did not fit the models with at least 50% probability were labeled as unknown (gray)..... | 81 |
| Figure 57  | Ten clinical tibial plafond fractures were puzzle solved. Volume renderings (3DCT) and segmented fragment geometries (Displaced) illustrate this series’ range in severity and variable fracture characteristics. Puzzle solutions (Reduced) provide ideal fragment positioning targets for restoring original anatomy.....                         | 85 |
| Figure 58  | For the case with the largest articular alignment error, a large articular defect was visually apparent on CT and the virtual reconstruction.....   | 86 |
| Figure 59  | Fracture energy calculations with puzzle solving agreed well with those reported in previous work (left). The two-dimensional original version and the 3D curve articular comminution metrics agreed (right).....   | 88 |

|           |   |     |
|-----------|---|-----|
| Figure 60 | Previously reported and puzzle solving-derived fracture severity measures are compared to the eventual development of PTOA at 2yrs post injury measured by KL scale (0 = no OA, 4 = severe OA).....   | 89  |
| Figure 61 | Two surrogate fracture patterns were reduced in a simulated fracture reduction surgery. When anatomically reduced, most fragments interdigitated with adjacent fracture surfaces. However, the posterior-lateral fragment of Pattern A (color purple) was highly unstable and was therefore especially challenging to reduce..... | 91  |
| Figure 62 | Left: The final fluoroscopic image taken during Resident 3's reduction of pattern B. Right: An accurate articular reduction is observed in a fluoroscopic image taken midway through resident 2's reduction of pattern A.....   | 92  |
| Figure 63 | The average reduction error for trials with, and without puzzle solving's assistance are compared.....  | 93  |
| Figure 64 | The base fragment from a cadaveric impact is shown (a). A segment of the cancellous fracture surface (arrow) that was detected visually and on the laser scan (b), but was not discernable on CT --causing there to be a cavity in CT iso-surface (low threshold, 100 HU).....  | 98  |
| Figure 65 | A color map of the surface deviation between manual and watershed segmentation geometries for Case 6 is shown. The majority of the native surface (left) differs by only 0.5mm, whereas there is greater disagreement on the fracture surface (right).....  | 99  |
| Figure 66 | The puzzle solution's articular alignment error was associated with fracture severity (left), and with the actual incongruities after surgical reduction (right). Theoretically, a single case (red marker, Case ID: 9) could have been reconstructed to substantially greater accuracy than what was physically achieved.....    | 100 |
| Figure 67 | Four puzzle solutions are compared to what was achieved surgically. Inspection of the virtual solution provides prognostic information.....   | 102 |
| Figure 68 | Application of puzzle solving technology to a prospective case. CT data (i) is segmented (ii) and fragment native surfaces are aligned to an intact template (iii-iv). Custom implants can be designed to fill segmental bone defects (v).....  | 104 |
| Figure 69 | Puzzle solving methods successfully reconstructed a comminuted fibula. Detailed information was provided to the surgeon prior to surgery.....   | 106 |
| Figure 70 | A cadaver ankle was shot with a 45 caliber round to produce a typical ballistic injury encountered in combat (a). CT data (b) and physical inspection (c) reveal a severely comminuted fracture with a large posterior defect.....  | 107 |

|            |  |     |
|------------|--|-----|
| Figure 71  | Puzzle solving derived injury severity metrics are compared to those established in earlier work. Although the magnitudes differ, each derivation accurately separates stable and arthritic joints by injury severity – except for one outlier. Both measured one case (red arrow, case ID 6) as having a relatively low severity injury, however that joint developed moderate PTOA after two years. .... | 109 |
| Figure 72  | Localized articular comminution is evident on Case 6’s injury CT (a) and on the virtually reconstructed plafond (b). Cartilage thinning is apparent in that region after two years with a dual contrast MDCT scan.....   | 110 |
| Figure 73  | The average articular error in the virtual reconstructions was associated with the severity of PTOA as measured by KL at 2 years. One outlier (Red marker - Case 3) developed PTOA with minimal deformation, but that case also had the second greatest fracture energy (30J). ....  | 112 |
| Figure 74  | Surgical simulation was successfully completed in five sessions. Fractured surrogate tibias were percutaneously reduced under the guidance of fluoroscopy. Meanwhile, surgeon hand motions were tracked with a Qualisys motion capture system, and synchronized to the video recording. ....   | 113 |
| Figure 75. | Fracture pattern A is shown with adjacent anatomy. The posterior-lateral fragment (purple) was relatively difficult for all surgeons to reduce due to its not having a lock-and-key fit.....   | 116 |
| Figure 76  | Restoration of normal anatomy is measured with navigation reference markers.....   | 119 |

## CHAPTER 1 - INTRODUCTION

Most fractures are relatively easily managed using well-established treatments such as orthoses, casts, external fixators, or internal fixation (plates, screws, intramedullary nails, etc.). The specific treatment that is appropriate for a given fracture depends primarily on the anatomic site involved and on the characteristic geometry and relative displacement/angulation of the fracture fragments. The goal of surgical management is to ensure stable fixation of the fragments in anatomically reduced positions during the two-to-three month period normally required to achieve osseous union. For low-energy fractures with little comminution, displacement and minimal injury to the soft tissues, these techniques are relatively straightforward with predictably satisfactory patient outcomes. Considerations differ markedly for high-energy injuries in which comminution and displacement are more severe. During these traumatic events (e.g. high-speed motor vehicle accidents), where substantial energy is delivered to the bone at a high rate, fragments are propelled through the surrounding soft tissues, severely disrupting the osseous and soft tissue anatomy. Oftentimes, dozens of individual fragments are involved, displaced appreciably from their site of anatomic origin and interspersed in a complex geometric pattern.

Especially troublesome are comminuted fractures that extend into an articular joint. These fractures carry considerable long-term morbidity and cost [1]. Advancements in the treatment of highly comminuted articular fractures have been impeded by unreliable severity assessments and a poor understanding of joint degeneration mechanisms. These high-energy fractures present with a network of complex characteristic features that each individually affect the eventual outcome. Observer-based methods for their assessment are compromised due to the inherent difficulties in describing the complicated fracture morphologies and other patient- and fracture-specific factors. Without a means to quantitatively decipher these complexities, treatment

decision-making has been largely based upon subjective empiricism. Fracture characterization using recently developed image analysis techniques has provided an objective basis for improving severity assessment, a necessary development in the quest for more favorable surgical and biological interventions.

In addition to the acute injury severity, clinical evidence suggests that precise fracture reduction is very important. The quality of an articular fracture's reduction not only affects the bone healing process, but it is also critical in avoiding cartilage contact stress elevations [2-3]. While diaphyseal fractures need only general alignment and stability to form abundant callus and to ultimately heal properly [4], intra-articular fractures fare better when the original anatomy is restored with ample inter-fragmentary contact [5]. In order for the limb to heal and function properly, it is essential that the original anatomy be restored with minimal surgical insult [6-7]. The degree of residual displacement that an ankle can tolerate is not well established [8], but other joints such as the hip have been shown to poorly tolerate even as little as 1 mm of residual displacement after articular fractures [9].

The trauma surgeon reconstructing a comminuted fracture faces a problem very much akin to puzzle solving, albeit with obvious additional complexities. Performing this geometric reconstruction, by matching fracture surfaces and fragment boundaries back together, is termed 3D puzzle solving. Muscle forces, combined with complex fragment displacements, intervening soft tissues, and interaction between fragments and fracture surfaces all serve to make it difficult to mobilize the fracture fragments. To partially or completely restore the osseous anatomy, traditional surgical treatment (open fracture reduction) exposes the fragments by a surgical approach through the damaged soft tissue envelope, so the surgeon can directly assess and reduce the fragments. The surgeon assesses fragment inter-digitations visually and by touch, effecting a sequential fragment reduction. This often requires considerable force and involves trial and error. Unfortunately each "error" prolongs the procedure and increases iatrogenic trauma to the

fragments and the surrounding soft tissues. Fracture reduction is deemed adequate when the surgeon judges that an optimal fit has been obtained between all relevant fragments, completing the fracture puzzle solution. The more extensive the surgical approach, the better the fracture is visualized and the easier it is to execute an open fracture reduction. However, wide surgical exposure comes at a significant price, including increased risk for wound healing failure, infection, joint stiffness, delayed fracture healing, and further damage to articular surfaces. To avoid such risks, an alternative is to use a limited approach, where fragments are manipulated percutaneously under fluoroscopic visualization. Unfortunately, the diminished visibility and accessibility can lead to a less than perfect reduction – a factor likely leading to the development of post-traumatic osteoarthritis [10-11], a poor clinical outcome regardless of osseous union. Although CT imaging is a useful tool for visualizing fracture patterns and displacements [12], it is often difficult to identify exactly how multiple bone fragments should be put back together in three dimensions.

Accurate and precise pre-operative planning, building upon modern medical imaging and knowledge of the pre-fracture anatomy, can provide important information for developing less invasive surgical techniques to reduce and fix articular fractures. Commercial pre-operative surgical planning software has been developed to aid in the reconstruction of long-bone fractures, but it is not designed to puzzle-solve complicated fractures (Mimics, (Materialise, Belgium) and TraumaCad (VoyantHealth, USA)). While useful for fixation planning for simple fractures, these early-generation systems are unable to deal with the complex geometries of comminuted articular fractures. In the last several years, new computational algorithms have been developed to achieve what effectively amounts to three-dimensional puzzle solving. Although initially developed for unrelated purposes (reconstructing archaeological relics), these methods can help to improve how comminuted bony fractures are reconstructed surgically. However, implementing puzzle solving for comminuted bony fractures involves several important

considerations not encountered previously. Many of the computational assumptions for puzzle solving of relics cannot be applied to orthopaedic trauma. In addition to human bones not being axisymmetric, bony fragmentation patterns and shapes significantly differ from the behavior observed in pottery and other archaeological relics. The complexities of natural bone specimens confound the development of this technology, and conventionally acquired clinical CT scan data afford less-than-ideal spatial resolution for achieving a clear delineation of fragment surfaces.

Toward orthopaedic application, a need was identified for more precise and controlled data to support algorithmic developmental work on 3D puzzle solving. Therefore, the present work started first with the task of developing a platform that utilized test specimens whose fragment geometries were precisely quantifiable, so that different computational approaches to fracture reconstruction could be investigated [13]. Novel methods for puzzle solving intra-articular fractures in an *in vitro* surrogate model were developed. The surrogate platform proved to be an effective vehicle for advancing a computationally tractable puzzle-solving framework that involves matching fracture fragments to an intact template. However, several important features inherent to the *in vivo* situation are much more challenging. Whereas surrogate geometries could be obtained from high-resolution laser scans, *in vivo* fragment geometries are necessarily acquired from lower resolution CT data. In addition, although simplified bone fracture surrogate materials were helpful in algorithmic development, the structure of peri-articular bone makes it much less homogeneous and more susceptible to plastic deformation (i.e., crush). In such cases, there could potentially be alignment errors introduced because fragment native surfaces might no longer precisely match the template geometry.

For these reasons, the next objective in the present work was to design new methods that would adequately accommodate *in vivo* complexities such that accurate reconstructions of highly comminuted articular fractures could be obtained. In

the first step toward that objective, effective image analysis techniques were developed for reliably extracting bone fragment geometries from CT data. Next, original geometric and anatomic bone classification approaches were developed to provide additional information to be used in the alignment step. New computational geometry methods were developed to grossly reduce fragment models and place them closer to their anatomic target – thereby improving the speed and stability of subsequent alignment steps. Lastly, fine fragment displacement adjustments were performed to restore original anatomy. In order to evaluate these methods, the hypothesis that aligning fragment periosteal and articular surfaces to the mirrored image of the non-affected contralateral tibia can restore the normal anatomy of human tibial plafond fractures was tested.

While it is intuitive that a detailed pre-operative reconstruction plan would make surgical management far less complex, objective data are needed to prove that there is clinical efficacy, and that the extra effort is warranted. Therefore, the final objective of the present work was to design and execute a surgical simulation experiment for quantifying utility in a well-controlled environment. Using surrogate bones within a physical model of the distal-most portion of the leg, orthopaedic surgeons reduced fractures with and without the aid of 3D puzzle solving. Surgeon performance and reduction quality were assessed with various quantitative metrics. In addition to documenting clinical utility, this experimental setup provides a useful platform for investigating how to integrate puzzle solving into practice. What appears to an engineer to be helpful may be irrelevant to the surgeon. In this setting, puzzle solving's strengths and weaknesses can be identified without harming a live patient.

From surrogates to prospective cases, the developments reported here document a significant advancement toward improving the treatment of comminuted intra-articular fractures. The computational 3D puzzle solving framework provides a heretofore unavailable patient-specific blueprint for fracture reconstruction planning. Having a suitable blueprint for restoring the original anatomy, it becomes possible for the surgeon

to pre-operatively explore less extensive surgical approaches, and to improve upon the present intra-operative trial and error approach, while still achieving accurate fracture reconstructions.

## CHAPTER 2 - LITERATURE REVIEW

### Comminuted Intra-Articular Fractures

#### Tibial Plafond Fracture

Comminuted intra-articular fractures are defined as fractures in which an articular joint surface is disrupted and the associated bone is fragmented into many pieces (Figure 1). Such fractures are commonly seen in the hip, knee, ankle, shoulder, and wrist. The tibial plafond fracture, (also known as a pilon fracture) is an intra-articular fracture involving the weight bearing area of the ankle joint. The prevalence of plafond fractures has been reported to comprise 7% of tibial fractures and less than 1% of lower-extremity fractures [14]. While they are not the most common injury, other more frequent joint fractures, such as the tibial plateau, share similar fracture characteristics. Therefore, new technologies developed for the ankle are likely to be successful elsewhere. One can begin to understand the mechanism and appearance of the tibial pilon fracture through the origin of its name. The distal end of the tibia is known as the “pilon” in French speaking countries. This translates to pestle or rammer, implying an axial compression configuration [15]. The fracture generally results from a compressive talar impact being axially applied to the distal tibia. Other forces such as shearing and bending become more influential as the apposition of the tibia and talus deviates from their neutral state [16]. A purely axial compressive force will generally produce an explosion of bony fragments, whereas torsion and shear forces produce oblique and split fractures to varying degrees. The fracture pattern can extend from the articular surface into the diaphysis, traversing both cortical and cancellous bone regions.

As with most intra-articular fractures, the severity of the tibial plafond fracture can be stratified according to the mechanism of injury, with knowledge of other patient factors. Injuries on the low end of the spectrum include minor falls and sports-related injuries, whereas those on the high end include falls from a height and motor vehicle

collision (MVC) [16]. A patient's long-term outcome is in large part determined by the fracture severity and the related cartilage damage. Numerous fracture classification schemes have been proposed, based upon general fracture characteristics, in an effort to guide treatment and predict outcomes. Proper treatment is especially important for intra-articular fractures, since they are at an increased risk for developing a degenerative condition known as post-traumatic osteoarthritis (PTOA). Unfortunately, inadequate and unreliable stratification of fracture severity has hindered this crucial step in patient treatment [17]. The current limitations with treating intra-articular fractures may partially explain the increased propensity for joint degeneration.



Figure 1 Radiographs and volumetric rendering from a high-energy tibial plafond fracture with severe comminution (~15 fragments).

### Soft Tissue Injury

Severe soft tissue injuries often accompany high-energy intra-articular fractures such as those of the tibial plafond. The rapid axial compressive force explodes the tibia, propelling the bone fragments into the surrounding tissues. The soft tissue structures provide varying resistance to the fragments. Sequelae include vascular laceration, compartment syndrome, hematoma, thromboembolic events, and skin necrosis [3]. Open wounds are reported in 20-25% of tibial plafond fractures, but severe internal injuries may also accompany closed fractures [18]. The acute injury not uncommonly presents with tense swelling and fracture blisters, reflecting the damage to the subcutaneous tissues (Figure 2). The more severe soft tissue injuries are associated with a high risk of infection. Thus, proper management of these injuries is in many ways as important as managing the skeletal damage, in terms of the limb's survival. The soft tissues need to be stabilized, and inflammation must be allowed to resolve prior to surgical fracture reduction.



Figure 2 A closed tibial plafond fracture with white and red fracture blisters presents evidence of severe soft tissue damage. In order to prevent complications, an external fixator is applied to stabilize the joint while the soft tissues are allowed to recover. After one to three weeks, the soft tissues are more tolerant to the surgical insult of definitive surgery.

For these reasons, it has been recommended that a two-stage surgical plan be implemented [19]. In the first stage, temporary external fixation is applied across the joint. After the soft tissue swelling has subsided, in approximately one to three weeks, definitive surgery is performed with internal fixation. This treatment approach offers a window of opportunity to incorporate more rigorous surgical planning into standard treatment methods. Soft tissue injury grading systems, such as the Tscherne for closed fractures and the Gustilo/Anderson for open fractures, are used to aid surgical approach and timing decisions [20] [21]. While the grading schemes may provide some insight as to the condition of the soft tissues, their moderate to poor inter-observer reliability has confounded their use as a basis for treatment decisions. To avoid the early complications associated with open reduction and internal fixation, some clinicians use a more limited approach with an articulated external fixator and internal fixation with percutaneous screws [22].

### Computed Tomography (CT)

Acquisition of CT data has become an integral part of orthopaedic research and clinical care. CT data are represented by images that are volumetric arrays of x-ray attenuation, commonly measured in Hounsfield Units (HU). Differences in musculoskeletal tissue densities allow radiographic attenuation to provide a clear delineation between them. Scanners are calibrated so that water is 0 HU and air is -1000 HU. Most soft tissues have attenuation values ranging from -100 to +100 HU, while cortical bone can range from 500 to 2000+ HU [23]. While plain radiographs remain clinically relevant, the superiority of CT scans for assessing complex fractures is widely acknowledged. Routine clinical care of articular fracture calls for the acquisition of pre-operative CT scans for fracture evaluation and surgical planning. Along with clinicians, scientists have long recognized the utility of CT in orthopaedic research, with a wealth of literature focused on measuring *in vivo* bone density and predicting mechanical properties

[24-25]. Ciarelli et al. investigated the capacity of CT-inferred densities to predict bone stiffness and strength [26]. They developed a statistically significant linear relationship between HU and density, supporting CT's capability to perform reliable measurements:  $\rho \text{ (g/cm}^3\text{)} = 0.11837 + 0.001141 \cdot \text{HU}$ , Rho et al. observed the relationship of  $\rho \text{ (g/cm}^3\text{)} = 0.047 + 0.001122 \cdot \text{HU}$ , (statistically significant) suggesting that CT is an adequate indicator for apparent density [27-28].

### Acute Fracture Severity and its CT-Based Assessment

Many consider the initial fracture severity to be the single most important prognostic determinant of long term joint health subsequent to trauma [8]. The degree of insult affects the joint's immediate survivability, its regenerative capacity, surgical treatment plan, residual defects and likely complications. Fracture severity occurs on a continuum, and it is manifest in a set of complex fracture characteristics, each with individual implications for treatment and outcome. Clinicians have long characterized fracture severity according to the perceived energy involvement, ranging from low to high [29-30]. Another principal component of fracture severity is the degree of bony fragmentation, or comminution. Fractures on the low end of the spectrum display easily identifiable fragments, and they respond well to more straightforward treatments. Complex fractures produce multiple fragments (4 or more), some with compromised vitality, and the disrupted tissues can pose extreme obstacles to achieving anatomic reduction and restoration of joint stability [3]. Surgical management is more complicated if the fracturing energy is sufficient to drive the fracture into the diaphysis or to substantially displace/rotate fragments, since mechanical and biologic stability is further compromised.

When considering a joint's ability to survive following intra-articular fracture, the damage to the cartilage may well be of comparable importance as damage to the bone. Since their severities are intimately linked through the energy transmission and fracture

process, the magnitude of ossified tissue insult can serve as an indicator of the propensity for cartilage degeneration [31]. Recently, a novel CT-based method to objectively measure fracture energy for fracture severity assessment was developed [32]. Using image analysis techniques, the energy absorbed during fracture was quantified by relating liberated fracture surface area and CT apparent bone density. That study demonstrated excellent agreement between the CT-based metric and expert severity assessments [32].

Intra-articular fractures predispose patients to post-traumatic osteoarthritis (PTOA), with associated chronic joint pain and decreased function. The success of articular fracture management is dependent on how the fracture is treated and on fracture type and severity. Articular fractures vary in their degree of articular surface disruption, overall comminution, fragment displacement / dispersal, and associated soft tissue injury. The severity of a fracture is an important determinant of long-term joint function, but it has not been amenable to objective quantification. The purpose of prior work was to correlate novel objective CT-based indices of intra-articular fracture severity [32] with subsequent joint degeneration. It was hypothesized that an injury severity metric that included objective measures of articular disruption, of fracture energy, and of fragment displacement/dispersal would be a useful predictor of PTOA.

Novel CT-based image analysis techniques were utilized to quantify acute injury characteristics in a prospective series of twenty tibial plafond fractures managed by articulated external fixation, with later definitive surgical fracture reduction performed after soft-tissue swelling had sufficiently resolved. The fracture energy was derived from the liberated surface area measurement, by multiplying inter-fragmentary surface areas times the energy release rate, the latter being a material constant that was scaled from CT intensities to account for variation in bone density within and between patients [33]. The degree of articular comminution was quantified by determining the amount of inter-fragmentary surface area present within 1.5 mm of the articular surface. It was expressed as a percentage of the intact surface area over the same portion of the distal tibia. PTOA

severity was assessed two years post-injury using the Kellgren-Lawrence (KL) radiographic grading scale. A predictive model was developed by linearly regressing these two-year KL outcomes on the CT-based severity metrics.

A combined acute severity score involving articular disruption and fracture energy successfully predicted PTOA severity ( $R^2 = 0.70$ ), whereas fragment displacement / dispersal and surgeon opinion correlated much less well with degeneration ( $R^2 = 0.42$  and  $0.47$ ). The concordance between the combined metric and PTOA severity was 88%. The findings of this study indicate that objective CT-based metrics of acute injury severity can reliably predict intermediate-term PTOA outcomes in this challenging class of articular fractures. The average of 8-10 hours of analyst time required to quantify injury severity posed a significant barrier to implementing these techniques clinically. Even though much of the algorithm is automated, certain operations (e.g., bone boundary segmentation) needed greater automation, to further reduce user interaction and total processing time. The results from this prior work nevertheless illustrate how quantitative biomechanical assessment of injury characteristics can provide new possibilities to improve fracture management and to guide PTOA research.

### Fracture Reduction and Treatment Techniques

A comminuted intra articular fracture is a challenging injury for orthopaedic surgeons to treat due to the complex anatomy and variable fracture morphology [34]. Accepted treatment protocol begins with an initial evaluation in the emergency department. If the fracture is assessed to be severe and to involve any risk of limb shortening/bony collapse, the limb is distracted to length, and placed in a splint or stabilized with an external fixator. The damaged soft tissue envelope is especially susceptible to complications, with rates ranging from 33 to 68% [35]. Therefore, the timing of fracture reconstruction surgery is generally delayed until the soft tissues are healthy enough to withstand the additional secondary insult of surgery [36].

Pre-operative planning is essential for properly managing these fractures. This process involves the surgeon understanding the fracture pattern, selecting the fixation strategy, and planning a surgical approach. Potential problems and likely complications can ideally be predicted and managed. Typically, plain radiographs and CT scans are acquired to aid the planning process [17, 37-38]. Although surgeons recognize the utility of planning, current methods for its execution are remarkably elementary. For long bone and less severe fractures, fragments are traced from the (two-dimensional) radiograph and reassembled over the normal x-ray of the contralateral limb (Figure 3). After the fragments are aligned, the fixation hardware and surgical approach is chosen. While simple to moderately fractured bones benefit from this technique, its implementation in highly comminuted fractures is not practical.

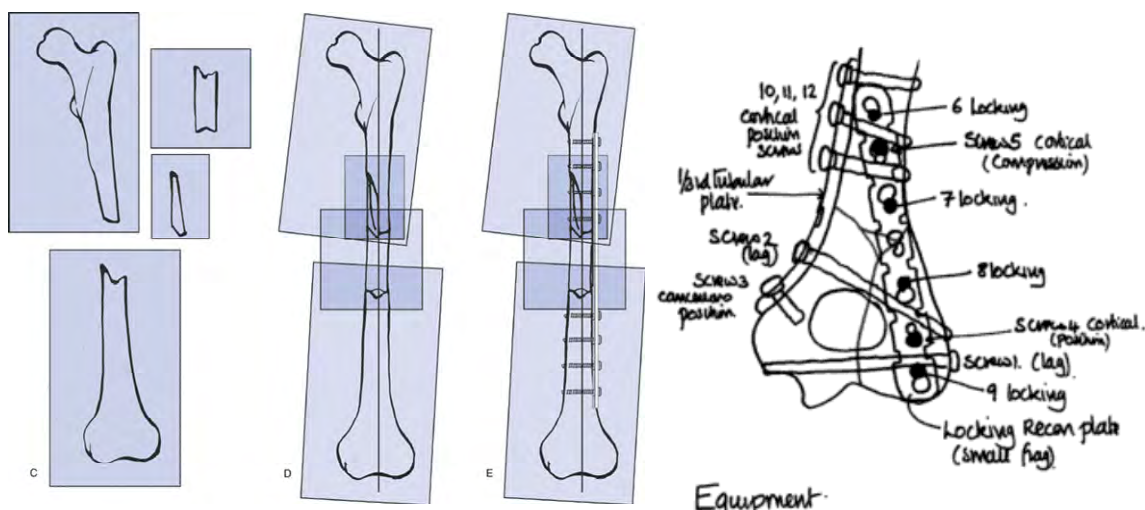


Figure 3 Conventional pre-operative planning method for reconstructing fractures.

The optimal surgical approach is open to debate, but the primary objectives are; anatomic reduction, limited iatrogenic trauma, and restoration of joint congruity and mechanical alignment [14, 39]. There are mitigating factors affecting the surgeon's

ability to achieve these objectives. Open reduction and internal fixation (ORIF) was historically the standard care for tibial plafond fractures. This procedure uses a direct approach which applies internal fixation to the fibula, reduces the tibial plafond and rigidly fixates the metaphysis with plates [40] (Figure 4, left). Due to the high rates of complications related to ORIF [41-42], some surgeons utilize less invasive techniques that minimize iatrogenic trauma at the expense of a less perfect reduction [22]. Rather than opening the joint with an incision through the compromised soft tissues, surgeons reduce the fracture percutaneously using various instruments (Figure 4, right). Video fluoroscopy is used to provide two-dimensional real-time visual feedback to the surgeon. Once positioned correctly, fragments are fixated to the diaphysis with screws, and an external fixator is then applied.

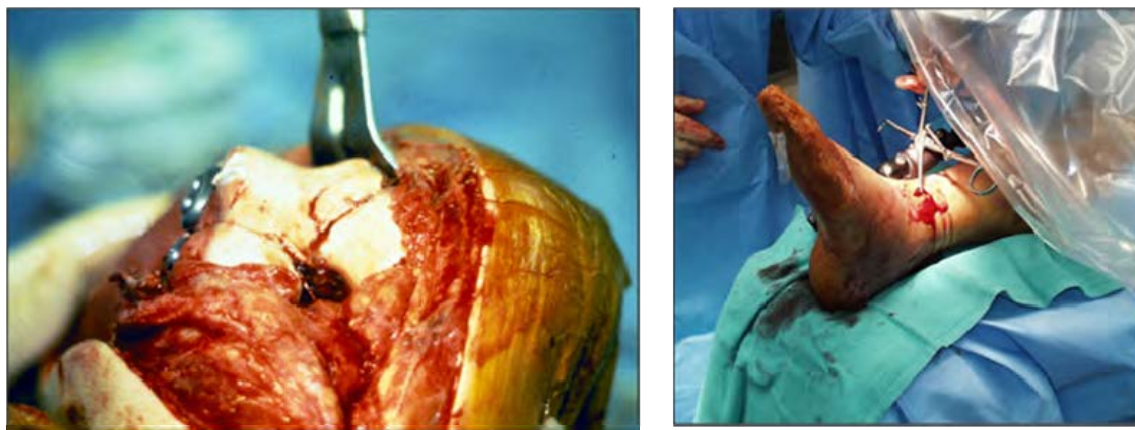


Figure 4 Open reduction internal fixation (left) and percutaneous/limited (right) surgical approaches illustrate the tradeoff between joint visualization and iatrogenic trauma.

Reducing an intra-articular fracture most often begins with the articular surface, starting with the least displaced fragment. (If one were to start with the metaphysis, relatively small mis-alignments would create large and unacceptable articular

incongruities.) After the articular surface is reconstructed, it is temporarily stabilized with small wires or forceps. Definitive fixation is achieved with screws. Next, the metaphyseal fragments are anatomically reduced with limited soft tissue disruption. After remaining gaps or defects are filled with a grafting material, the articular block is reattached to the diaphysis with various fixation options [43].

Precise articular reduction has been shown to be important in obtaining good functional outcomes, but the concomitant surgically induced soft tissue damage may cause severe complications [7]. While these objectives are based on 40 years of clinical experience, an incomplete understanding of the primary factors affecting outcome continues to limit improvements in the success of this treatment [44]. This is illustrated by perfectly reduced joints still experiencing poor outcomes, while joints with residual incongruities can have a positive outcome. Regardless of surgical technique or success, it is difficult for a patient to recover from the tibial plafond fracture [39]. The documented results of clinical and functional outcomes vary, with poor results ranging from 30-50% [45]. There are high incidences of early and late complications, including wound breakdown, infection, nonunion, joint stiffness and post-traumatic osteoarthritis [46]. Treatment advancements have been hindered by the inability to discern and measure the complex characteristics of the tibial plafond fracture. Their individual and collective effect on joint health and surgical response remains unknown without reliable identification.

#### Post-Traumatic Osteoarthritis

Trauma to articular cartilage from impact, fracture, and/or abnormal loading has been shown to strongly correlate with degenerative joint changes. The changes to the cartilaginous composition and structure, and an associated constellation of physical symptoms (joint pain and stiffness) constitute a disorder known as post-traumatic osteoarthritis (PTOA) [47]. PTOA is a painful and debilitating disease that greatly

affects patients' functional abilities, with implications to their general health status. The degree of functional impairment due to osteoarthritis of a single lower extremity joint is severe. Saltzman et al. observed it to be equivalent to that of congenital heart failure [48]. PTOA is not an uncommon disease, with clinical studies of patients with joint injuries showing its incidence as high as 54% [49]. In addition to physical and mental impairment, the economic impact of PTOA is profound. It is estimated that lower extremity PTOA alone imposes a roughly \$12 billion annual burden on the economy, with around \$3 billion from direct health expenses alone [1].

PTOA-inducing impact injuries can range from relatively lower energy, non-fracturing events to severe high-energy disruptions of the articular surface [50]. The variable combinations of tissue damage elicit different repair responses, ranging from matrix macromolecule repair to the formation of fibrocartilaginous tissue [47]. Even though numerous studies have shown that fracture of the articular surface is closely associated with eventual PTOA development [51], the specific biomechanical and cellular mechanisms leading to PTOA remain poorly understood [52]. Articular fractures are complex injuries, with a host of characteristics that might predispose a joint to PTOA development. It has been hypothesized that the likelihood of PTOA is governed primarily by three pathomechanical factors: (1) the acute injury severity, (2) residual joint instability, and (3) elevated contact stresses due to residual incongruity. However, the relative importance of each of these interdependent factors on PTOA development is widely debated.

Many observers feel that the acute fracture severity is the main determinant of eventual outcome, regardless of fracture treatment [8, 53]. Studies consistently show that the magnitude of the mechanical insult to the cartilage is directly related to the immediate destruction of cartilage structural and cellular components, in addition to long term biochemical changes, and therefore related to the severity and speed of PTOA development [49]. Clinicians have long suspected this relationship, with observation of

increased PTOA propensity with greater fracture severity, even for some joints with excellent surgical restoration of joint congruity [8].

Accepted surgical protocol calls for the reduction and stabilization of the fragmented articular surface, in part to avoid the deleterious effects of residual joint surface incongruities. It is believed that chronic exposure to abnormal contact stresses from incongruous regions is one of the leading pathomechanical factors for PTOA development. Residual incongruities are often associated with high-energy fractures that had significant fragment displacement. However, articular step-offs can occur across the severity spectrum. The incongruity tolerance remains to be identified, but clinical observation shows that 1-4mm step-offs are associated with a high incidence of PTOA [54].

Joint instability is the third main pathomechanical factor for PTOA. Instability refers to the altered joint kinetics and kinematics following injury to the articular surface or supporting soft tissues [55]. The altered joint contact patterns and loading rates may evoke irreversible cartilage damage. The tolerance of instability varies between joints, but instability has clinically been shown to be a likely indicator for joint degeneration[56]. The interaction between these three pathomechanical factors and PTOA development is complex, and it is currently viewed by many as a “black box” [52]. While the three are clearly related, the circumstances and conditions under which they individually dominate is unknown.

### Computer Vision and Assistance in Orthopaedics

#### Bone Segmentation from CT Data

The treatment of articular fractures has greatly benefited from CT imaging. Whereas fracture lines and fragment displacements are difficult to appreciate from plain radiographs, CT improves visualization of relevant fracture characteristics with volumetric data [57]. This information facilitates fracture classification and reduction

planning. But in order to move beyond visualization with computational modeling, bone fragment geometries have to be extracted from the CT data. Segmentation of bone boundaries is both an active research area and a lucrative commercial market. There are well-established techniques for extracting normal bone anatomy from CT. Using methods such as active contours, graph cuts, level sets, adaptive thresholding and edge detection, many techniques are able to identify the majority of bone edges [58-60]. Since human bones are similar in shape for much of the population, many of those algorithms exploit that *a priori* knowledge, and create generic models that can be deformed to fit specific patients [61].

However, comminuted fractures present an especially difficult segmentation problem. Bone fragments not only vary in shape, but also in tissue composition. Furthermore, patterns of fracture comminution are highly idiosyncratic. Fragments often include both cortical and cancellous bone, tissues with very different radiographic appearances. Whereas cortical bone has a relatively uniform CT intensity, cancellous bone is quite heterogeneous due to its variable density and architecture. Furthermore, non-displaced fracture surfaces typically have weak edge signals, making them difficult to demarcate both visually and computationally. No segmentation technique has been identified in the literature that automatically segments all comminuted bone fragments. Algorithms typically implement semi-automated approaches where automatic algorithms are used to identify most of the bone edges, then a trained user manually edits those results by separating and/or fusing objects into appropriate geometries [62-63]. A fully automatic CT fragment segmentation method would greatly advance computer assistance in orthopaedics. Clinicians and scientists would be permitted to explore new technologies without being limited by that laborious process. Although it is doubtful that such a tool will be developed in the near future, progress toward advancing computational orthopaedics should not be impeded. Without an established technique, it is essential that new segmentation methods are validated in some reliable manner.

## Computational Reconstruction Methods

Accurate and precise pre-operative planning, building upon modern medical imaging and upon knowledge of the pre-fracture anatomy, can provide information instrumental for planning less invasive articular fracture surgery. Computational techniques hold strong potential to contribute in this area, and there are several noteworthy studies. A detailed survey of the computer vision field is beyond the scope of the present document. Algorithms for matching objects based on their shapes have been applied in the past to the assembly of (2D) jigsaw puzzles [64-66]. However, jigsaw pieces have similar sizes with easily identifiable sites that need to be matched. Also, the task of registering complementary fragments is much simpler than reassembling broken objects in the situation where there may be missing fragments and material deterioration. Solving more difficult puzzles involving physical fracture surfaces is an emerging area of research [67-72]. Examples of successful puzzle solving in full 3D situations remain limited [69, 73-74]. The primary path taken in dealing with fragments of arbitrary shape has been to base assembly efforts on matching the fragments' break curves, i.e., the edges of the surfaces along which the fragments physically broke apart [69, 73]. The initial stimulus for that technology had been the reconstruction of culturally/historically important relics such as broken pottery and broken sculptures, recovered from archaeological sites [75]. For that type of application, computational puzzle solution has taken as its input the 3D surface geometry of each of the recovered fragments as quantified by laser scan, with geometric reconstruction performed by matching individual fracture surfaces and fragment boundaries.

Implementing puzzle solving for the orthopaedic situation of highly comminuted intra-articular fractures involves several considerations not encountered in precedent archaeological work. Bone fragment surfaces tend to be more highly irregular, and they can frequently lie in very close proximity to one another (or even in partial contact), making discrimination of individual fragments sometimes difficult. To compound

matters, to quantify the boundaries of the bone fragments in clinical fracture cases, one must rely upon segmentation of CT scan data, which are subject to partial volume effects. Fortuitously, two aspects of bone fractures are actually more advantageous than for archaeological fractures. First, bone fragments have spatially varying distributions of density, which can be measured from CT scan data and therefore constitute additional basis for registration. Second, for unilateral fractures of an extremity, the intact contralateral bone represents a reasonable mirrored template against which to reconstruct the fracture [76-77].

### Computer Assisted Orthopaedic Surgery

The literature regarding virtual reconstruction of bone fragments is relatively sparse, compared to the very large body of research on the topics of bone segmentation and medical image registration. Early efforts in this area included a technique for reconstructing a simple two-fragment bone fracture [78]. More recent work has focused on developing the algorithms to support image-based reconstruction systems [79-80], including even a complete fracture reassembly environment [81]. Methods for virtually reducing displaced acetabular fractures have received notable attention recently. Due to the hip's anatomic complexities and poor visualization, engineers have developed computer tools to train for, and aid surgical interventions. Cimerman and Kristan have developed pre-operative methods for reducing and planning fixation in pelvic and acetabular structures [82]. After fragments are manually segmented from CT data by a specialized engineer, surgeons manually move and rotate fragments to reduce the fracture. Afterwards, the fixation method is chosen and a printout records the pre-operative plan (Figure 5). Citak et al. have also developed virtual planning software for acetabular fracture reconstruction. Their technology allows for surgeons to rehearse fragment manipulations and ultimately assess the accuracy of reduction [83]. Although

these methods have not been tested clinically, users of the software were shown to have decreased the simulated surgical time after serial trials.

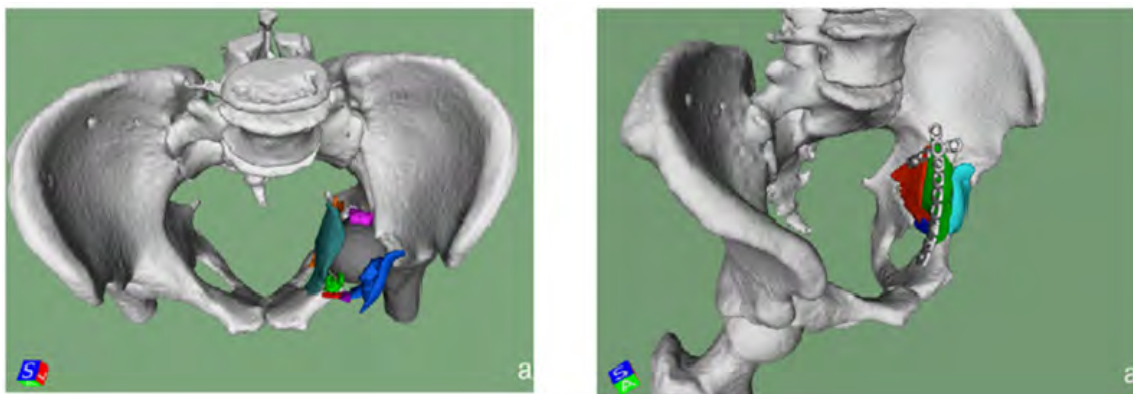


Figure 5 Virtual reduction and fixation for pre-operative pelvic and acetabular surgery.

Suero and Citak have recently piloted reconstruction methods in a small series of tibial plateau fractures [84]. In that work, recently commercialized software for image segmentation and 3D reconstruction were applied to a series of five patients. Since few details about the segmentation or virtual reconstruction algorithms were provided, it is difficult to assess and compare that work to others. However, the manuscript did state that the segmentation process involved some intensity thresholding method, and that fragments were ‘painted’ in the sagittal, coronal and transverse planes. From that information, it is likely that their method is semi-automated. After visual inspection, it appears that the segmentation technique would benefit from additional refinement or post-processing. The less dense metaphysis seems to have been problematic, much of the tibial surface is deeply pitted (Figure 6). Although questions remain regarding the technical details of this work, it is clear that many engineers and surgeons are recognizing the utility of computer assisted surgery in complex joint fractures, and are attempting to develop new technologies for improving treatment methods.



Figure 6 Suero et al. present segmentation results for an example C1 tibial plateau fracture. Although the authors state that the total planning time was 167mins for this case, no virtual reconstruction results are put forth.

While advances are being made in computer assisted orthopaedic surgery, many of these methods require the user to manually reposition fragments, a particularly challenging task for comminuted fractures. However, some are introducing computer vision algorithms to aid the assembly problem. Chowdhury et al. have investigated the specific problem of automated multi-fracture craniofacial reconstruction [85]. The fracture fragments of the mandible are typically displaced with clearly defined bone borders and non-deformed fracture surfaces (Figure 7).



Figure 7 CT images of an example mandibular fracture case are presented.

These authors used a two-stage approach: the first approximately apposed the fracture surface using the Maximum Weight Graph Matching algorithm, and the second then used the Iterative Closest Point (ICP) algorithm to finalize the registration (Figure 8). Whereas previous methods relied on experienced users for manual classification, the graph matching algorithm was developed to automatically identify fracture surfaces. This pairwise registration approach was able to accurately reduce the mandible from several fragments. However, this method assumed that a fragment had only one or two fracture surfaces, which mated to a single other fragment. High-energy comminuted fractures would severely complicate this combinatorial first phase, since fragment fracture surfaces may match to many other fragments. Furthermore, this alignment algorithm assumes that fracture surfaces are not plastically deformed. While this might be consistent with the typical mandible fracture, bone fragments from other anatomic sites can often be deformed. If fracture surfaces were mated in such cases, the general shape of the reconstructed bone would differ from the original anatomy.



Figure 8 Initial, intermediate and final mandibular reconstruction stages are shown.

In addition to Chowdhury's group, Roser et al. have investigated the clinical efficacy of pre-operative virtual planning in facial reconstruction procedures [86]. In a

retrospective study of mandibular osteotomies, prefabricated surgical plate templates and cutting guides were designed from virtual reconstruction information. To do so, pre-operative CTs were processed by an external company, and 3D models of the facial bones were generated. Surgery was then planned in collaboration with surgeons and the modeling company, and the custom guides and plate templates were manufactured. The pre-fabricated plate was then used by the surgeon as a template to pre-contour the final reconstruction plate. Post-operative CTs were then analyzed and the surgical outcome was superimposed onto the pre-operative virtual plan to assess accuracy. Compared to manual graft placement methods, the results from this work suggest that the patient benefited from virtual planning with more accurate osteotomies. However, the final contour plate did not reproduce the geometry of the prefabricated template. Rather than manually contouring a plate, rapid prototyping could be used to address these limitations in reproducibility.

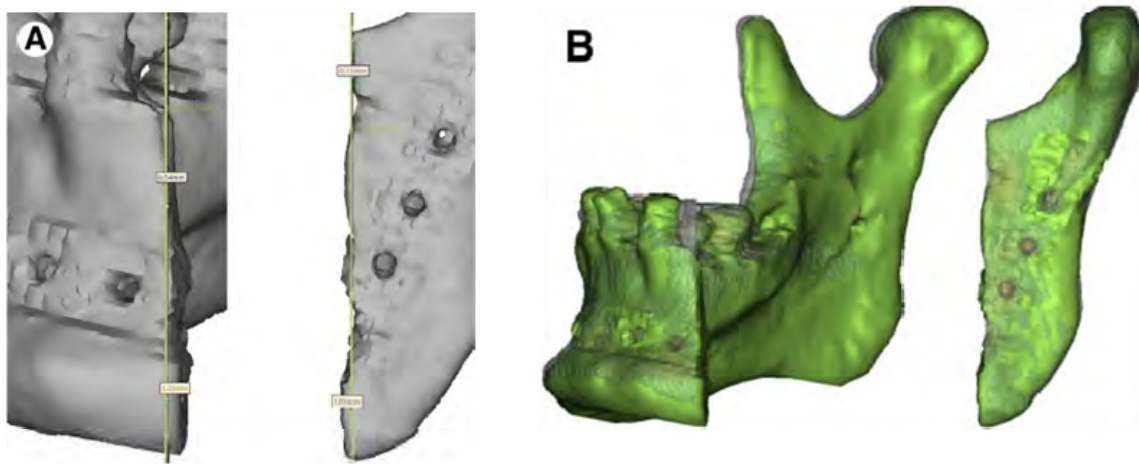


Figure 9 A virtual mandibular osteotomy is compared to what was surgically achieved. The virtual plan (green surface) is superimposed on the post-operative isosurface.

Willis et al. recently reported a methodology for semi-automatic reconstruction of highly comminuted bone fractures, developed to aid in treatment planning [87]. The software aligns bone fragment fracture surfaces derived from segmentation of volumetric CT scan data. The user interactively selects fracture-surface patches, in pairs that coarsely correspond, after which an optimization step is performed to automatically solve the corresponding N-body rigid alignment problem (Figure 10). In such a virtual interactive environment, the user is able to influence the reconstruction process, and to examine multiple potential reconstruction scenarios. In a subsequent paper [88], new algorithms were introduced to improve accuracy of anatomic restoration, using an alignment functional that allowed idiosyncratic geometric surface variations (ridges and valleys) to more heavily influence the final alignment solution, yielding results which were highly encouraging visually.

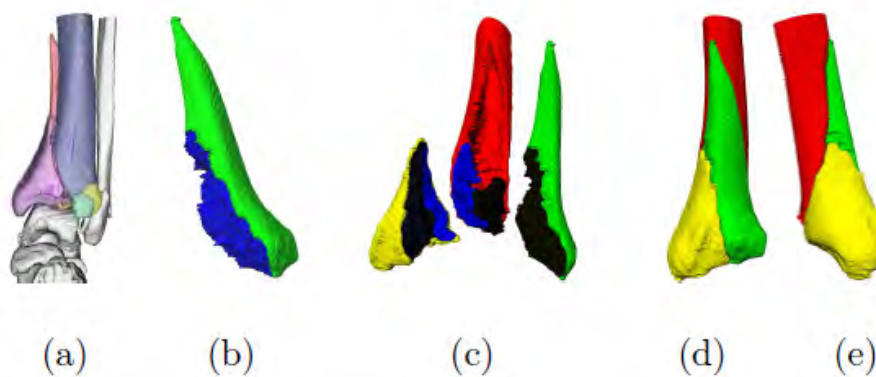


Figure 10 A tibial plafond fracture is segmented (a). Bone fragment fracture surfaces are identified (b) and interactively matched to corresponding fragments (c). Fracture surfaces are then aligned with a modified iterative closest point algorithm.

## Summary

Although significant advancements in comminuted peri-articular fracture treatment have been made in recent years, there remain high rates of both short- and long-term complications. In addition to problems with bone and soft tissue healing, post-traumatic osteoarthritis commonly develops. Research indicates that both acute injury severity and residual incongruities are primary factors for its onset. Given current categorical severity assessment methods, and crude two-dimensional reconstruction planning methods, surgeons are limited in their capacity to address those factors that are causing PTOA. Computer assistance offers new capabilities for investigating the pathomechanical determinants of PTOA and new treatment techniques. Others have recognized such benefits, and have started researching potential clinical applications. The groups that have made the most progress have focused on facial reconstructions. While their complex combinatorial algorithms have been effective for matching cranio-maxillofacial fragment fractures surfaces, a high-energy joint fracture is a very different problem. With the presence of cancellous bone, new complexities are introduced. In addition to segmentation difficulties, plastic deformations of fracture surfaces become more likely. The matching problem becomes much more complex when the correspondence between mating surfaces is distorted. The present document details a new fracture reconstruction planning approach, where fragment native surfaces are matched to an intact template. Native surfaces were identified as the optimal datum, since they are less susceptible to plastic deformation, and are better demarcated on CT. Of course there are tradeoffs with this approach, but the results from this work suggest that this approach is highly effective.

## CHAPTER 3 - MATERIALS AND METHODS

### A Development Platform for 3D Puzzle Solving

As a next step toward clinical application, algorithmic refinements of 3D puzzle solving benefit greatly from the availability of more precise and controlled data. The complexities of working with natural bone specimens confound systematic development of this technology, and conventionally acquired clinical CT scan data afford less-than-ideal spatial resolution from which to obtain fragment surfaces. Puzzle solving work therefore began with the creation of a development platform utilizing test specimens whose fragment geometries were precisely quantifiable, so that novel methods for fracture reconstruction could be quantified against an objective gold standard.

#### Surrogate Fabrication

Methodology was developed for generating fragmentation/dispersal patterns typical of comminuted articular fractures, but in surrogate test specimens. Using anatomy derived from the intact contralateral CT of a 6 foot male fracture patient, a NURBs surface was generated from an isosurface. Dr. Matt Frank from the Iowa State University then machined five identical replicas of a human distal tibia from blocks of high-density polyetherurethane foam (manufactured by General Plastics, Tacoma Washington). The surrogate material was developed to exhibit structural and fragmentation behavior comparable to that of native human cortical bone. When suitably doped with BaSO<sub>4</sub>, the material has comparable radiographic appearance as cortical bone [89]. Dr. Frank's innovative rapid machining technology was used to manufacture the distal tibia geometry, working off models generated from CT segmentations of intact anatomy [90]. The processing instructions for the computer numerically controlled machining were derived using advanced geometric algorithms for toolpath planning and fixturing [90].

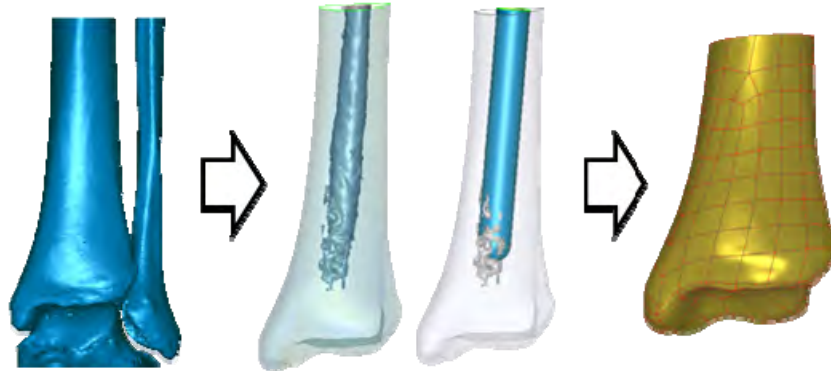


Figure 11 Process for surrogate tibia creation. From a CT isosurface, the endosteal and native surfaces of the tibia were modeled for generating NURBs surfaces. Surrogate material was then machined from the CAD model with rapid prototyping.

The external (native: periosteal and articular) surfaces of the surrogate distal tibias were indelibly color-dyed, to allow later distinction between native and endosteal bone surface equivalents, and so that fracture-liberated surfaces could be distinguished from native surface. The native-equivalent surface was also marked with alphabetic graffiti, to enable later unambiguous determination of the original location of fracture-generated fragments. A desktop 3D laser scanner (NextEngine Model 2020i; NextEngine, Inc., Santa Monica, CA) was then used to capture the geometry (resolution  $\pm 0.13$  mm) and surface appearance (color texture, 160 points/cm) of the surrogate tibias. Finally, these surrogate test specimens were encased in cylinders of dense hydrocarbon gel (a clear, highly occlusive emollient from Calumet, L.P) designed to replicate the resistance to bone fragment traversal through surrounding soft tissues during the fracture event (Figure 12 a). The entire physical test preparation was then CT scanned en bloc.

#### Fracture Generation

The test specimens were impacted using an instrumented drop tower, to cause highly comminuted fractures involving 5-15 fragments. A steel cylinder (7.6 kg mass)

was released from a selected height to deliver the necessary (empirically determined) kinetic energy. A talus analog, molded of polymethyl methacrylate, provided an anatomically matching proximal surface for tibio-talar contact, and had a flat distal side for flush impactor contact. The fractured specimens were then again CT scanned, with the fragments at their spontaneously-displaced/interspersed positions in the gel (Figure 12).

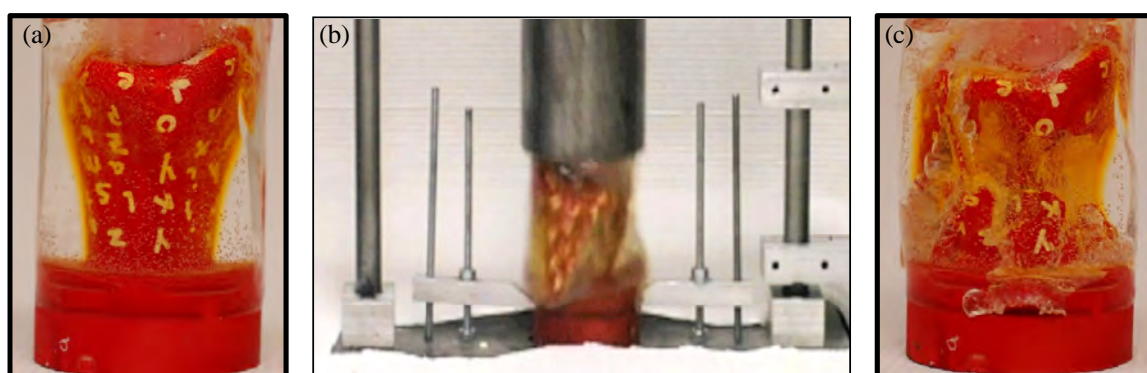


Figure 12 The polyetherurethane distal tibia was encased in a soft tissue simulant (candle gel) (a) and an instrumented droptower was used to create comminuted fractures (b), similar to those clinically observed such that fragment displacement would replicate *in vivo* patterns (c).

Subsequently, the fragments were removed from the gel, and their surface geometries were individually laser-scanned (gold standard for fragment surface geometry) (Figure 13). This ordered developmental platform provides clinically relevant data for investigating 3D puzzle solving algorithms, without hindrance by the many confounding factors involved in dealing with actual bone fractures.

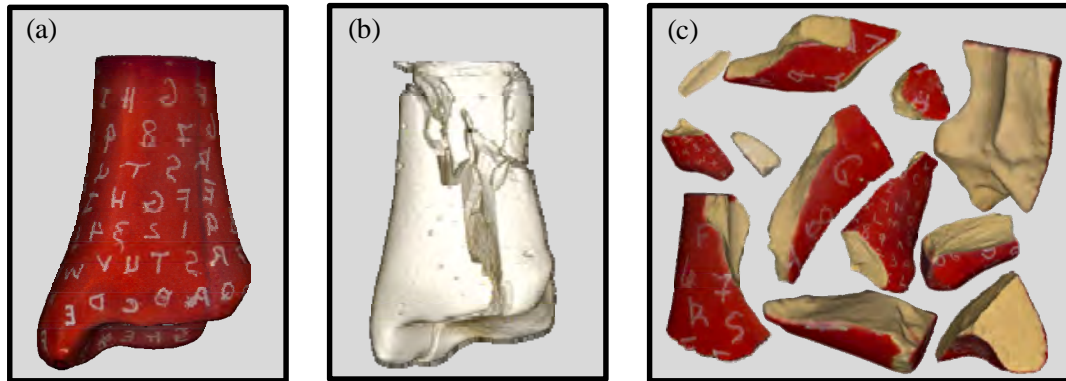


Figure 13 Distal tibia replicas were 3D laser scanned before and after fracturing (a, c). Post-fracture CTs provided visual confirmation of comminution and a data set for investigating segmentation techniques (b).

The fracture morphologies generated by the surrogate testing protocol were similar to the morphologies seen in clinical fracture cases. As with tibia plafond fractures, the replica tibias' articular surfaces were fractured anterior-posteriorly and/or medial-laterally through the weight bearing region. The replicas fractured into between 8 and 14 discrete fragments of varying sizes, with 2-5 of those being articular. Post-fracture fragment volumetric comparison showed that approximately 95% of the pre-fractured volume was recovered in the form of manipulably-sized fragments. The remaining volume was accounted for by “dusting” (crumbling of material), and/or by the decision to discard fragments that were judged as too small ( $\sim 0.5\text{cm}^3$ ) to be feasible for physical manipulation in a surgical setting.

### Native Surface Identification

#### Texture- and Color-Based Identification

The reconstruction algorithm began with native surface identification performed in MATLAB (Figure 14). Since the surrogate tibia's outer surface was colored red prior to impact, the pre-existing surface could be reliably distinguished from the fragment's *de*

*novo* fractured surface using an automatic texture (color) classification program. The data acquired from laser scanning provided red, green and blue (RGB) values for each vertex in the fragment mesh. To simplify the color classification process, the RGBs were converted to the hue saturation value spectrum (HSV). This enabled the red native, yellow/brown fractured, and green endosteal surfaces to be accurately distinguished using a single parameter, the hue value. From the fragment's hue histogram (Figure 14, right), three threshold values were chosen. Vertices with hue values between the first and second thresholds ( $\sim 0.07 - 0.22$ ) were classified as fractured. Vertices between the second and third ( $\sim 0.22 - 0.45$ ) were classified as endosteal and the remaining vertices were classified as native. The results from this step served as the gold standard from which alternative surface classification algorithms could be systematically investigated.

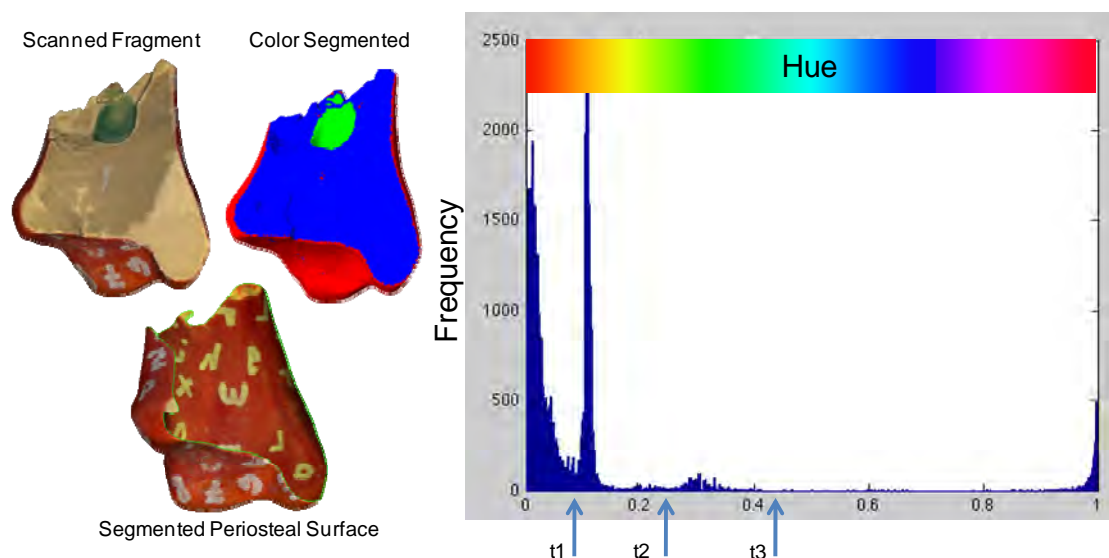


Figure 14 Fragment surface classification according to color (hue). Using the precise color information that was obtained during laser scanning, fracture surfaces (color blue) were automatically and accurately separated from the endosteal (green) and the periosteal and articular (red) surfaces with thresholding.

### Surface Classification with Region Growing

Since human fractures of course cannot be distinguished based on color (at least not from CT), native surfaces were also identified from geometric information. During high-energy impact loading, bone fractures as a brittle solid, and its fragment fracture surfaces tend to be relatively flat. Looking ahead toward surface classification in clinical cases, a method to separate surrogate fragment surfaces into discrete patches was developed using a region-growing algorithm that propagated patches up to boundaries of high curvature (Figure 15).

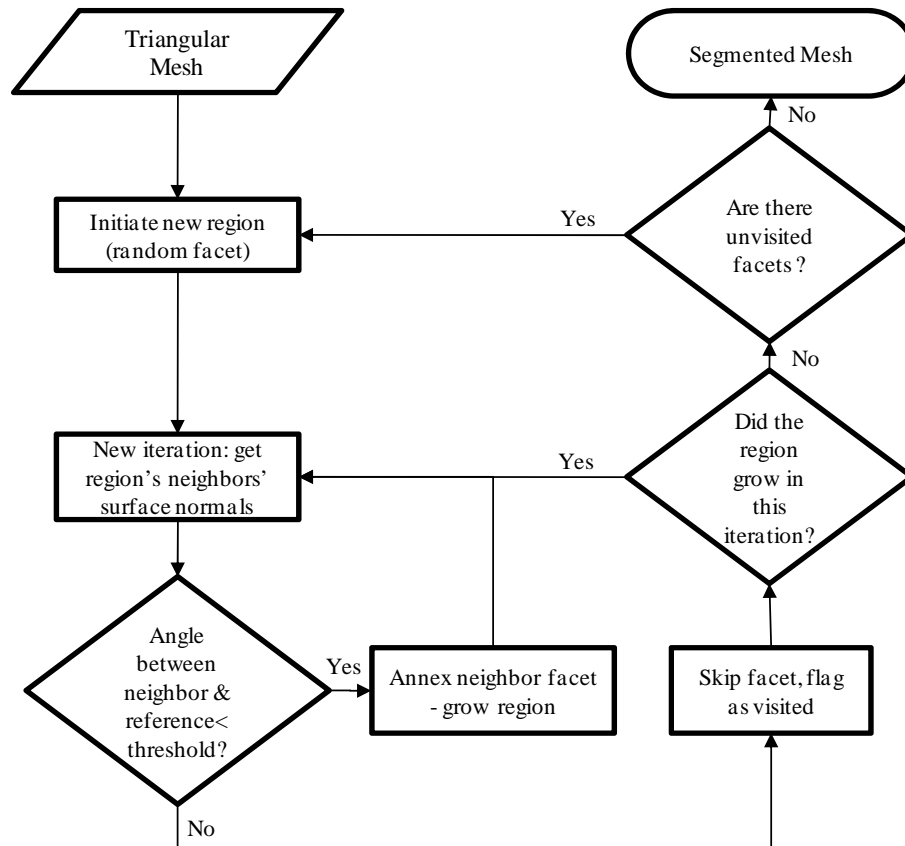


Figure 15 Fragment surface classification was performed with a region growing algorithm.

The algorithm started with the seeding of a random facet on the fragment's surface representation (triangular mesh), and then proceeded by analyzing how neighboring facets were oriented relative to the seeded facet. If a neighboring facet's surface normal direction deviated by less than a threshold angle from the seeded region, the facet was annexed. A facet whose normal deviated from the seeded region by greater than the threshold was classified as an edge, and not analyzed in future iterations. This algorithm continued until the grown region no longer had any neighboring facets that satisfied the surface normal criterion. A new region was then seeded on a randomly chosen as-yet-unvisited facet, and the process repeated. The required surface normal deviation threshold was determined empirically, and was found to consistently be approximately  $10^\circ$  (Figure 16).

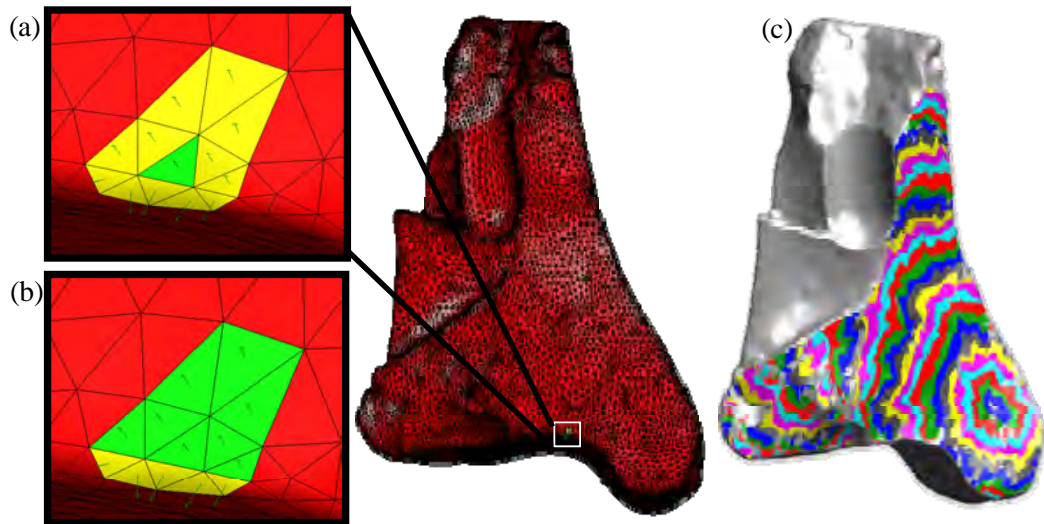


Figure 16 A random facet seeded the region growing algorithm (a). A patch's 1-ring neighbors (yellow facets) were annexed into the patch if their surface normal vectors deviated less than a defined threshold (b, green facet). Otherwise, facets were marked as visited and passed over (b, yellow). Patches iteratively propagated up to borders of high curvature (c).

Due to the tibia's shape and fracture behavior, each fragment had only one discrete native patch, and that patch had the largest surface area. To assess this algorithm's performance, the overlapping surface area between the gold standard (color identification) and the native surface as identified by the region growing algorithm were measured. With precise geometries and sharp fracture boundaries separating periosteal from fracture surfaces, this algorithm performed well with greater than 99% agreement.

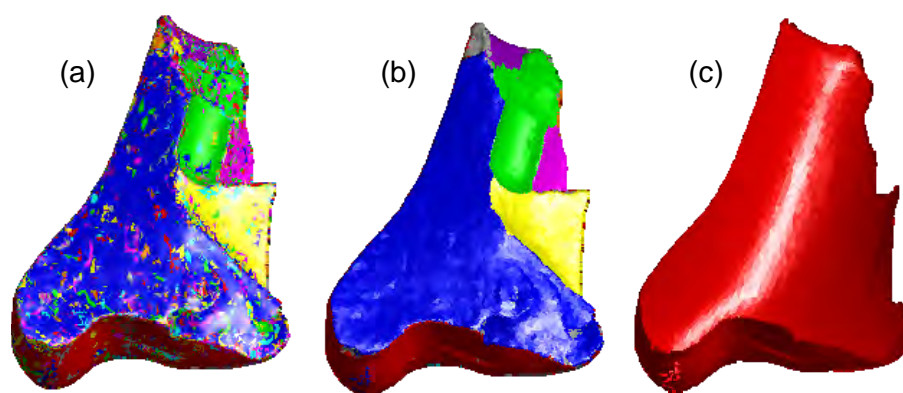


Figure 17 Surface classification results from the region growing algorithm are shown. After the surface normal analysis (a), the classification is refined (b), and the patch with the largest surface area was determined to be native surface (c).

### 3D Puzzle Solving Method

The tibia replicas were then methodically reconstructed by matching fragment and intact native surfaces using Geomagic Studio software's built-in iterative registration function (Geomagic, Inc., Research Triangle Park, NC U.S.A.). This function started by automatically bringing the fragments' surfaces into rough alignment with the template, by aligning their centers of mass and principal axes. However, some fragments lacked sufficient geometric variation for this step to execute automatically. This occurred when attempting to match diaphyseal fragments that had cylindrical or relatively flat shaped

native surfaces. In these instances, rough alignment had to be done manually with the user designating three pairs of surface points that were in nominal correspondence. After the automatic or manual rough alignment, fragments were sampled at a user-specified resolution, and the closest points computed on the intact template for each point sampled. Next, an iterative closest point (ICP) algorithm was executed: the sums of squares of distances between the sample pairs were minimized over all the rigid motions that could align the two objects [91]. Having done this, the program re-computed the closest points on the template and established the final spatial alignment transformation. Using this alignment function, the intact bone was reconstructed, starting with the fragment having the largest native surface area. The puzzle-solving algorithm proceeded by individually aligning the remaining fragments, moving in turn from largest to smallest. The accuracy and speed of alignment were improved by successively reducing the ICP algorithm's search area, by deleting regions of the template that had already been successfully matched to a fragment (Figure 18).

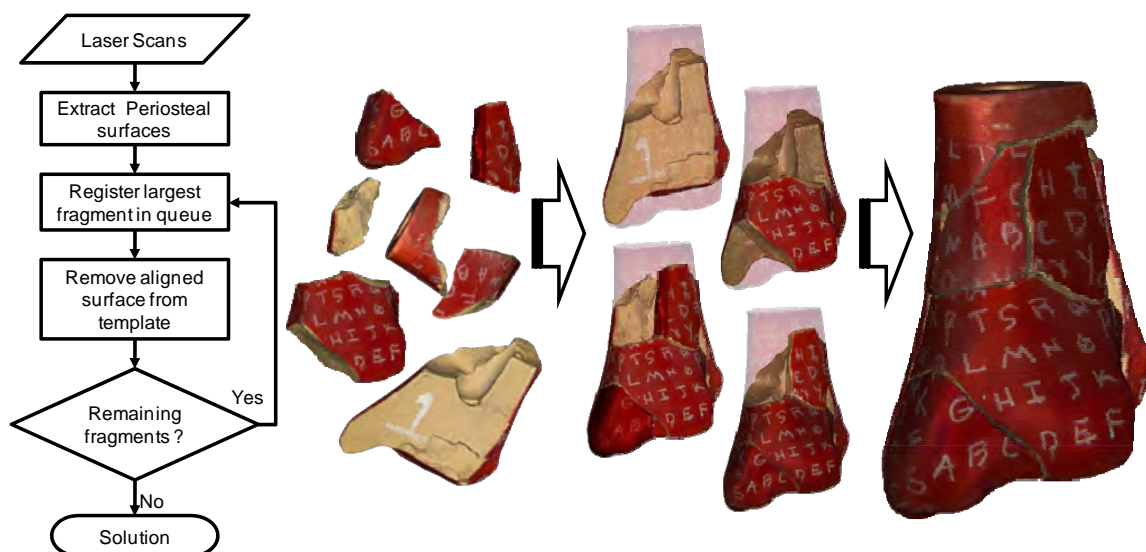


Figure 18 A surrogate fracture puzzle solution is shown. Anatomic geometry is restored using a semi-automatic virtual bone fragment reconstruction system.

Computational puzzle solutions were thus executed for each of five surrogate distal tibia replica fracture cases. The accuracies of the puzzle solutions were quantified by calculating the distances between the intact template and the fragments' native surfaces, and the distances between mating interior/fracture surfaces. The difference between the spatial volumes enclosed by the aligned bone surrogate fragments versus that of their intact (pre-fracture) specimens was used as an additional measure of surface reconstruction accuracy.

### *In vitro* Cadaver Testing

Once effective 3D puzzle solving methods were established for surrogate fractures, the next logical step in progression of complexity was to reconstruct cadaveric fractures. By introducing biologic variability and complexity, cadaver specimens were expected to challenge puzzle solving algorithms, while still affording the "ground truth" to be measured *in vitro*. It was thought that such specimens would be ideal for investigating the practicality of puzzle solving algorithms when fragment geometries are derived from clinical CT data. Whereas laser scanned surfaces provide high resolution surface information, the resolution of CT derived geometries are lower by a factor of 10 (0.05 vs. 0.5mm). Not only does resolution decrease, but the accuracy of the geometric representation largely depends upon the segmentation technique. In addition to imaging limitations, cadaver specimens introduce biologic variability such as heterogeneous structures (cancellous and cortical bone), and the greater potential to plastically deform during fracture. However, the algorithm's capacity for dealing with such difficulties can be better assessed since it is possible to laser scan and physically reconstruct cadaver fragments. For these reasons, cadaver fracture reconstruction was piloted for developing a more complex platform for algorithmic development. The methods developed in the surrogate model were subsequently used to reconstruct a fractured cadaver tibia to its pre-injury state using CT and laser scan data.

### Cadaver Specimen Preparation

A lower extremity was obtained from the deeded body program. Although the donor's age and sex were not available, an orthopaedic surgeon evaluated the specimen and its bone quality based upon visual and radiographic inspection. It was assessed to be similar to that of a healthy middle-aged man. The joint capsule and soft tissues of the ankle were preserved so that a more physiologic intra-articular fracture could be generated. The soft tissues were only dissected from the inferior side of the talus, and from the proximal shaft of the tibia, so that they could be potted in bone cement (PMMA). To improve fixation, two screws were placed in the distal tibia directed radially, and four into the talus directed longitudinally (Figure 19).



Figure 19 The process of preparing the cadaveric specimen is shown. With the joint capsule intact, the proximal shaft of the tibia and the inferior talar surface were potted in PMMA. A steel platen for impactation was attached to the talar side.

To better control the impact dynamics and to avoid plantar/dorsiflexion motion, a 3cm diameter stainless steel platen was attached to the talar PMMA block and positioned so that the drop tower's energy would be transmitted across the ankle's axis of rotation. The tibial PMMA block was firmly attached to the base of the drop tower. The specimen

was then impacted with a 7.5 kg steel mass dropped from a height of 1m (nominally 75 J impact) (Figure 20). Afterwards, CT scans of the fractured specimen were acquired with the same scanner used to obtain pre-fracture data. For the purposes of laser scanning, all soft tissues were dissected, and the bone fragments were air-dried for 48 hours. To improve surface recognition, fragments were dusted with magnaflux particles prior to scanning. Fragments were laser scanned using the NextEngine device.



Figure 20 A drop tower delivered 50-75J of kinetic energy to cadaver ankle joints in order to produce a clinically relevant tibial plafond fracture.

CT scans of the fractured and contralateral limb were segmented using a semi-automated 3D image analysis approach. The cadaveric tissue's CT appearance was slightly different than previously analyzed in vivo clinical cases. Although the joint capsule remained intact, the proximal end of the distal tibia was exposed. During specimen preparation, this free end allowed fluids and marrow to drain. Fluid loss from the soft tissues caused muscle, tendon and adipose tissues to have an increased CT intensity (+100HU). Having similar intensities, some soft tissues were indistinguishable from less dense regions of cancellous bone (Figure 21a, b). Also, marrow drainage from

the intramedullary canal and trabecular network caused an influx of air, causing the inner regions of cancellous bone to display increased intensity gradients. The trabecular structures ( $>300$  HU) were surrounded by pockets of air ( $-1000$  HU). These artifacts complicated the process of segmenting bone with intensity based segmentation techniques.

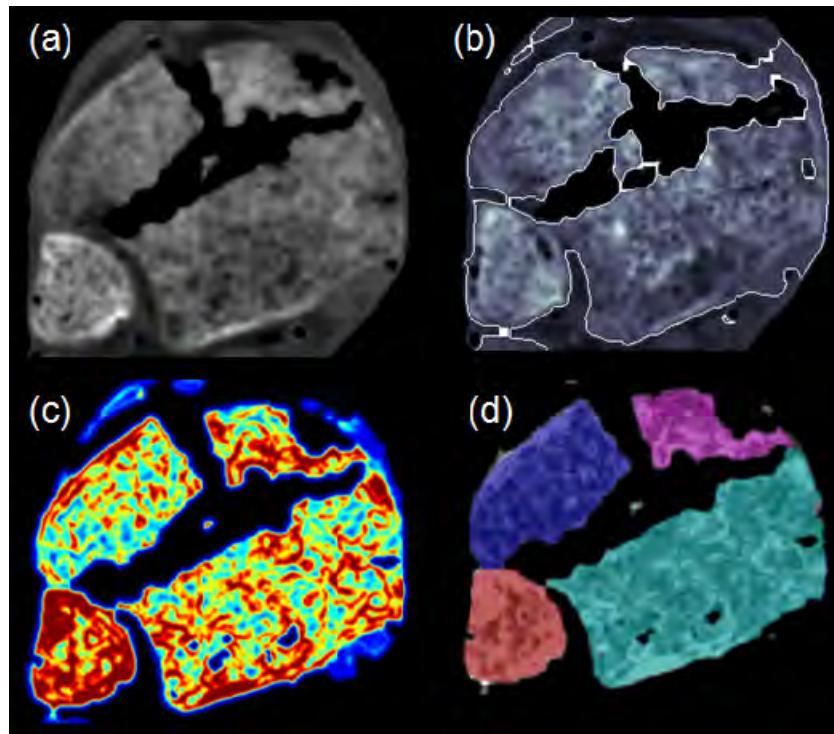


Figure 21 Since the cadaveric CT (a) could not be reliably segmented from intensity information (b), image texture (c) was analyzed to yield discrete fragment segmentations (d).

A 2D texture based approach was used to exploit these non-physiologic gradients and to allow for bony structures to be discernable. This analysis was done using a MATLAB program that filtered the original image volume with a local standard deviation filter. Each output pixel in the feature image (the image to be segmented)

contained the local standard deviation of the 5x5 pixel neighborhood around that location in the original CT data (Figure 21c). The resulting feature image had a high signal response in those problematic cancellous areas, while soft tissues had a relatively lower response because of their more homogeneous structure. Next, the soft tissues and other background pixels in the feature image were set to 0 by a user defined standard deviation threshold. Finally, the resulting feature image was imported into ITK-snap and semi-automatic bone segmentation with active contour methods were performed (Figure 21d) [92]. After discrete fracture fragments were segmented, triangular meshes were exported for puzzle solving. An intact template was created by segmenting the prepared specimen's (pre-fracture) CT scan with the same technique as was used for the fractured bone.

The fractured cadaver tibia was reassembled using the methodology developed in the surrogate platform. The fractured bone's base fragment (i.e., the proximal segment of bone, which remained intact) was first identified, and the dispersed collection of bone fragments was then queued for reconstruction. The base fragment model was aligned to a proximal subset of the reconstruction template. Fragments were subsequently aligned to the pre-fractured geometry in order from largest to smallest. The cadaveric tibia impact yielded a similar fracture configuration as was observed in the surrogate test specimens, albeit with some additional depression at the articular surface (Figure 22). A similar degree of reconstruction accuracy was obtained over the majority of the surface, with higher inaccuracies (on the order of 1 to 2 mm) at the edges of a few fragments.

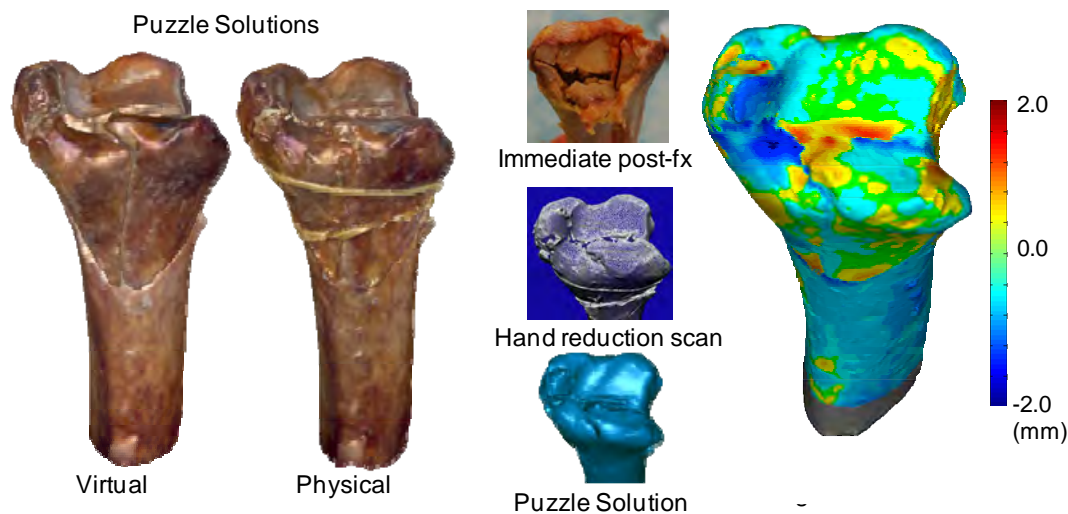


Figure 22 Virtual and physical reconstruction results for the cadaveric tibia are shown.

After the cadaveric fragments were manually reassembled, the construct was laser scanned to produce a reference for virtual comparison. The similar results between virtual and physical puzzle solutions suggest that aligning native surfaces restored this specimen's original anatomy. However, the limitations encountered during this experiment discouraged further cadaveric work. In order to produce clinically relevant fractures, it is essential to obtain specimens with good bone quality. Unfortunately, the specimens that are most often available have questionable bone quality due to age-related degeneration, and therefore have fracture behavior that is more likely to crush rather than fracture as a brittle solid. Consequently, the drop tower method proved unsuitable for fracturing a specimen with results similar to a severely comminuted clinical case. Although it is desirable to simulate the *in vivo* environment while being able to perform *in vitro* assessments, doing so involved introducing new complexities that counterbalanced any benefit. Rather than pursuing technologies that would only be relevant to cadaveric analyses, efforts were directed toward developing algorithms for immediate clinical application. Although limitations were encountered, the results from

the cadaveric experiment supported the *in vivo* efficacy of the native surface alignment methodology.

### Development and Application to Clinical Cases

Matching native fragment bone surfaces to an intact template proved to be an effective and computationally tractable reconstruction methodology with *in vitro* application both to surrogate models, and to a cadaveric fracture. Similar to the complexities encountered during the cadaver study, limitations in CT resolution and weak fracture edge signal complicate clinical segmentation, and combined with the bone's susceptibility to plastic deformation (i.e., crush) contribute to making the 3D puzzle more difficult to solve. These factors invariably introduce alignment errors, since segmented fragment native surfaces may not precisely share the same shape as the template. Substantial technical advancements were needed in order to make the algorithms more robust to variance. The first objective in advancing 3D puzzle solving methods for clinical application was to improve the image segmentation techniques. It was deemed critical that bone fragment geometries be extracted from CT with minimal user guidance, and in a practical amount of time. Only with capable automatable CT segmentation methods can puzzle solving ever become a clinically relevant tool.

### Patient Management

Ten tibial plafond fractures were retrospectively studied (Table 1). The fractures ranged in severity from moderate to severe, with AO/OTA classifications ranging from B1 to C3. Acute clinical management had involved the application of an external fixator to provisionally stabilize the fracture and to restore limb length. Prior to any further treatment, CT scans had been acquired of the fractured limb, and of the uninjured contralateral limb. Definitive surgical fracture reconstruction was delayed from one to two weeks until swelling had subsided, at which time the soft tissues were more tolerant

to surgery. Surgical fracture reduction had been performed using a limited approach, under fluoroscopic guidance. Bone fragments had then been stabilized with screw fixation, and a post-operative CT scan had been obtained to assess reduction quality. The prevalence of joint degeneration was graded from standing radiographs obtained at one and two year follow-ups, using the Kellgren-Lawrence (KL) scale [93]. Patient number 7 did not return for follow-up after definitive surgery.

Table 1 Ten tibial plafond fracture patients were retrospectively analyzed in this study.

| Patient ID | Sex | Age | Classification | Mode of Injury | KL Grade |
|------------|-----|-----|----------------|----------------|----------|
| 1          | M   | 21  | B13            | fall (30 ft)   | 4        |
| 2          | M   | 34  | C11            | fall (18 ft)   | 4        |
| 3          | M   | 24  | C23            | fall (12ft)    | 3        |
| 4          | F   | 36  | C11            | MVA (20mph)    | 0        |
| 5          | M   | 20  | C13            | ATV            | 0        |
| 6          | M   | 41  | B21            | fall (20 ft)   | 2        |
| 7          | M   | 21  | B22            | MVA            | N/A      |
| 8          | M   | 29  | B12            | ATV            | 0        |
| 9          | F   | 38  | C32            | MVA (50mph)    | 2        |
| 10         | F   | 48  | C11            | fall (1.5 ft)  | 1        |

### CT Segmentation

Before new virtual reconstruction algorithms could be advanced, novel image segmentation techniques needed to be developed to provide accurate geometric models of the bony anatomy from *in vivo* CT scan data. Bone fragment boundaries are especially difficult to demarcate when fragments are abutting other fragments. In addition, the intensities of the osseous structures may overlap with some of the surrounding soft tissues, making them difficult to distinguish (Figure 23).

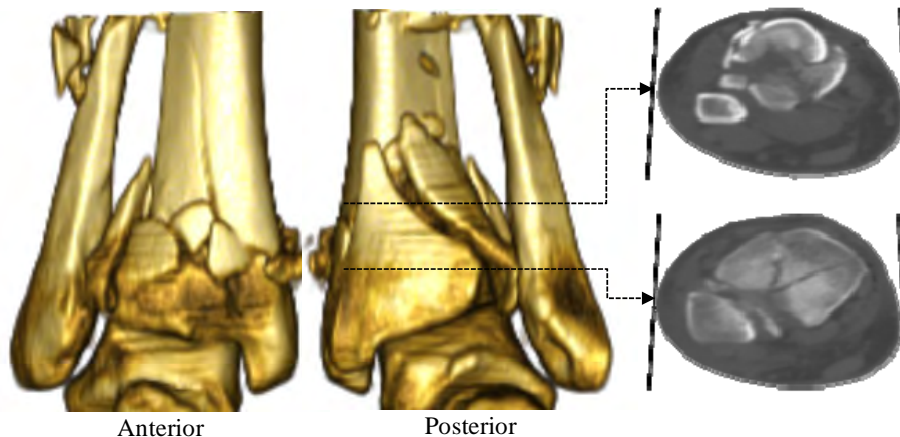


Figure 23 Illustrative CT data for a comminuted tibial plafond fracture.

A largely automated image segmentation methodology was developed to extract bone surface geometries from pre- and post-surgical reduction CT scans (Figure 24). The image segmentation algorithm used a 3D watershed transform [94], implemented in the MATLAB image processing toolbox (MathWorks, Inc; Natick, MA, USA). With a watershed analysis, image data can be conceptualized in 2D as a topographical map, where basins are separated by ridge lines (Figure 25). A common limitation to watershed analyses is over-segmentation, i.e. separating of an object into too many parts. In musculoskeletal CTs, variable bone density causes small local variations in the image data. These regional differences can be erroneously treated as separate basins and ultimately discrete objects.

A novel approach was used to pre-process and manipulate the image data in a series of logical steps so that ridgelines did not intersect objects of interest, i.e. bone fragments. Generally, the image data were manipulated by imposing regional minima in fragment regions, analogous to carving a single basin for each fragment. This approach ensured that individual objects would not be connected. A watershed algorithm was then applied to first flood those regions/seeds, and expand their boundaries up to the edges of other fragments or other non-osseous tissues

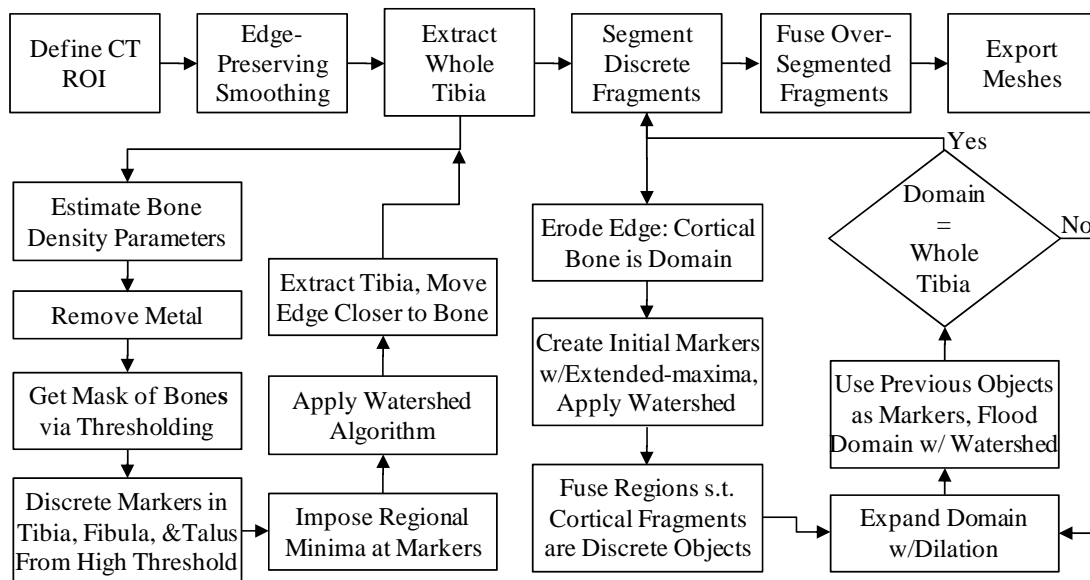


Figure 24 A flowchart of the image analysis technique for extracting bone fragment geometries from clinical CT data.

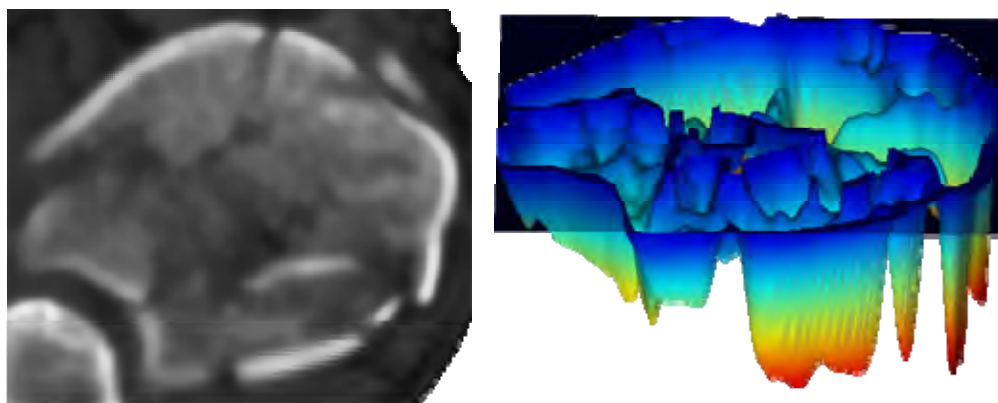


Figure 25 In a watershed segmentation, the intensity of a CT slice (left) can be conceptualized topographically in 2D (right) where fragments correspond to basins, and ridgelines to fragment boundaries.

The novelty of this watershed implementation was in the method and sequence for defining the appropriate seeds needed to yield accurate fragment models. In the first phase of this segmentation algorithm, the fibula and talus were removed from the image

dataset (Figure 26). Separate seeds were placed in the tibia, talus and fibula using simple intensity thresholding. The threshold level was set as the minimum intensity that would reliably separate the tibial and talar subchondral surfaces (typically  $>500\text{HU}$ ). After imposing minima upon the seeds, the watershed algorithm was applied. This successfully segmented the tibia, fibula and talus into multiple objects. The tibia was automatically extracted with *a priori* knowledge of what structures are found in the most distal and proximal slices. A label array was created from the watershed's output. All objects connected to a plane containing the most distal CT slice were identified as talar/foot bones. The largest 2D object in the most proximal plane was deemed to correspond to the tibia, while all other labels in that plane were fibular. The fibula was removed and all remaining objects were identified as tibial and fused together. The entire distal tibia was then extracted for further analysis.

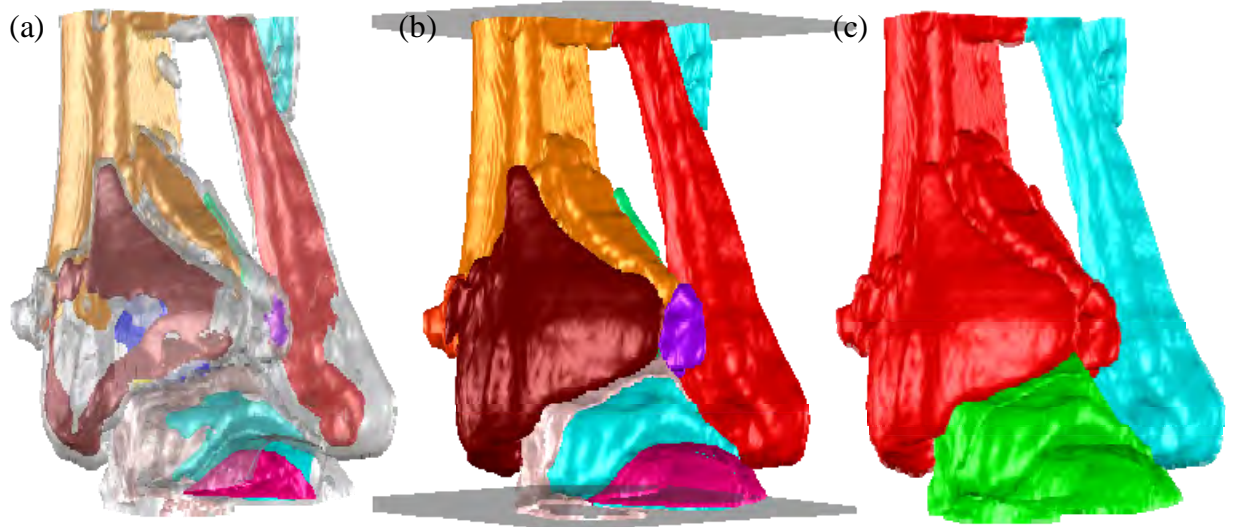


Figure 26 Very dense volumes within the gross bony structure are identified from thresholding (a) and used as markers for a subsequent watershed implementation (b). All objects connected to the most distal plane (talus), and the second smallest object connected to the proximal plane (fibula) were removed from the volume for tibial analysis.

Next, the tibia was further segmented so that each fragment would be a single object. Since there was little variation in intensity in the regions between many fragments, simply thresholding the image was not an effective approach. To solve this problem, it was necessary to identify an isolated region within each fragment that could seed a second watershed operation. It was observed that the vast majority of bone fragments contained one continuous piece of non-cancellous (subchondral or cortical) bone. Since these relatively dense pieces of bone were not connected, they provided ideal regions for seeding the watershed algorithm. Using an intensity threshold (typically  $>500$  HU), a mask of all cortical bone was created (Figure 27 a).

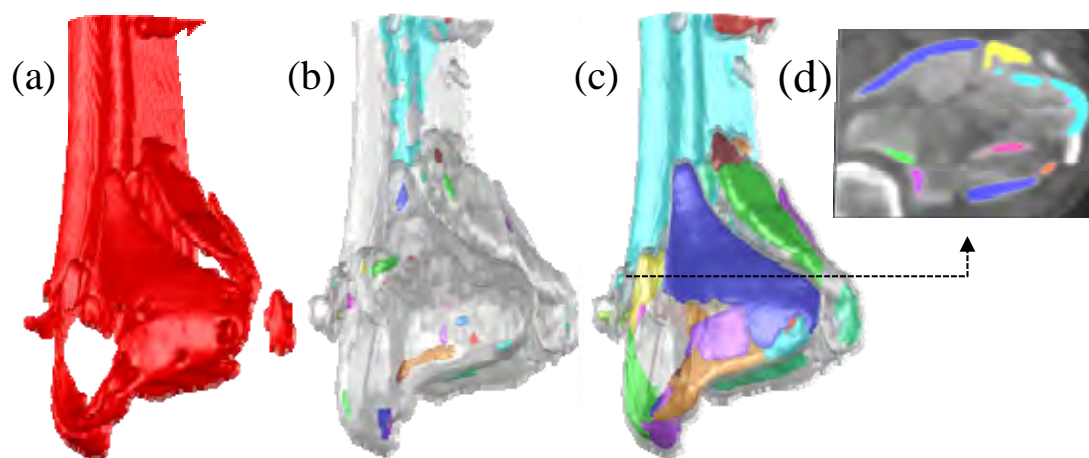


Figure 27 The cortical mask (a) was analyzed and new markers were identified from an extended maximum transform (b). After imposing minimum at those sites, a watershed operation propagated boundaries up to cortical edges (c, d).

Although some cortical fragments were still connected in the resultant mask, they were separated by groups of voxels with intensities lower than the fragments' inner regions. If a larger threshold were initially chosen such that all cortical fragments were separated, significant portions of cortical tissue would be invariably lost. An extended

maxima operator was used to then generate discrete seeds within the cortical masks. This operator identifies groups of voxels that have intensities that are greater than their immediate surrounding by a specified threshold (Figure 27b). For these data, an extended maxima threshold of 80HU (i.e., regions with intensities within 80HU) reliably placed at least one seed in each fragment, and the watershed algorithm then flooded the remaining cortical mask (Figure 27c).

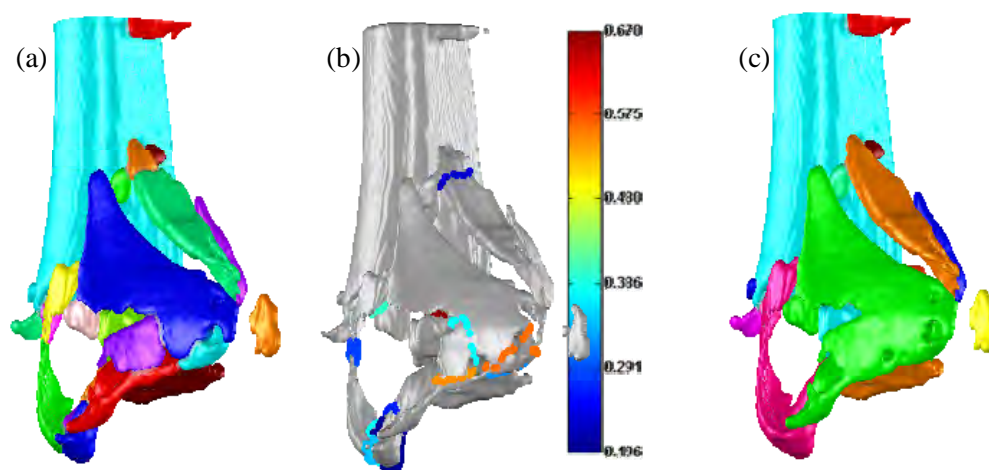


Figure 28 Over-segmented fragments (a) are analyzed (b) and automatically fused (c).

In order to identify and correct overly-segmented cortical fragments (Figure 28 a), an automatic detection and fusion algorithm was developed. Typically, the surface of an over-segmented fragment is flat/convex along erroneous boundaries, whereas boundaries separating distinct fragments lie along concavities. Convex hulls were fit to sub-volumes along inter-fragmentary boundaries in order to distinguish between these two geometric features. First, the voxels that intersected two fragments and the tibial surface were flagged for analysis (Figure 28 b). Next, convex hulls were fit to 2.5x2.5x2.5 mm sub-volumes about those flagged voxels on the tibia's binary mask surface (Figure 29). The

difference in volume between the convex hull and the tibia mask was measured, and used as criterion for determining whether the boundary dissected a single object. If two objects that shared a border had an average volumetric difference  $<0.4\text{mm}^3$ , they were fused (Figure 28 c), if not, the two objects remained separate. Lastly, those cortical objects were used as seeds for a final watershed operation to recover the whole tibia volume (cortical and cancellous). From the segmented volume (Figure 30 b), meshes of the bone fragments were created with uniform triangle sizes of  $0.1\text{mm}^2$  (Figure 30 c).

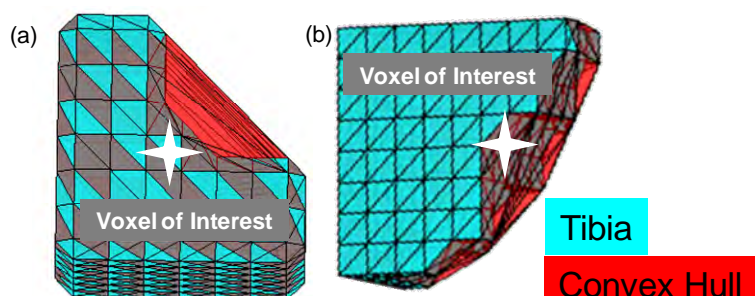


Figure 29 Convex hulls are fit to a  $2.5 \times 2.5 \times 2.5$  sub volume of the tibia's mask, centered at a voxel that intersects two or more fragments and the outer tibial surface. The difference in volume between the convex hull and sub volume was quantified. Concave locations (a) had volumes  $> 0.75\text{mm}^3$ , convex locations were  $< 0.3\text{mm}^3$

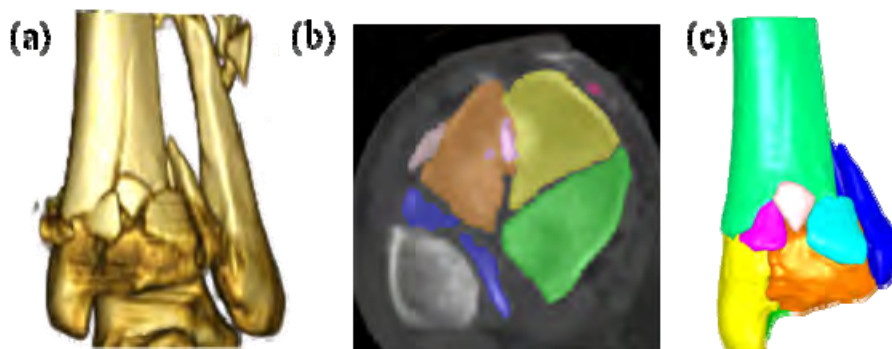


Figure 30 Clinical CT data of a comminuted tibial plafond fracture are shown (a). Novel image segmentation techniques were developed for generating discrete fragment models that could be spatially manipulated and reduced (b, c).

### CT Derived Fragment Geometry Validation

In order for puzzle solving to be clinically relevant, it is critical that accurate fragment geometries are derived. It would be ideal to assess the watershed segmentation approach in a cadaver study, where precise fragment geometries could be obtained from laser scanning. However, limitations encountered during pilot *in vitro* fracture experiments (see above) discouraged the pursuit of cadaveric work. Cadaveric specimens are most often aged, and do not have the same fracture behavior as the bones involved in most clinical fracture cases. Therefore, to support the accuracy of the watershed approach, segmentations were assessed against geometries generated from manual methods.

A trained user segmented each case's largest articular fragment with an interactive Cintiq® display tablet (Wacom Co, Toyonodai, Kazo-shi, Saitama, Japan). Assessment of accuracy was performed by comparing the segmentation results for the fragment as a whole, and the periosteal, articular, and fracture surfaces, individually (Figure 31). While comparison of all fragments in a fracture case would provide the most robust analysis, the added benefit was deemed to not be worth the additional effort required. In addition to the substantial labor investment that would be needed for that analysis, the largest articular fragment contains all relevant bone types (cancellous, cortical and subchondral) and fracture surfaces. Therefore, if there were discrepancies, they would most likely appear in an articular fragment. Furthermore, the accuracy of articular segmentation is paramount since precise joint reduction is the primary surgical objective.

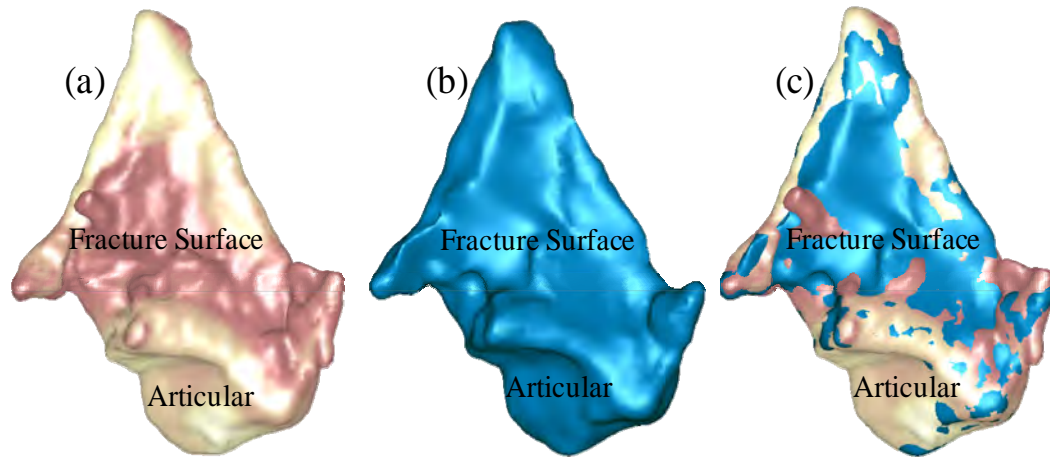


Figure 31 Example fragment comparing the watershed segmented fragment (a), to the manually segmented fragment (b). Accuracy was assessed by the distance deviation between the two registered fragments (c).

### Fragment Mesh Segmentation and Classification

Fragment and intact native surfaces provide the primary input for the 3D puzzle solving approach. *De novo* fracture edges were removed from fragment meshes using the region-growing algorithm described above. *In vivo* fracture surfaces tended to have significant surface variations, causing the algorithm to separate them into many smaller surface patches. By contrast, the native surface (periosteal and articular) identification was smooth, resulting in a single contiguous set of patches. Similar to the surrogate analysis, the set of patches with the largest surface area was therefore reliably identified as native.

Having knowledge about the fragment's anatomic classification allows one to develop more intelligent reconstruction algorithms. For example, an algorithm that prioritizes joint congruity would need to have the articular surface identified. Also, knowing that a surface patch corresponds to the diaphysis, metaphysis or subchondral plate (articular) provides useful information for coarsely aligning fragments and for improving overall algorithmic performance. The distal tibia's variable tissue

composition and radiographic appearance were exploited to develop classification methods suitable for this purpose. Different regions of a bone have a density that characteristically varies from the outer surface to the interior. Similar to other long bones, the proximal portion of the distal tibia, the diaphysis, is made up of solid dense cortical bone ( $>1000\text{HU}$ ). The distal diaphysis transitions into the metaphysis, the widest section of bone with less dense and porous cancellous bone encased in a thin cortical shell (cortex). The epiphysis is at the end of the long bone with articular cartilage at the joint surface, below that is relatively dense subchondral bone (Figure 32).

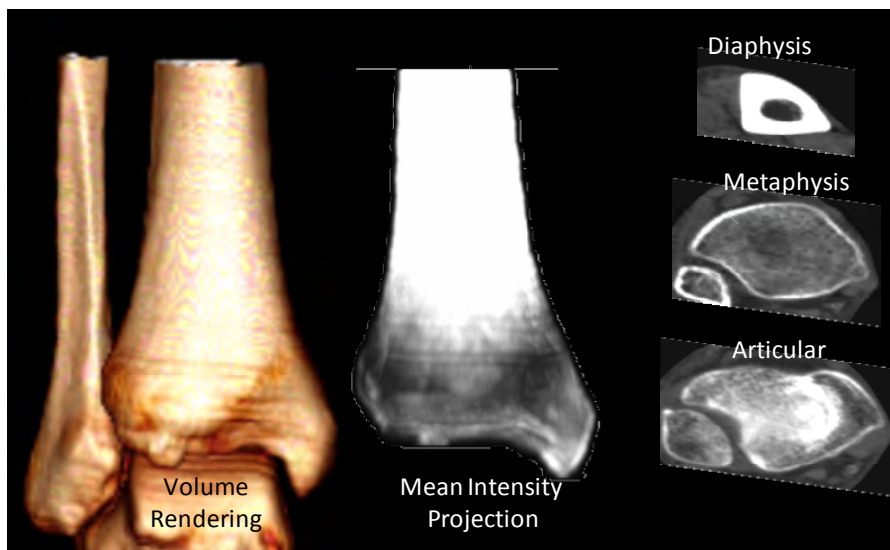


Figure 32 CT appearance of the distal tibia anatomy. Relative to the tibia's outer surface, the CT intensities vary with characteristic profiles along the inward surface normals for each anatomic region (diaphysis, metaphysis and articular).

These characteristics were used to computationally classify anatomy by modeling how CT intensities change over a distance along an inward-directed surface normal. The classification process started with a training phase where the user selected patches on the intact tibia's mesh that corresponded to the diaphysis, metadiaphysis, metaphysis and

subchondral plate. Density profiles were collected at each facet on the triangular mesh by measuring the HU intensity at 1mm increments from the surface. Analysis of the training data corroborated the observation that different bone types had distinctive density profiles. Cortical bone in the diaphysis had the profile with the largest intensity peak about 1-2 mm from its segmented boundary. For the metaphysis, the curve also peaked after 1-2 mm with approximately 25% of the peak diaphyseal intensity. Once sampling passed through the cortical shell, the profile leveled off to the average cancellous intensity. With its subchondral density being greater than the cortical shell, but less than the compact bone of the diaphysis, the articular surface had a profile intermediate to the middle of the diaphyseal and metaphyseal profiles.

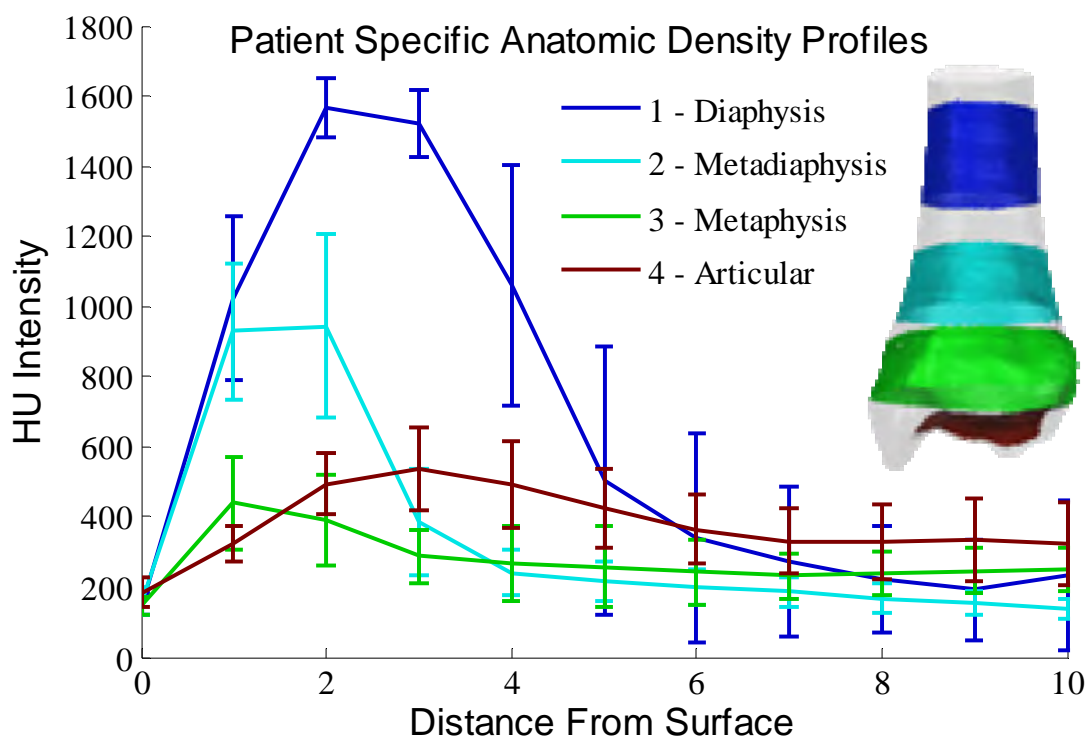


Figure 33 Different bone structures of the distal tibia display characteristic CT intensity profiles.

Gaussian mixture models were generated from the set of profiles for each anatomic type. It would be ideal for training to be automatic and not require the user to identify anatomy on the intact tibia. Therefore, in addition to patient-specific models, a single set of population-based models were also generated. First, density profiles for each patient were normalized to the maximum HU observed in their CT dataset. Normalized profiles were compiled from all ten patients for each tissue type, and a set of population based models were generated. Training error was measured by reclassifying the labeled intact patches and calculating the percentage of facets whose labels were incorrect. The patient-specific Gaussian mixture models fit well to the training data, with errors of only; diaphysis= 2.34%, metadiaphysis= 6.21%, metaphysis= 7.89% and articular= 16.14%. The compiled data fit the models with greater error; diaphysis= 10.2%, metadiaphysis= 20.9%, metaphysis= 27.0% and articular= 38.8%.

Next, density profiles for fracture fragment native surfaces were collected at each facet, and the facet's probability for belonging to each model from the patient-specific, and compiled sets, was calculated (Figure 34). Facets that did not fit to a model with more than 90% probability were classified as unknown. Since each surface patch (from region growing separation) is either all periosteal or articular, the whole patch was labeled according to maximum occurrence (i.e. area). If more than half of the patch's area was unknown, it remained without label. In order to assess the intensity profile algorithm's accuracy, results were compared to manual patch classifications made by an experienced user. The percent of surface area that was correctly classified with certainty (>90%) by the algorithm was calculated.

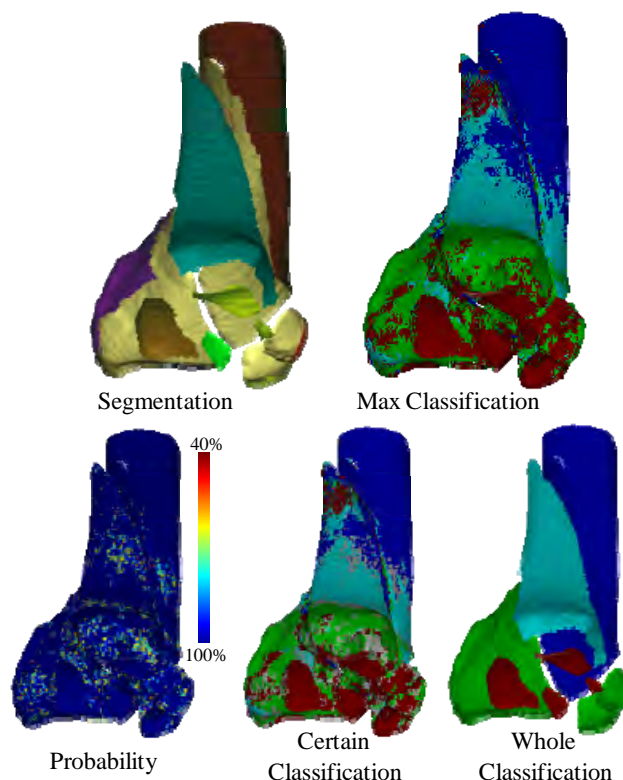


Figure 34 For assessment, a trained user manually segmented the tibia by anatomy. Tibia's mesh was classified by maximum probability. Then surface patches (groups of facets) received the one label that was most frequently detected. Computer and human classification results were in excellent agreement.

### Fragment Position Initialization

Iterative closest point (ICP) algorithms have been shown to effectively align bone fragments in previous surrogate and cadaveric work, but ICP performance depends greatly upon fragments' initial displaced positions. The computational speed and probability for an accurate solution was inversely proportional to the magnitude of fragment displacement. Leveraging the results from the surface classification, and from *a priori* knowledge about typical fracture morphology, a series of algorithms were therefore developed that positioned each fragment closer to their anatomic target in order to improve alignment speed and stability.

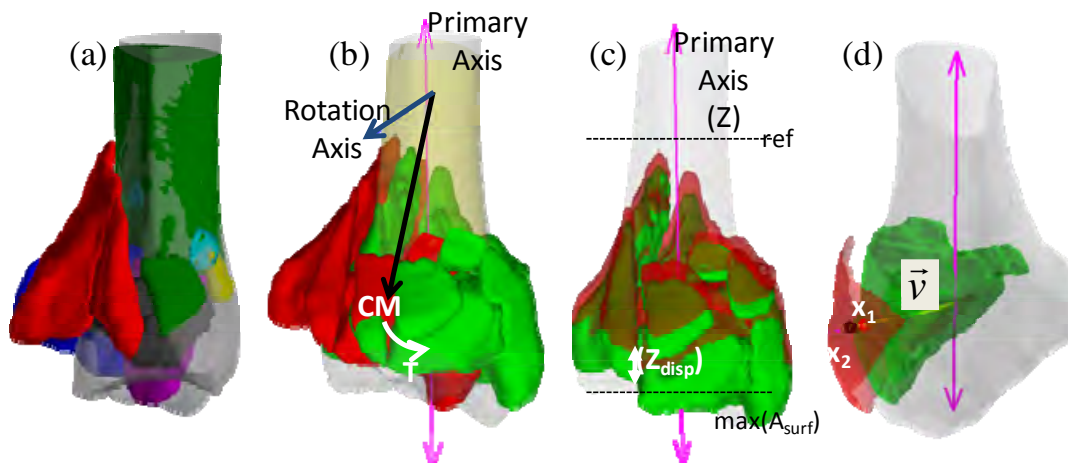


Figure 35 Displaced fragments (a) are grossly reduced with a series of algorithms that computationally mimic the surgeon's intra-operative actions. First, axial alignment is restored by shifting the constellation of fragments toward the template's primary axis (b). Next, limb length is restored by longitudinally translating fragments such that articular patches are at the same level as the template's (c). In the final step in gross reduction, fragments are translated and rotated radially such that the overlap between periosteal patches and the template is maximized.

Fragment position initializations started with registering the diaphysis of the intact template to the fractured tibia's most proximal segment (Figure 35 a). Next, gross axial alignment was restored by shifting the constellation of fragments toward the template's longitudinal axis. To do so, principal component analysis was used to identify the primary axis of the intact template. A vector that connected a proximal point on the intact template to the center of maximum of the constellation of fragments was found. Fragments were rotated about the cross product of the primary axis and the center of mass vector until they aligned (Figure 35 b). Fragments were then rotated such that their average articular surface normal aligned to the template's average articular surface normal. Then, limb length was restored by translating fragments along the longitudinal axis until fragment and template articular surfaces were at the same level (Figure 35 c). That process began by measuring the maximum longitudinal displacement between the

fragments' and template's articular patches ( $Z_{\text{disp}}$ ). Articular fragments were independently translated along the longitudinal axis such that they were at the same level as the intact template's articular surface.

All non-articular fragments were subsequently translated by a magnitude that was determined by their location relative to the articular fragments (AF), and according to their position along the longitudinal axis (between ref and max). This approach ensured that the most displaced fragments, i.e. articular fragments, were matched to the template, while non-articular fragments were distributed along the axis in evenly. Then, vectors ( $v$ ) from the primary axis were projected outward in the transverse plane through each fragment's center of mass, passing through the template at ( $x_1$ ) and the fragments periosteal surface at ( $x_2$ ). Fragments were then translated radially along that vector by the distance ( $x_2 - x_1$ ) and rotated such that the fragment's periosteal surface normal aligned to the surface normal of the overlapping template region. A moderate improvement in Geomagic's ICP performance was detected. For instance, a large articular fragment's alignment duration decreased from 10 seconds to 7 after initialization (Figure 36 c, d).

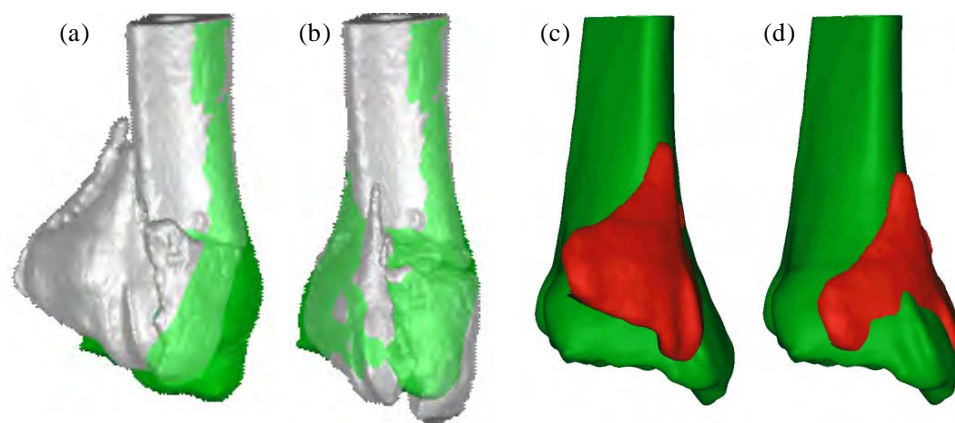


Figure 36 Displaced (a) and initialized (b) fragments are shown for an illustrative case. Alignment processing time was reduced. For an example fragment, the ICP computational time was reduced from 10s in its original position (c), to 7s after initialization.

## Finalizing Fracture Reduction

Lastly, ICP was implemented to make precise final alignment adjustments. In the order from largest to smallest native surface, ICP was used to implement rigid affine rotations and translations of each fragment, such that the cumulative distance between fragment-template surfaces was minimized (Figure 37 f). The accuracy and speed of alignment was improved by iteratively reducing the ICP search space as each new template/fragment match was achieved.

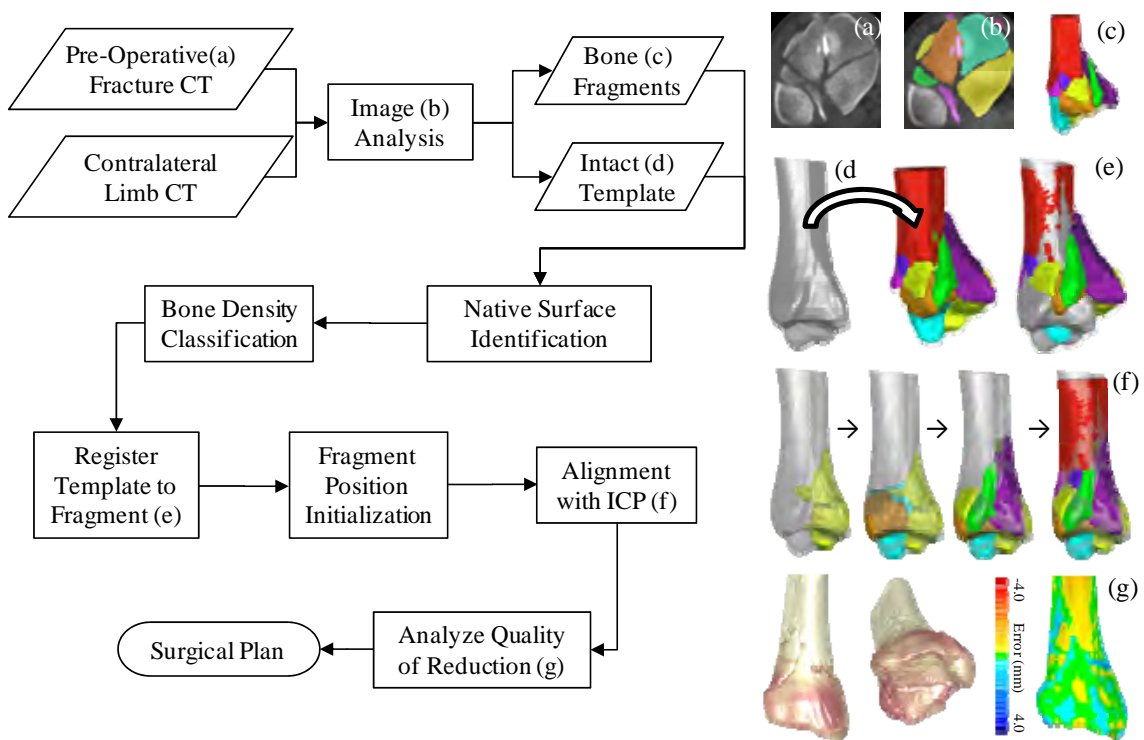


Figure 37 A flowchart of the puzzle solving process. Intact template and fragment geometries are generated by analyzing pre-operative CT data. Native surfaces (periosteal and subchondral) are then segmented and classified from geometric and bone density information. The fracture is then reduced by first registering the template to the fracture's base fragment, then grossly positioning fragments in a series of initialization steps, and finally precisely aligning fragment-template surfaces with an iterative closest point (ICP) algorithm.

### Accuracy Assessment

Puzzle solution accuracies were quantified by calculating distances between the intact template and the reduced tibia's native surface (Figure 37 g). Since the articular surface is the most clinically important to precisely reduce, it was isolated from the periosteal surface and compared to the intact anatomy. To illustrate the clinical utility of 3D puzzle solving, virtual reconstructions were also compared to the physical reconstructions achieved surgically, based upon segmentations of post-operative CT scan data (Figure 38).

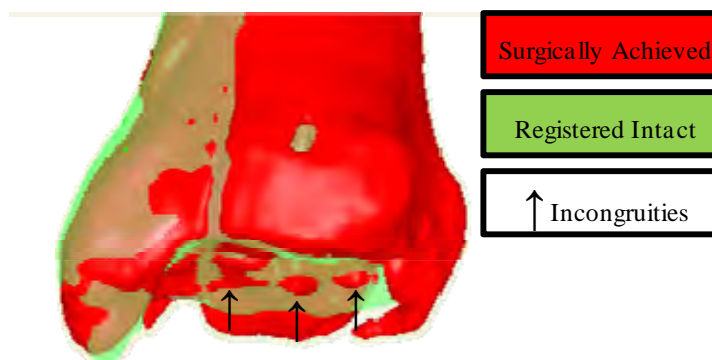


Figure 38 Residual incongruities (Case ID 2) were visible after the intact template was registered to the surgically reconstructed plafond. Quality of reduction was quantified by measuring the distance deviation between the physically reconstructed articular surface and the template. The average articular deviation for this case was 1.1mm.

### CT-Based Fracture Severity Assessment

The obtaining of the 3D puzzle solution enables additional capabilities, including the ability to improve fracture severity assessment. In previous work, CT-based techniques to objectively quantify fracture energy and articular comminution were developed and implemented in a series of twenty tibial plafond fractures. The results from that study showed that the objective metrics were highly predictive of degeneration

and were in strong agreement with expert subjective opinion. However, there were some compromises made in that prior work. Ideally, the energy release rate along fragment edges would be scaled pixel-by-pixel according to the immediate density inferred from the CT image intensity. Unfortunately, partial volume effects and high intensity gradients at the bone edges prevented a reliable pixel-based scaling (Figure 39, arrow). Now with puzzle solution, the *de novo* surfaces could be aligned to their original anatomic location in the intact CT volume, where without partial volume effects, accurate pixel-by-pixel energy release rates could be derived (Figure 39, right).

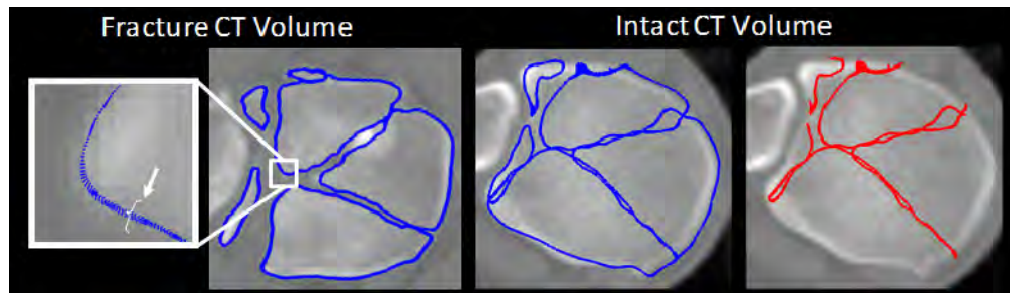


Figure 39 Fracture surface CT intensities queried from the intact CT volume provide for reliable measured and subsequently improved fracture energy analyses.

Starting anew, fracture energy was quantified in the series of ten virtually reconstructed clinical cases. The amount of mechanical energy absorbed by the bone during fracture was quantified using linear elastic fracture mechanics. Fracture energy calculated with previously reported methods [95] were compared to new measures derived after puzzle solving. The puzzle solving fracture energy analysis scaled *de novo* area by facet-specific energy release rates. After puzzle solutions were obtained, fracture surface meshes extracted with the region growing algorithm were transformed and registered to the intact CT volume. As prescribed by fracture mechanics, the facet surface areas were divided in half (since crack propagation created two new surfaces). Next, the

specific bone density ( $\rho_a$ ) that each facet intersected was calculated from CT image intensity using a power equation, ( $HU = 10^{2.87} \rho_a^{1.45}$ ) [28]. Then, facet-specific energy releases rates were calculated by multiplying those densities by the ratio  $12 \text{ kJm}^{-2}$  per  $1.98 \text{ gm}^{-3}$  [96]. Finally, fracture energy was calculated by summing the products of fracture facet surface area and respective energy release rates over all fracture surfaces.

Articular comminution may itself be indicative of the propensity for PTOA. Previously, it was assessed by measuring the amount of interfragmentary surface area involved at the articular level. Specifically, the location of the articular roof was identified, and the *de novo* area within a 1.5mm window was measured and normalized to the intact surface area. This measure loosely reflected the degree of articular comminution, but when articular fragments were longitudinally displaced, the comminution of interest could be shifted outside the measurement window. The algorithms developed for puzzle solving made it possible for the limitations of previous methods to be addressed. Using the fragment surface classification algorithms, articular fractures edges became now explicitly identifiable. A new articular injury metric was formulated by measuring the total arc length of articular fracture lines, normalized to the intact plafond (Figure 40).

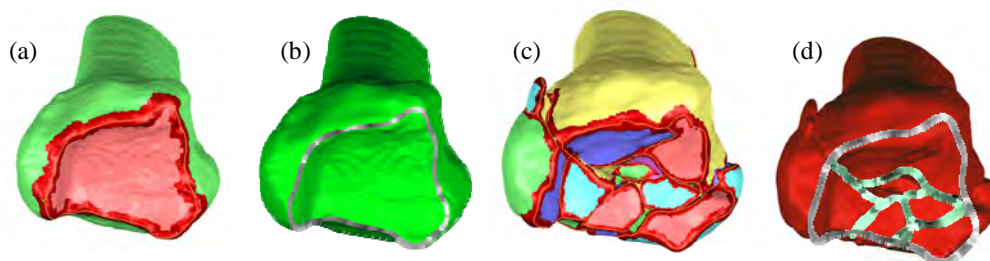


Figure 40 High curvature areas were identified on the intact template (a) and the fractured bone (c). The ridgeline along the malleoli (b, silver curve), and the fracture surfaces (d, green curve) were extracted. Articular insult was quantified by the fracture curve's length, normalized to the intact's.

The agreement between previous and new fracture severity measures was assessed using concordance. This approach enables the comparison of two different metrics whose methodologies and variables are different (i.e. ordinal ranking vs. continuous metric). Concordance assessment first requires an ordering of all values from lowest to highest, followed by comparisons between pairings of values. The concordance rate is defined as the ratio of concordant pairs to the total number of possible pairings, ranging from 0.5 (chance), to 1 (perfect agreement). The resultant sample probability estimates the likelihood that any two data points are a concordant pair, i.e. that they will be ranked in the same order by both metrics.

In addition to inter-metric comparison, the capability for the new fracture energy and articular comminution metrics to predict joint degeneration was examined from the severity of PTOA, as indexed by the patients' two-year follow-up KL scores. Even though it is difficult to make statistically based conclusions given the small number of sample points, these data will help elucidate general trends relating fracture severity to PTOA and possibly guide future research directions.

#### Quantifying the Clinical Utility of 3D Puzzle Solving

Limited approaches minimize the likelihood of complications when compared to more invasive surgical techniques such as open reduction and internal fixation (Figure 41). Although the secondary surgical trauma is decreased with limited approaches, the diminished visibility and accessibility can lead to a less perfect reduction. Three-dimensional (3D) puzzle solving methods have the purpose of improving reduction quality while minimizing the secondary surgical insult. Surgery with a limited approach would seemingly be far less complex if a clear pre-operative reconstruction plan were available. To support this claim with quantitative data, a controlled surgical simulation study for fracture reduction was designed where key variables that reflect surgical complexity were measured.



Figure 41 In limited approach fracture reduction, bone fragments are percutaneously manipulated under fluoroscopic guidance.

Using surrogate materials, this study compared simulated fracture surgeries performed with and without the aid of 3D puzzle solutions. While the simulation does not replicate every anatomic and surgical detail, it provides a controlled environment for quantifying tangible indicators of utility, i.e. duration of surgery, extent of fragment motion in the course of the surgery, and final reduction quality. This work aimed to show that reassembling a fracture under simulated surgical constraints is simpler with a 3D puzzle solution.

Hypothesis: In a simulated reconstruction of a comminuted intra-articular fracture, access to the 3D puzzle solution will reduce surgical time, minimize the secondary surgical insult, and improve the quality of reduction.

#### Specimen Preparation

The injury chosen for this experiment was a three segment tibial plafond fracture. This injury poses a challenging, yet solvable problem (with and without puzzle solution in hand). Reducing more comminuted fractures may be attempted in future studies after greater experience is gained with the experimental protocol. To produce these specimens, distal tibia replicas were fabricated from the same polyetherurethane foam as used in the prior surrogate models, and they were then fractured in a drop tower. Fracture energy was

delivered by a 7.5 kg mass released from a height of 0.5m, which impacted an artificial talus molded from PMMA (Figure 42).

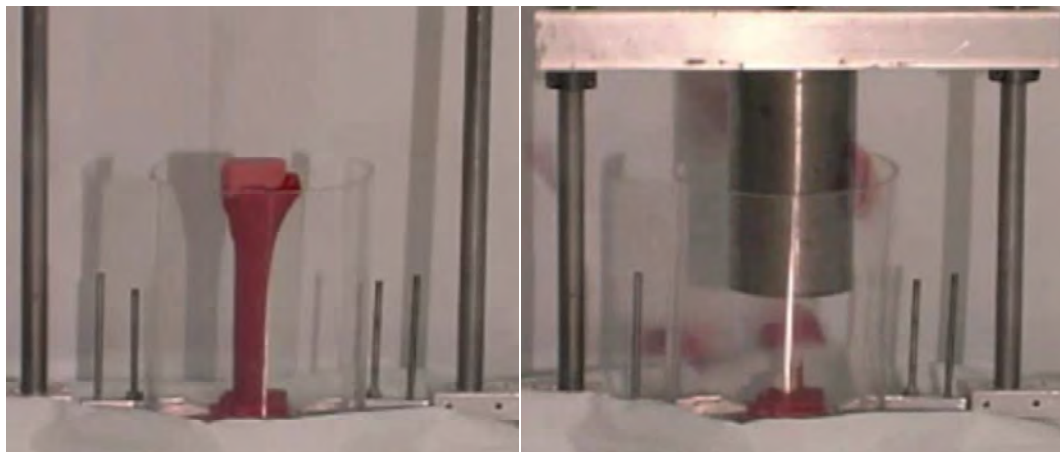


Figure 42 A surrogate distal tibia is impacted with a drop-tower to produce a three segment fracture.

To control for complexity between fracture reduction trials, each operator reduced the same two fracture patterns twice. Specimens were replicated by first molding fragments from silicone rubber (TinSil® 70 Series RTV, U.S. Composites). Replicas were then casted using a 16 lb/ft<sup>3</sup> density polyurethane foam that was doped with barium sulfate (15% by weight), a radio-opaque contrast agent. To imitate the denser subchondral plate's radiographic appearance, the fragment's weight bearing region was painted using glue that was doped with a high concentration of barium sulfate (40%). Original and casted fragments were laser scanned to verify that the cast/molding process produced accurate replicas. The average error between casted fragments was less than 0.2mm.

Original fracture fragments were apposed in a moderately displaced configuration by an experienced orthopaedic surgeon, and very lightly held together with very low-

strength glue that was applied just at inter-fragmentary point contacts (Figure 43). A PMMA impression was made of the displaced configuration's articular surface and used as a template for positioning casted fragments in the same configuration as the original. Laser scans of the original and casted constructs verified that configurations were replicated with sub-millimeter accuracies.

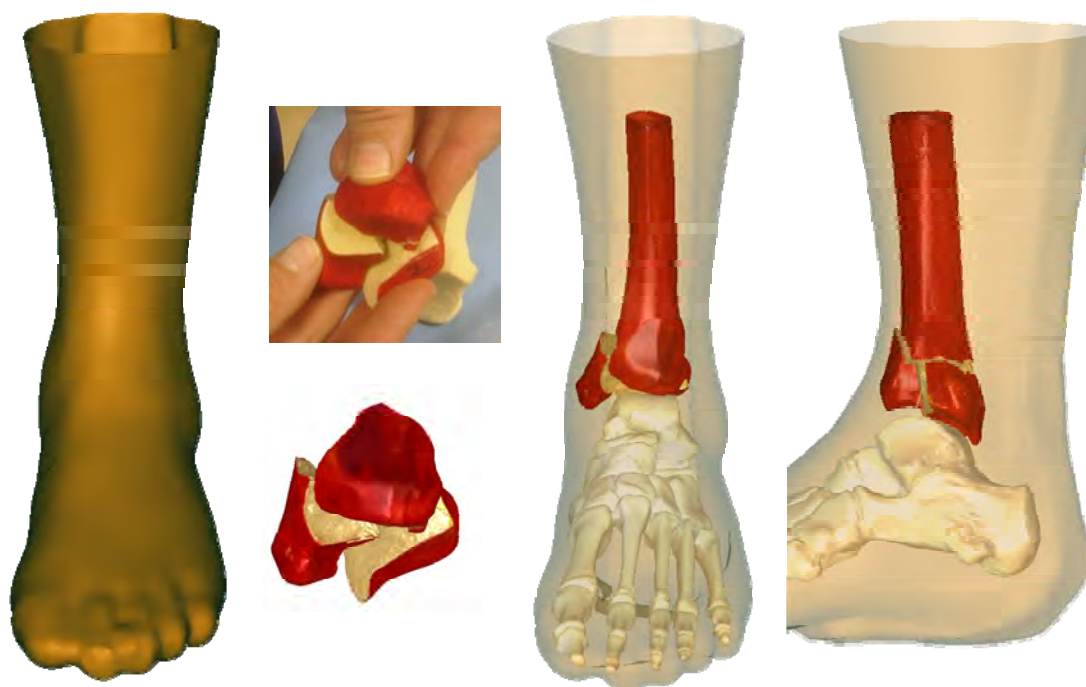


Figure 43 Fractured surrogate fragments were virtually apposed to replicate a moderately displaced pattern that was physically configured by an orthopaedist.

Using this approach, fragments were very lightly held in reproducible positions of displacement, and readily separated upon manipulation. The fracture constellation was then placed inside of a foot and ankle model manufactured by Sawbones Inc (Figure 44). These models are commonly used for arthroscopic and injection training. The model conforms to the normal anatomy of the lower limb, with an overlying soft flesh-colored

plastic that allows for palpation. In addition to the fractured tibia, all other normal osseous structures were present.

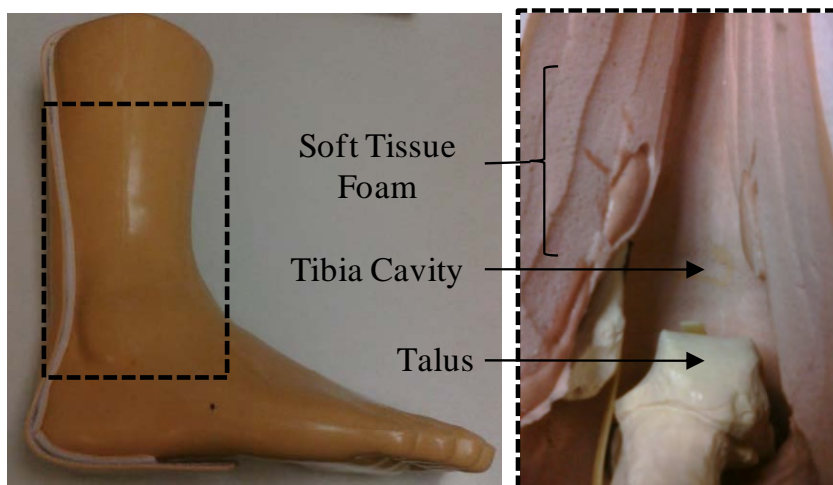


Figure 44 Foot and ankle model obtained from Sawbones. Muscle and soft tissues are simulated with homogenous foam that encased in a outer skin-like material. There is normal anatomy (fibula, talus, etc.) adjacent to the tibial cavity where the fracture surrogate tibia resided.

A limitation of these models is that only the global mass of soft tissue is represented: individual anatomic structures such as muscles, ligaments, neurovascular structures, etc. are not separately distinguished. Also, fragment soft tissue attachments that would otherwise restrain fragment motions during reduction are absent. Even so, senior orthopaedic residents and an experienced orthopaedic traumatologist confirmed that these models reasonably simulated the *in vivo* experience. Pre-operative CT scans were obtained, one for each fracture pattern. The surgical access site for each pattern was pre-determined to be approximately 2 inches in length, located anteriorly, thus adhering to the limited approach philosophy.

## Study Design

A set of ten clinicians were divided into two groups (1, 2), and each group reduced the same fracture pattern twice. Group 1 reduced the fracture with puzzle solving, and then three weeks later, reduced the fracture without puzzle solving (three weeks was judged a suitable amount of time for memories to have faded). Group 2 reduced the fracture without puzzle solving, then after three weeks with puzzle solving. To diminish the effects from the learning curve, operators were allotted 15 minutes to practice on a dummy specimen at the beginning of each session.

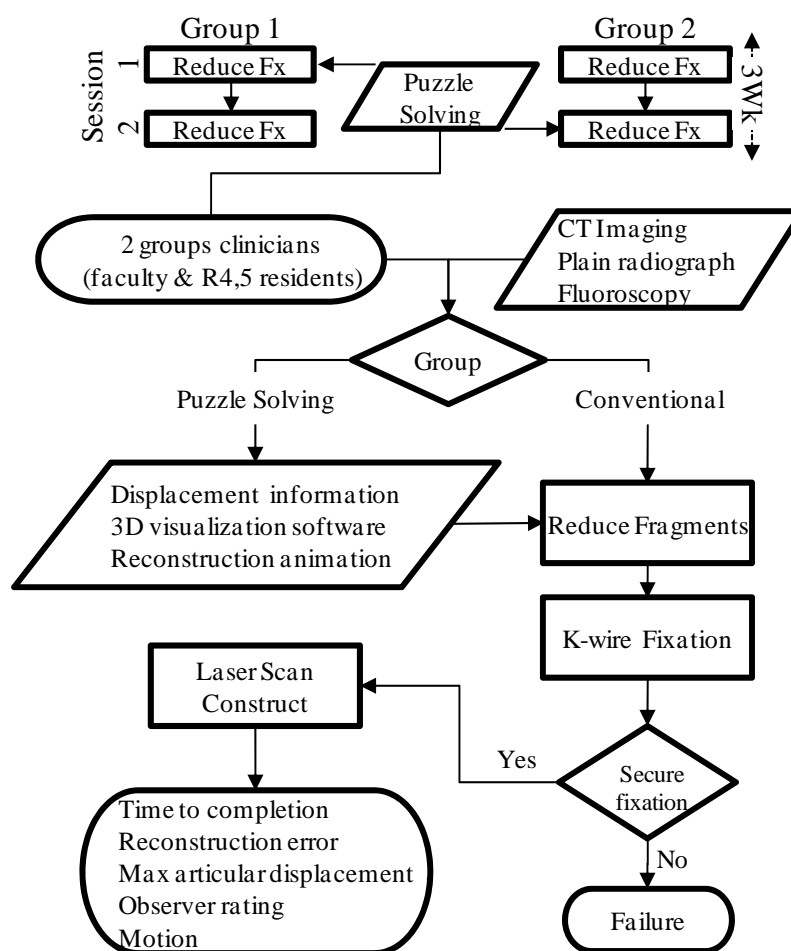


Figure 45 The protocol for surgical simulation and post-reduction evaluation is shown.

Both groups had access to conventional pre- and intra-operative imaging; plain radiographs, axial CT imaging, and fluoroscopy. Reductions were performed with a limited approach using standard reduction tools, and fragments were stabilized with K-wires (Figure 46). The objective of fixation was to rigidly stabilize the construct such that all fragments were in some way connected to the base fragment and were not free to rotate. All surgeries were timed to the moment at which the operator declared to have reduced and stabilized the fracture. Fracture reductions were scored according to a series of criteria. Points were given on a sliding scale with full credit if completed within 15 minutes. No “time to completion” credit was given to those trials that exceed 30 minutes. Operators were told that the primary objective was to successfully restore and stabilize original anatomy within 15 minutes. Secondly, operators aimed to minimize hand/fragment motions and time to stabilization.



Figure 46 A surgical simulation trial is depicted where fragments are percutaneously manipulated under fluoroscopic guidance, and fixed with k-wires.

3D puzzle solutions were generated for each fracture specimen by matching fragment native (periosteal and articular) surfaces to a pre-fractured template. For surgical trials with puzzle solving assistance, fragment-specific translations and rotations were provided to the surgeon numerically and visually with animations. Custom

software allowed for complete visualization control in 3D (Figure 47). In addition to rotating, translating and zooming at will, the operator could hide or visualize any structure. This program was running on a table-side laptop, and was available for as long as desired before the trial started.

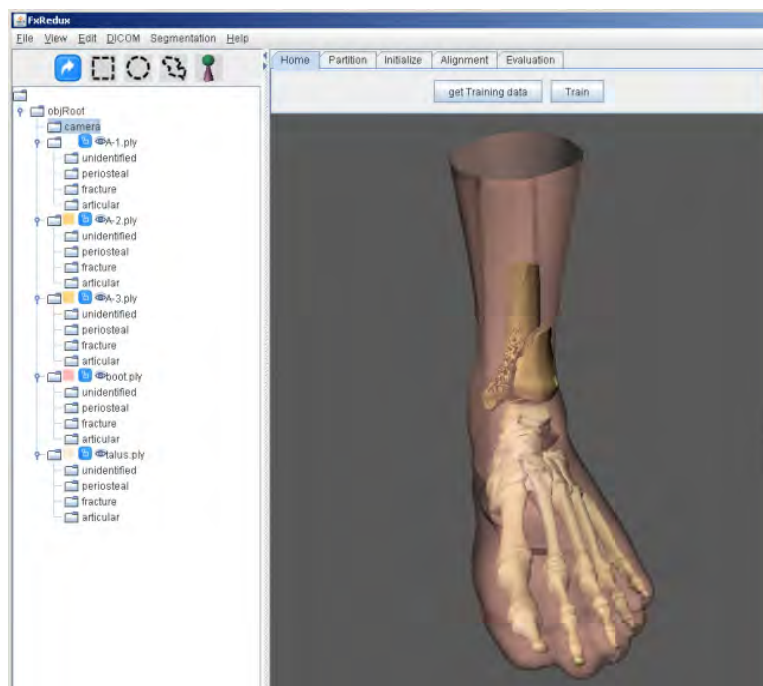


Figure 47 Custom puzzle solving software provides comprehensive visualization capabilities. The user could hide and/or change the transparency of all individual models. Animations also demonstrated the trajectories for precisely reducing fracture fragments.

The degree of surgical insult was indexed in terms of the cumulative motion of the surgeon's hands during fragment manipulation. A Qualisys motion capture system tracked passive markers that were attached to the back of each hand, with data capture at a frequency of 100Hz (Figure 48). Only those gestures that resulted in some physical contact with the specimen were considered to be significant. Synchronized video was collected and analyzed, to discard any irrelevant gestures.

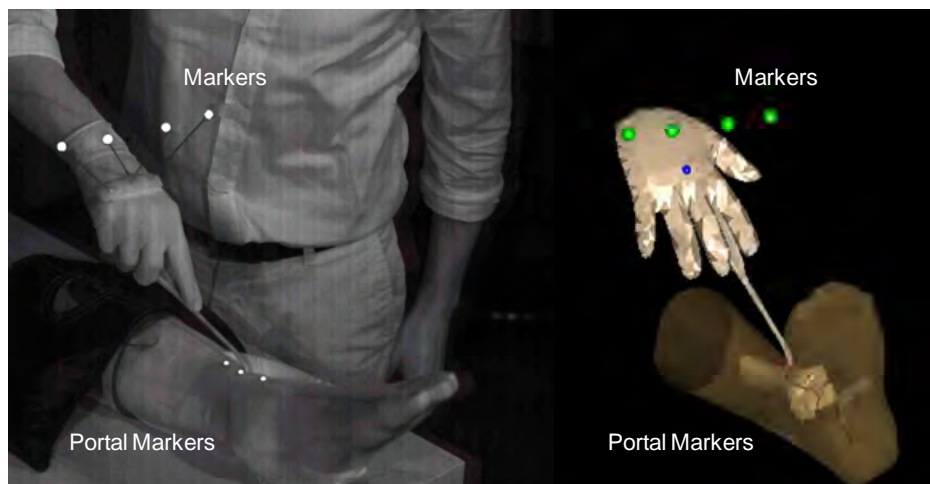


Figure 48. Hand motions were tracked with a Qualysis motion capture system. Fiducial markers attached to the back of the hand are located in space and registered to pre-simulation models.

#### Performance Assessment

Reconstructed specimens were extracted from the foot model and inspected. Constructs were deemed non-stabilized, and therefore a failure, if all fragments were not secured to the base fragment. Stabilized constructs were laser scanned for further analysis. Reduction accuracy was quantified by comparing the reduced fragments' native surfaces to the pre-fracture geometry. Error was calculated as the average distance between the two surfaces. Since articular reduction was deemed especially important, the maximum deviation between fragment and template articular surfaces was determined. Score points were deducted if the articular deviation was greater than 2mm, a reasonable threshold since joints with greater incongruities are likely to degenerate. In addition to those objective measures, an experienced surgeon reviewed the video recording and graded the operator's "expertise" with the Objective Structured Assessment of Technical Skills Skill (OSATS) test (Appendix B). With subjective scoring of dexterity, iatrogenic trauma, and likely outcomes, the OSATS is a validated method for assessing a trainee's technical skill [97].

Motion data were post-processed in MATLAB and the cumulative motion (Euclidean distance) was calculated. Since the fragments' motions were grossly related to hand motions, the degree of surgical trauma could be estimated from this quantity, providing a basis to quantify the effort, or the “trial and error” involved in reducing a fracture with versus without the aid of puzzle solving. In addition to cumulative hand motion, the number of discrete actions was estimated. Hand velocities were calculated from the positioning data, and smoothed with an averaging filter (window width = 11). Initially, time-points at which acceleration was near zero were flagged as instances of discrete hand actions. However, signal noise resulted in an overestimation of hand motions. As an alternative, local minima in the velocity trace were identified with MATLAB's 'imextendedmin' function. With a threshold of 10mm/s, that method was not as susceptible to error as the acceleration-based method. The correspondence between local minima and discrete actions were subjectively validated from the synchronized video recordings (Figure 49).

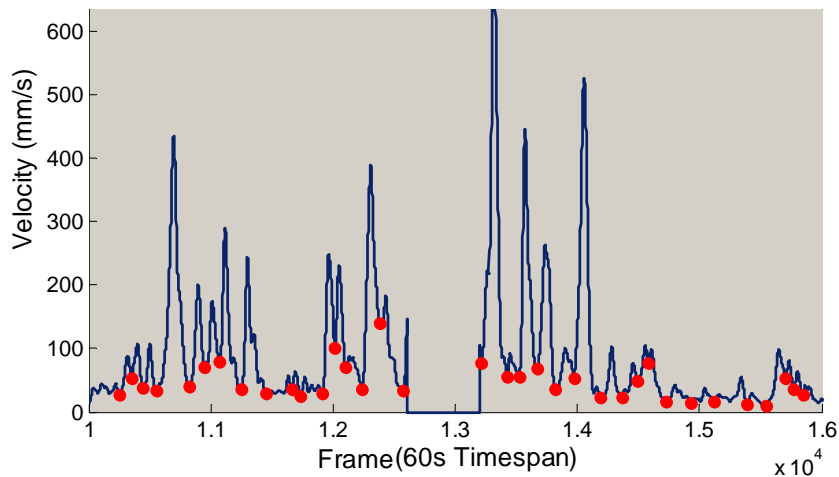


Figure 49 A sample plot of a surgeon's hand velocity during the simulation. Red dots represent instances of discrete actions. From the synchronized video data, time periods when the surgeon's hands were not touching the model were excluded from analysis (e.g. time period encapsulating  $1.3 \times 10^4$  s).

Since the sample size was relatively small, non-parametric tests were used to determine the statistical significance of puzzle solving assistance. A Fischer's exact test was used to investigate the null hypothesis that success is equally likely with and without puzzle solving. This statistic calculates the significance of the deviation from the null hypothesis. To further examine the benefits of puzzle solving, the group of successful reconstructions had their continuous data analyzed with a Wilcoxon signed-rank test for paired samples. This allowed determination of whether or not puzzle solving significantly affected reduction error, cumulative motion, and surgical duration times.

## CHAPTER 4 - RESULTS

### Surrogate Fracture Reconstruction

The fracture morphologies generated by the surrogate testing protocol successfully replicated the types of morphologies seen in clinical fracture cases. As with tibial plafond fractures, the replica tibias' articular surfaces were fractured anterior-posteriorly and/or medial-laterally through the weight bearing region. The replicas fractured into between 8 and 14 discrete fragments of varying sizes, with 2 to 5 of them being articular. Post-fracture fragment volumetric comparison showed that approximately 95% of the pre-fractured volume was recovered in the form of manipulably-sized fragments. The remaining volume was accounted for by “dusting” (crumbling of material), and/or by the need to discard fragments that were too small ( $\sim 0.5\text{cm}^3$ ) to be feasible for physical manipulation in a surgical setting. Figure 50 illustrates the puzzle solutions obtained for the five replica tibias.



Figure 50 Although some dusting was observed at the most proximal segment of the tibia, the articular and metaphyseal bone volume was preserved during impact. Subsequently, the 5 replica tibias were accurately reconstructed by matching native surfaces to the pre-fractured template.

The accuracies of the puzzle solutions were quantified by calculating the distances between the intact and the fragments' periosteal surfaces, and the distances between mating interior/fracture surfaces. The difference between the spatial volumes enclosed by the aligned bone surrogate fragments versus that of their intact (pre-fracture) specimens was used as an additional measure of volumetric reconstruction accuracy. With respect to the intact template, computational surface alignment yielded precise geometric reconstructions, with accuracy of fit to the whole intact template ranging from 0.03 to 0.2 mm (Figure 51.c).

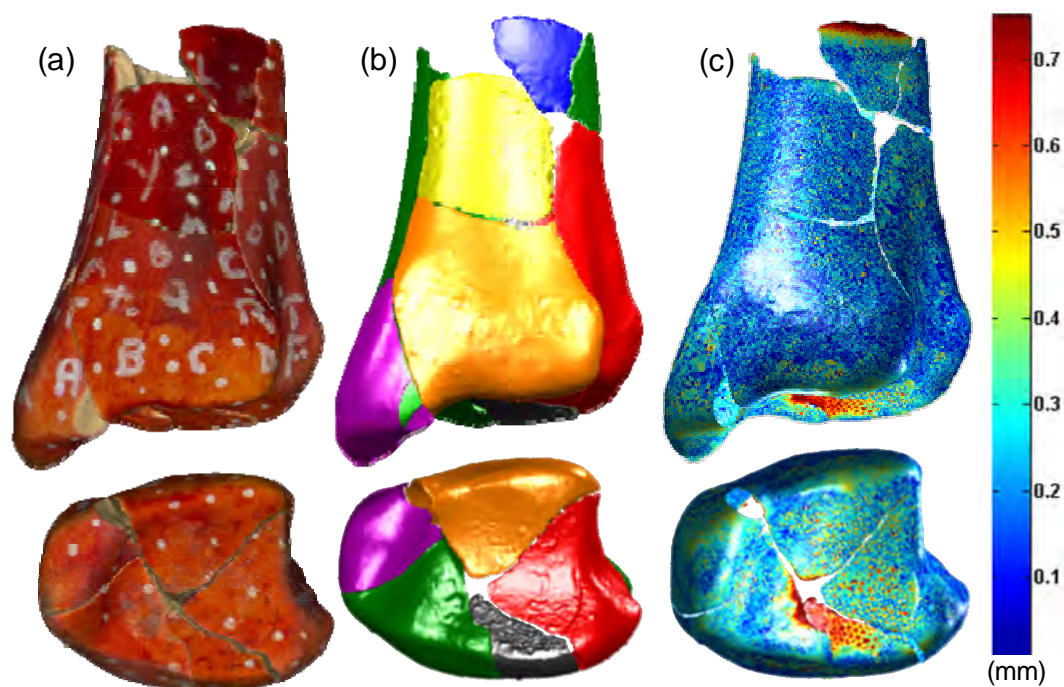


Figure 51 Reconstruction of the whole bone (top row) and the articular surface (bottom row) is shown for a typical surrogate tibia (a). Individual segmented fragments are shown color-coded (b). The pre- and post- fracture periosteal surface distance deviation calculations (c) verified that the original anatomy was accurately restored.

Both articular and non-articular (e.g. diaphyseal) fragment's native surfaces aligned well to the intact template (Figure 52). Although fracture surfaces aligned relatively well for both articular and non-articular, greater inter-fragmentary gaps were observed for non-articular fragments, indicating a small loss in material volume (Figure 52,right). That material loss was evident in some diaphyseal fragments, and likely was caused by the experimental setup. The tibia's proximal end was in contact with the drop-tower's steel base. Upon impact, the proximal diaphyseal was driven into that much denser material, a non-physiologic occurrence. Since dusting was isolated to within 0.5-1.0cm of the proximal end, articular and metaphyseal fragments were not affected.

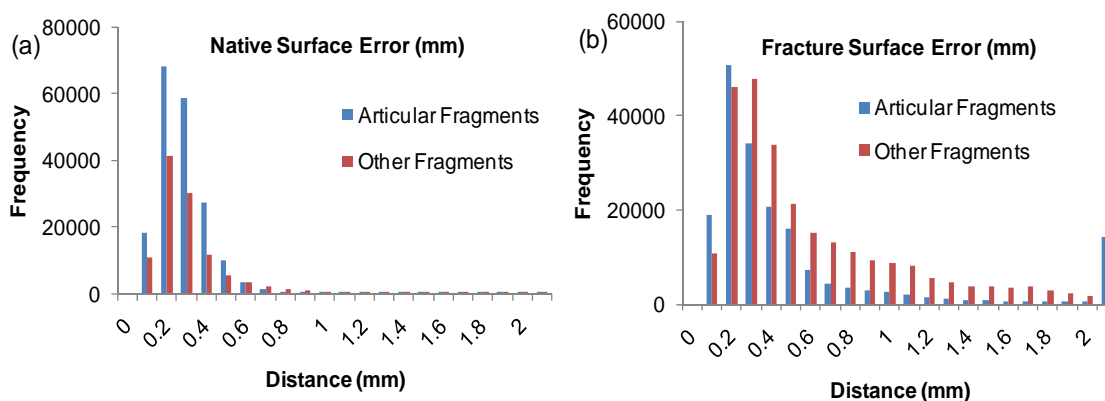


Figure 52 Histograms comparing native (i.e., periosteal) (a) and fracture (i.e. interfragmentary) surface (b) alignment errors for both articular, and non-articular fragments, for the five surrogates.

Given that clinical outcomes are especially affected by residual articular incongruities, the alignment accuracy specific to the weight-bearing region was separately calculated. Although some regions were plastically deformed during the impact event, the articular surface was congruent, and matched to the intact template within an average absolute error of 0.13mm. Proximities of internal fracture surfaces in the surrogates were less accurate, averaging 0.85mm, and they demonstrated a bimodal

distribution. Internal fracture surfaces tended to be either very well aligned to one another, or else they had distinct gaps, in some instances exceeding 1mm.

## Puzzle Solving Clinical Cases

### CT Segmentation

The image analysis techniques developed for puzzle solving purposes greatly expedited what was previously a very labor-intensive process. In prior methods, intensity based segmentation methods has been used to identify preliminary bone boundaries, and then a trained user edited the segmentation manually. Whereas that process typically required 8-10 hours per case [13], the new watershed-based method enabled the processing of each case in less than 20 minutes, with minimal user intervention. There was a range in comminution severity among the ten tibial plafond fracture cases that were analyzed. The number of fragments ranged from 4 to 11, of which between 2 and 6 were articular fragments. If intervention was required, much of the user guidance dealt with manually fusing over-segmented fragments. The automatic fusion algorithm worked well when erroneous boundaries traversed flat areas on a fragment's surface. However, some boundaries resided in concave regions and were therefore discarded by the automated algorithm. In those instances, the user manually clicked on both objects and the program fused their boundaries in less than 5 seconds. Other manual intervention involved editing small subvolumes of cancellous boundaries with ITK-Snap. That effort was mainly necessary for one case whose CT data had an abnormally low-resolution (1.0mm slice spacing). Beyond those two issues, the CT segmentation technique was mostly automatic, computationally inexpensive, and from visual inspection, highly accurate (Figure 53).

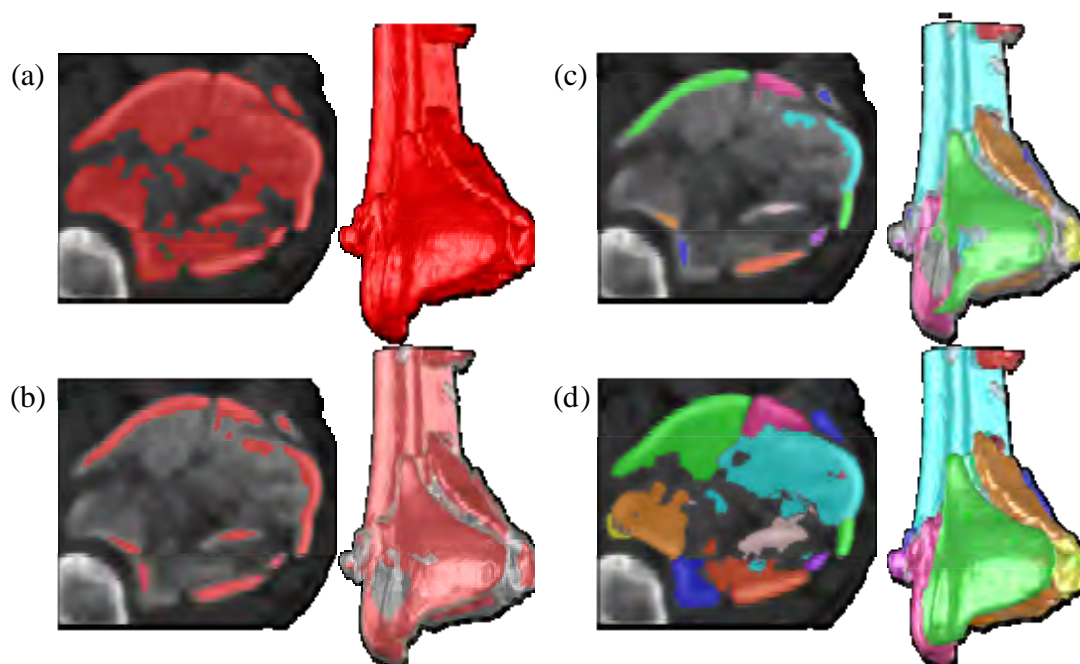


Figure 53 Novel image analysis techniques were developed for generating discrete fragment models that could be spatially manipulated and reduced. The process started with extracting the whole tibia (a), then non-cortical tissues were masked out (b). Individual cortical fragments (c) were used as seeds from which bone boundaries propagated (d).

Even though visual assessment suggested watershed segmentation to be highly effective, a validation study was conducted to quantify its accuracy. In that study, an expert user manually traced each case's largest articular fragment with an interactive display tablet. Comparison between manual and watershed segmentations showed an average unsigned distance difference of only  $0.55 \pm 0.22$  mm for all ten cases. When native and fracture surfaces were analyzed separately, it was evident that the user and watershed methods were in greater disagreement as to where the fracture surface boundary resided (Figure 54). While native surfaces only deviated  $0.34 \pm 0.24$  mm on average, the fracture surfaces deviated by  $0.99 \pm 1.43$  mm. One patient (Case 5) displayed a relatively greater degree of deviation between methods on the fracture surface. Visual inspection of the watershed segmentation confirms some erroneous loss in cancellous

bone volume. The error in segmentation is likely a consequence of this case's relatively poor CT resolution (1.0 mm slice spacing). Although the fracture surface may have had greater error, the native surface was accurately segmented (0.3mm) and therefore, the puzzle solution itself was not affected. Since the average difference between the computer and human for the 10 cases was the size of a single voxel, watershed segmentation techniques were deemed accurate.

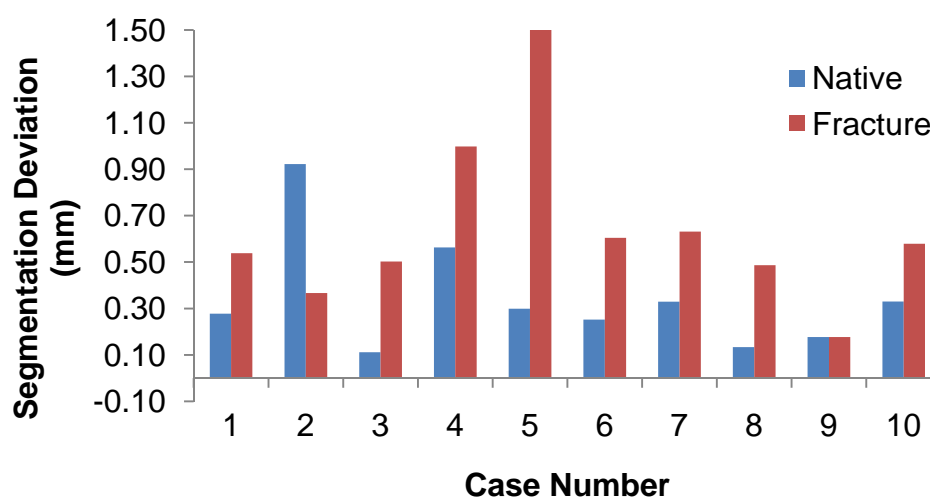


Figure 54 The deviation between watershed and manual segmentation results is shown for each case. There was better agreement on the location of the native boundaries than there was for the fracture boundaries.

### Surface Classification

Native surfaces were reliably classified as periosteal or articular by matching density profiles to both patient-specific and compiled population Gaussian mixture models (Appendix A.). Facet profiles that did not fit any of the four anatomic models with more than 90% probability did not meet the certainty threshold, and were therefore classified as 'unknown'. In order to assess the intensity profile algorithm's accuracy, its results were compared to visual classifications made by an experienced user. The

intensity profile algorithm with patient-specific models correctly classified 76% of the articular surfaces, and 77% of the periosteal surfaces. The compiled models accurately classified 60% of the periosteal and 59% of the articular surfaces (Figure 55). Classified mesh facets were then grouped into patches by the region-growing operation. Each patch was classified according to the maximum occurrence of periosteal or articular labels. If 50% or more of the patch was comprised of facets labeled as ‘unknown’, the whole patch was not labeled. With this classification and thresholding approach, both periosteal and articular patches were correctly identified in all cases.

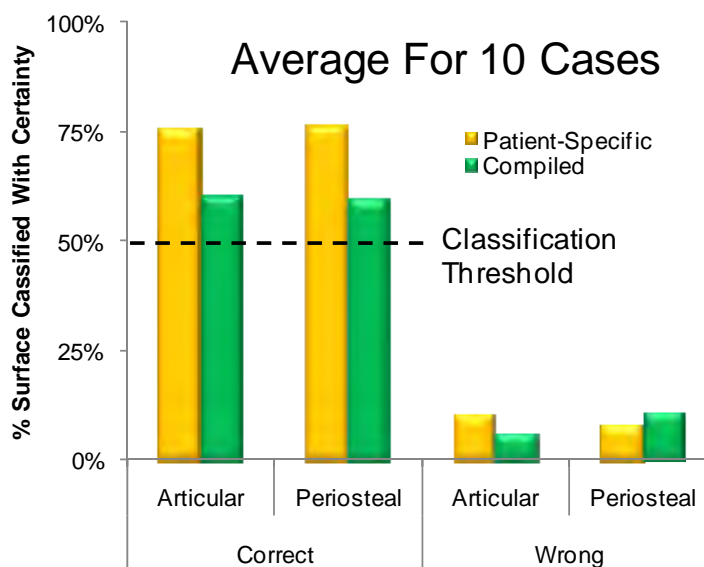


Figure 55 The accuracy of patient-specific vs. compiled classifications for total articular and periosteal areas is reported. Whole patches were given a single label if 50% of their surface area matched a model with 90% probability.

From visual analysis, the classifier performed well in the diaphysis and metaphysis with both patient-specific and population-based models. Although much of the articular surface was correctly identified, some areas of the malleolus were erroneously marked as articular. This was not surprising considering its unique shape

and density composition. The malleolus has a relatively homogenous density distribution, with magnitudes somewhere between cancellous and cortical bone. Another density model specific to the malleolus was investigated. However, it proved to be problematic. While some of the malleolus was classified correctly, other surface labels were changed from an accurate label to an inaccurate malleoli label. Therefore, malleoli models were not used in the final classification algorithm. Aside from modeling bone density, the malleolus' unique convex geometry could be as an independent feature in future classification algorithms. Even though some malleoli were problematic, both puzzle solving and fracture severity assessment algorithms greatly benefited from the ability to computationally recognize clinically important features.

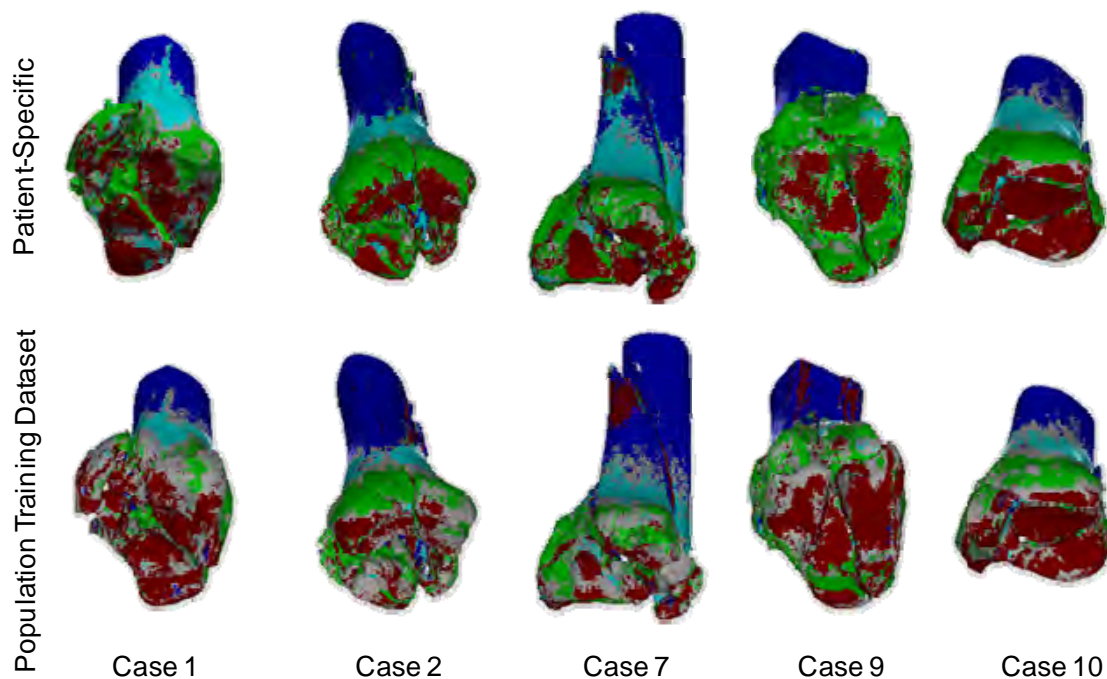


Figure 56. Five cases display surface density classification results using patient-specific and compiled population models. The majority of diaphysis (blue), metadiaphysis (cyan), metaphysis (green) and articular (dark red) surfaces were recovered. Regions that did not fit the models with at least 50% probability were labeled as unknown (gray).

A method for anatomically classifying fracture surfaces may assist geometry-based region-growing in future algorithms. Even though the majority of native surfaces were smooth and contiguous, some had irregularities that caused the region-growing algorithm to erroneously exclude some segments. It was hypothesized that fracture surfaces would not fit well to any Gaussian model, and could therefore be identified and distinguished from the native surface by improbability. Surprisingly, however, 82% of the facets on the fracture surface fit to one of the models with more than 90% probability. Developing models specific to fracture surfaces could potentially be used to make classification more discriminating. However, many of their inward surface normals point in unpredictable and variable directions. Measuring density profiles at these oblique angles would skew the measurements and introduce substantial variation in the statistical models. Therefore, efforts to improve fracture/native surface segmentations should concentrate on modifying the geometric-based approach.

#### Fragment Position Initialization

The automatic fragment initialization algorithm placed the fragments closer to their anatomic target. This was quantified by comparing displaced and initialized fragments, relative to their reduced positions. Specifically, the fragment's center of mass in each position was located, then the distance between displaced versus reduced was compared to the distance between initialized versus reduced (Table 2). Except for the two cases with the least amount of displacement (Cases 6 and 10), the average distance was reduced after initialization. It was expected that computation time for alignment would decline since fewer rotations and translations would have to be performed by ICP. However, there was only a ~30% reduction in computation time. Since Geomagic is a highly refined commercial product, it is likely that greater improvements in speed would be observed in less advanced ICP implementations. While the improvement in speed was less than expected, some fragments, particularly those that had little surface variation and

were highly displaced, could be aligned only if initialization was performed. If ICP was applied without initialization, Geomagic could not always place fragments correctly. If the fragment was considerably displaced from the template, Geomagic's alignment algorithm would expand the search space. Because Geomagic does not account for physical realities, that search space sometimes included improbable segments of the template. For instance, a displaced posterior diaphyseal fragment might be aligned to the anterior metaphysis. By incorporating *a priori* fracture pattern and anatomic information, the initialization algorithms placed fragments near their target, thereby improving the stability of Geomagic's ICP.

Table 2 In order to improve speed and stability, a series of algorithms grossly reduced each fracture prior ICP. The average distance between fragments in their displaced versus reduced positions, are compared to the average distance between fragments in their initialized versus reduced positions.

|             | Gross Reduction Results: Fragments' Average Distance (mm) |                         |
|-------------|---|-------------------------|
| Case Number | Displaced vs. Reduced                                     | Initialized vs. Reduced |
| 1           | 10.74   | 5.75                    |
| 2           | 7.61  | 4.71                    |
| 3           | 4.27  | 2.95                    |
| 4           | 4.56  | 4.40                    |
| 5           | 18.12   | 11.07                   |
| 6           | 1.51  | 2.38                    |
| 7           | 5.85  | 4.94                    |
| 8           | 4.63  | 3.01                    |
| 9           | 10.95   | 6.66                    |
| 10          | 2.07  | 2.87                    |

After the initialization process, Geomagic's ICP algorithm performed precise adjustments, and accurately aligned each fragment to the intact template in less than one minute (Figure 57). Larger fragments having relatively high surface variation, such as the articular fragments, were quickly aligned. Smaller fragments with more planar surfaces took more time to align. With less surface variation, the ICP test space was less constrained, and therefore greater translations and rotations had to be evaluated by the algorithm. Manual intervention was required for some of those fragments. In many of those instances, fragments were centered near the correct position, but were inaccurately rotated (e.g. upside-down). Accuracy of alignment was quantified by the average deviation between template and fragment surfaces with Geomagic Qualify. The virtual reconstruction accurately restored normal anatomy in all ten clinical cases. The average surface deviation was only 0.39 mm (standard deviation 0.50 mm) (Table 3).

Table 3 Alignment error for overall native (periosteal and articular combined) and periosteal/articular surfaces individually are shown. The periosteal surfaces aligned better to the intact template than the articular surface.

| Case ID | Average Alignment Error (mm) |            |           |
|---------|------------------------------|------------|-----------|
|         | Native                       | Periosteal | Articular |
| 1       | 0.50                         | 0.45       | 0.85      |
| 2       | 0.45                         | 0.35       | 0.75      |
| 3       | 0.35                         | 0.35       | 0.35      |
| 4       | 0.35                         | 0.30       | 0.30      |
| 5       | 0.30                         | 0.30       | 0.35      |
| 6       | 0.35                         | 0.40       | 0.60      |
| 7       | 0.40                         | 0.30       | 0.45      |
| 8       | 0.35                         | 0.35       | 0.45      |
| 9       | 0.30                         | 0.35       | 0.40      |
| 10      | 0.60                         | 0.60       | 0.65      |
| Average | 0.40                         | 0.38       | 0.52      |

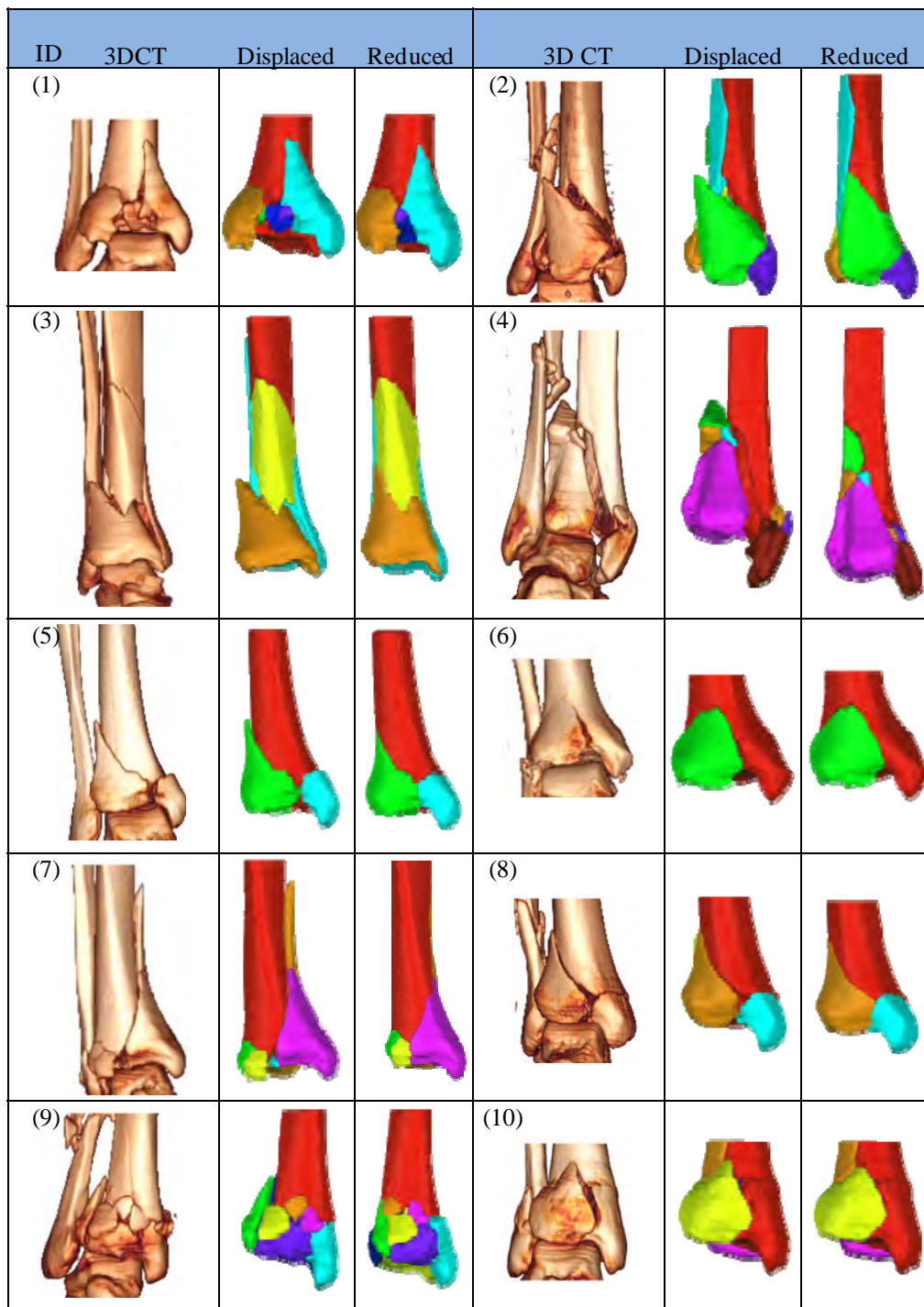


Figure 57 Ten clinical tibial plafond fractures were puzzle solved. Volume renderings (3DCT) and segmented fragment geometries (Displaced) illustrate this series' range in severity and variable fracture characteristics. Puzzle solutions (Reduced) provide ideal fragment positioning targets for restoring original anatomy.

The articular surfaces were generally congruent after virtual reconstruction. However, five cases (Cases 1, 2, 6, 7, and 10) displayed some crush from the impact event. These cases had an average articular alignment error of  $0.66\pm 0.17$  mm, whereas cases without crush averaged  $0.37\pm 0.11$  mm. The relatively large error in articular alignment for Case 1 was visually confirmed as being due to an apparent articular defect in the central weight bearing region (Figure 58). In addition to articular distortion, several cases displayed clear evidence of cancellous crush with gaps between fracture surfaces. In the most severe instance, the distance between one fragment's superior surface and another's inferior surface was 10 mm (Case 9). The majority of bone fragments were not plastically deformed, however, but rather fit well to both the intact template and to adjacent other fragments.

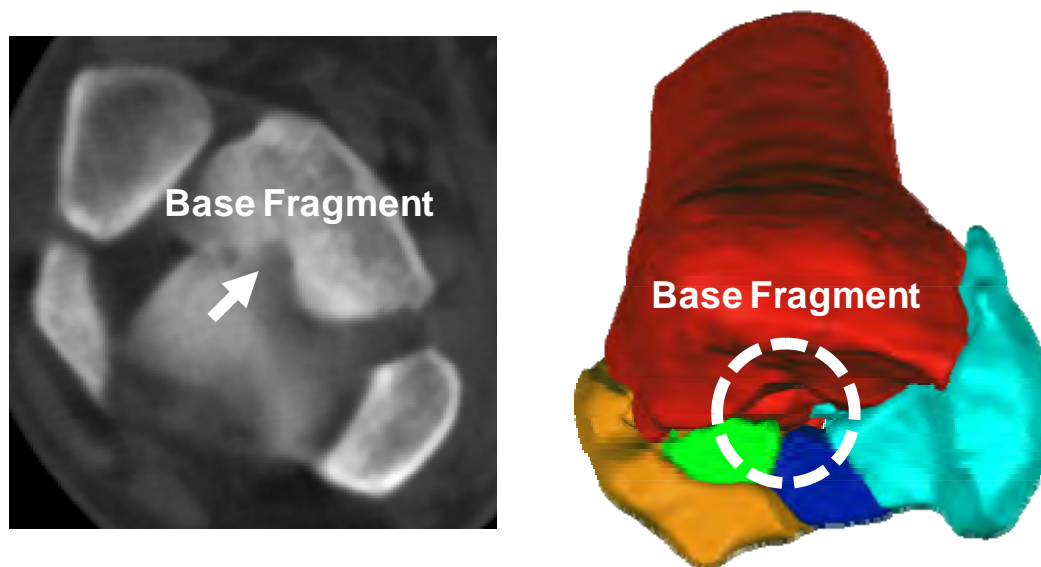


Figure 58 For the case with the largest articular alignment error, a large articular defect was visually apparent on CT and the virtual reconstruction

Three-dimensional visualization of displaced and virtually reconstructed joints provides useful information for treatment. Compared to viewing CT in two-dimensions, the degree of comminution and specific fracture characteristics are easier to understand with CT volume renderings (Figure 57, 1<sup>st</sup> and 4<sup>th</sup> columns). However, some fracture edges and cracks are not always discernable, thereby making comminution more difficult to appreciate. In addition, the amount of articular disruption cannot be judged, since the joint surface is hidden by the talus. Accurate CT segmentation from the watershed method resolved those issues by extracting non-tibial anatomy, and color coding individual fragments (Figure 57, 2<sup>nd</sup> and 5<sup>th</sup> columns). In addition to providing detailed positioning instructions, inspection of the 3D reconstruction (Figure 57, 3<sup>rd</sup> and 6<sup>th</sup> columns) and alignment data enables one to identify segmental defects, deformations, and to better plan definitive fixation.

#### Injury Severity Assessment

Due to the influence of partial volume effects blurring fragment boundaries in fractured CT data, reliable voxel-by-voxel energy release rates could not be formulated with the previously reported methodology. The original fracture energy measurements scaled liberated surface area by three categorical energy release rates. Those rates were calculated from statistical modeling of diaphyseal, metaphyseal and cancellous tissue types. Now with puzzle solving, fracture surfaces could be registered to the intact CT data where partial volume effects are minimal, thereby enabling the calculation of voxel-by-voxel energy release rates. Interestingly, the average difference between previously reported energy measures, versus the new measures derived with puzzle solving was only  $2.9 \pm 3.0$  J (Figure 59). With 93% concordance, both methods were in excellent agreement (Figure 59 left). The articular comminution metrics were normalized to the maximum observation for these ten patients. The average difference between the 2D liberated area

derived measure, and the 3D arc length measure was  $14 \pm 10\%$ , with a concordance of 67% (Figure 59 right).

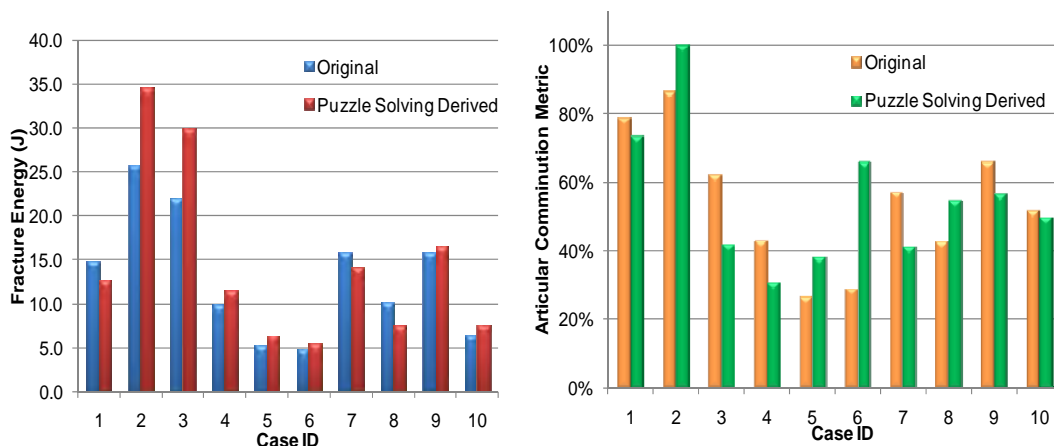


Figure 59 Fracture energy calculations with puzzle solving agreed well with those reported in previous work (left). The two-dimensional original version and the 3D curve articular comminution metrics agreed (right).

Since both articular comminution and fracture energy contribute to the joint's predisposition to degeneration, a comprehensive severity measure was formulated by combining the two measures. With equal weighting factors, previously derived and new measures were combined, normalized, and compared against the severity of PTOA two years after injury. A regression model was not developed as done in previous methods, because the population size was relatively small. But these equal weighting factors were similar to those previously regressed factors (0.48, 0.52). Previous and new acute severity scores were in general agreement, with a concordance of 82%. Both metrics displayed strong predictive capabilities for joint degeneration (Figure 60).

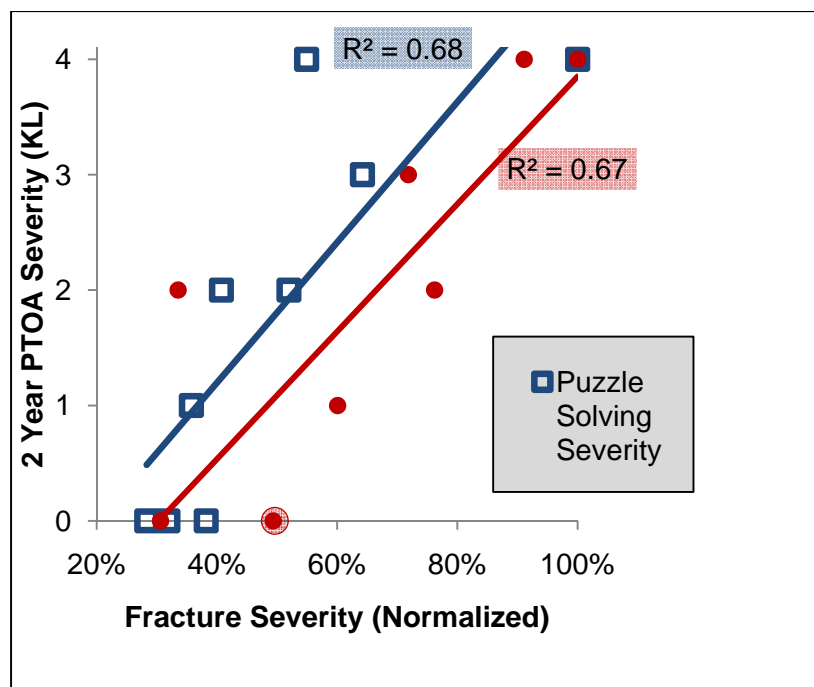


Figure 60 Previously reported and puzzle solving-derived fracture severity measures are compared to the eventual development of PTOA at 2yrs post injury measured by KL scale (0 = no OA, 4 = severe OA).

### Surgical Simulation

The protocol outlined in the methods section is an on-going effort. Unfortunately, the residents' busy schedule and difficulties in obtaining fluoroscopy has impeded the progress of this study. Preliminary results for five complete simulation sessions are presented below, with the acknowledgement that no statistically significant conclusions can yet be made due to the limited number of observations (Table 4).

Since it was recognized early in the study that progress would be slower than expected, the first trial in each session was not framed as a “dummy” trial. Instead, surgeons were informed that the first and second reductions were of equal importance so that preliminary comparisons between trials with versus without assistance could be made. It is recognized that these initial comparisons are confounded by familiarity gained in performing the first trial, and by the difference in fracture complexity.

Ultimately, this slight modification in protocol will not affect the final analysis outlined in the METHODS section.

Table 4 Results from the first five surgical simulation sessions are reported.

| Resident    | Pattern          |         | Fixation Success     |         | Duration (s)      |         | Fluoro Shots     |         |
|-------------|------------------|---------|----------------------|---------|-------------------|---------|------------------|---------|
|             | With             | Without | With                 | Without | With              | Without | With             | Without |
| 1           | A                | B       | +                    | +       | 1108              | 1682    | 39               | 35      |
| 2           | A                | B       | -                    | +       | 1461              | 1211    | 34               | 65      |
| 3           | A                | B       | +                    | -       | 542               | 561     | 177              | 23      |
| 4           | A                | B       | +                    | +       | 1827              | 725     | 56               | 35      |
| 5           | B                | A       | +                    | +       | 653               | 726     | 19               | 29      |
| Resident ID | Total Error (mm) |         | Articular Error (mm) |         | Cumulative Motion |         | Discrete Actions |         |
|             | With             | Without | With                 | Without | With              | Without | With             | Without |
| 1           | 0.47             | 1.12    | 2.56                 | 3.20    | 104309            | 137250  | 942              | 2933    |
| 2           | -                | 1.07    | -                    | 3.50    | 138838            | 124371  | 1597             | 993     |
| 3           | 0.62             | -       | 2.69                 | -       | N/A               | 57417   | N/A              | 382     |
| 4           | 0.71             | 0.65    | 3.10                 | 2.73    | 107213            | 36156   | 943              | 394     |
| 5           | 0.80             | 0.55    | 2.78                 | 2.57    | 27483             | 38393   | 318              | 388     |

As of September 30, 2010, two pilot and five complete surgical simulation sessions had been completed. In one of the pilot sessions, a senior traumatologist subjectively confirmed that the specimen and setup simulated the intra-operative experience well. In each complete session, a fourth or fifth year orthopaedic resident reduced two fracture patterns, one pattern without puzzle solving, and the second with puzzle solving (Figure 61). In four of the sessions, pattern B was reduced without assistance in the first trial, and in the second session, pattern A was reduced with the puzzle solution. In the fifth session, pattern B was first solved with puzzle solving, and pattern A was solved without during the second. In Resident 3's first trial, the data failed to transfer from the Qualysis' on-camera memory and was permanently lost. When residents are tested in the second session, pattern B will again be reduced first, but access to puzzle solving will be reversed.

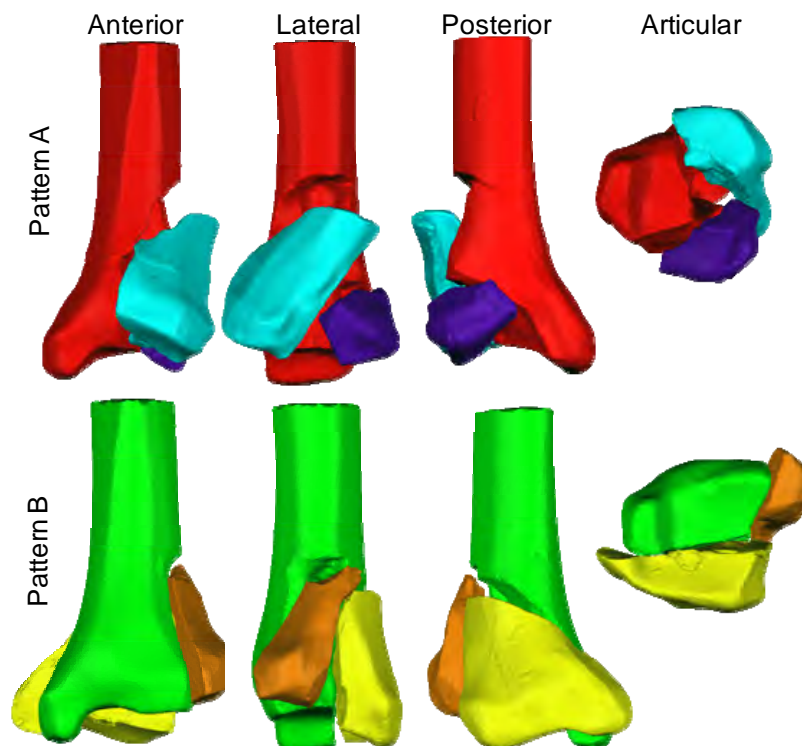


Figure 61 Two surrogate fracture patterns were reduced in a simulated fracture reduction surgery. When anatomically reduced, most fragments inter-digitated with adjacent fracture surfaces. However, the posterior-lateral fragment of Pattern A (color purple) was highly unstable and was therefore especially challenging to reduce.

Before the results from the first five sessions are presented, it is important to note the substantial difference in reduction difficulty between the two patterns. Although both are three- segment fractures with similar fragment sizes, the posterior-lateral fragment in pattern A makes this pattern especially difficult to reduce. This was spontaneously stated verbally by all residents. Since that fragment did not have the “lock and key” effect that the smaller fragment in pattern B had, it was less constrained by adjacent fragments, and moved more freely. Furthermore, there was no direct access to that fragment. Therefore, its placement required greater skill and control. Because 4 of the 5 sessions had pattern

A reduced with assistance, the benefit to having the puzzle solution may be artificially diminished.

Residents successfully reduced 8/10 fractures, and secured them with k-wires. There were only two failures. Resident 3 appeared to have fixed pattern B on fluoro (Figure 62 left), however, the k-wire failed to penetrate the posterior fragment (Figure 61, orange fragment). The second failure occurred in Resident 2's reduction of pattern A with puzzle solving. Though it was a failure, it is worth mentioning that the fracture appeared to have been reduced to a high degree of accuracy after ~930s, but in an effort to further perfect the quality of reduction, the posterior-lateral fragment k-wire was removed, and additional maneuvering was performed (Figure 62, right). During subsequent reduction maneuvers, that fragment migrated further, and further away. Ultimately, the fragment flipped upside down near the talus and the resident had to abort the trial. If the resident had stopped earlier, it is likely that the trial would have been successful.

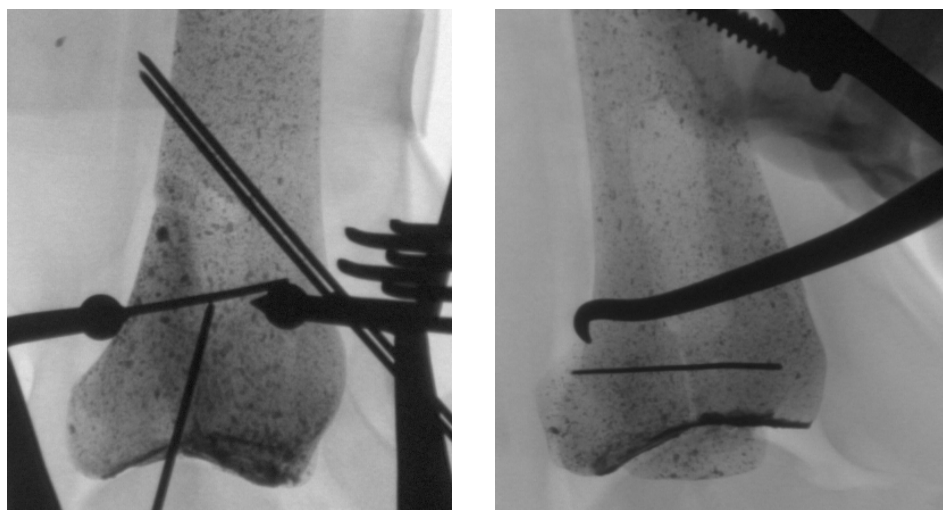


Figure 62 Left: The final fluoroscopic image taken during Resident 3's reduction of pattern B. Right: An accurate articular reduction is observed in a fluoroscopic image taken midway through resident 2's reduction of pattern A.

The results from the first five sessions suggest there to be a wide range in surgeons' technical abilities. Even though reduction accuracies were mostly consistent across residents (Figure 63), the time, motion, and number of discrete actions needed to perform those reductions varied greatly. For instance, Resident 5 was able to reduce Pattern A in 653seconds, but Resident 4 took almost three times as long. As expected, surgical duration corresponded to greater cumulative and discrete motions. While there was substantial inter-subject variation, intra-subject performance varied less (as measured by duration and motion), except for Resident 4 who struggled with Pattern A.

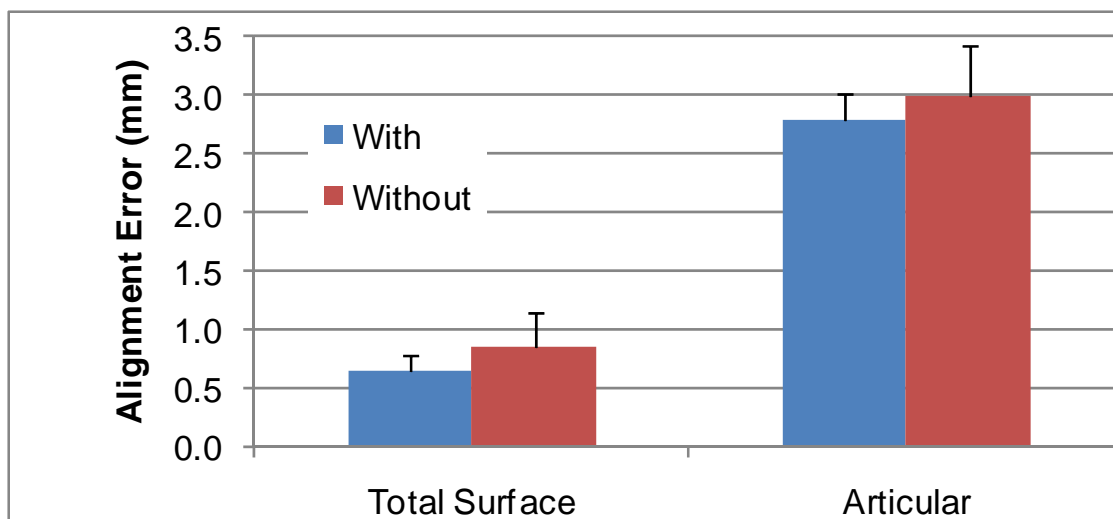


Figure 63 The average reduction error for trials with, and without puzzle solving's assistance are compared.

## CHAPTER 5 - DISCUSSION

Without computational aid, surgeons have to cognitively plan the reconstruction from a stack of 2D CT slices or from a 3D volumetric rendering. This task is particularly challenging in comminuted fractures where fragments are appreciably displaced, and where some fragments may even be missing. While surgeons try to position fragments such that the weight-bearing surface is as smooth and congruous as possible, results are often substantially imperfect. The virtual 3D puzzle solving methods here reported hold great potential for improving the care of these difficult injuries. By having a blueprint for restoring the original anatomy, it becomes possible for the surgeon to perform less extensive surgical dissections, and to lower the number of mismatches of candidate fragments, while still achieving accurate fracture reconstructions.

Existing intra-operative navigation tools developed to aid in the reconstruction of long-bone fractures are not designed to puzzle-solve complicated fractures. While useful for fixation planning for simple fractures, these early-generation systems are unable to deal with the complex geometries of comminuted articular fractures. Various groups have developed virtual environments wherein fracture reduction is pre-operatively planned by manually manipulating 3D models [98]. Those computational tools have been shown to improve reductions and reduce surgical time. Although such methods may be applicable to 3-segment fractures, it is impractical to manually reconstruct more highly comminuted fractures, in the clinical setting. The governing objective of this research was to develop a clinically practical technology. Specifically, puzzle solving methods have to reliably generate accurate reconstruction plans for a wide range of fracture morphologies expediently, and with minimal user intervention. With the successful application to a clinical series of comminuted tibial plafond fracture series, 3D puzzle solving is quickly advancing toward achieving that objective. Furthermore, inspection of the virtual

reconstruction was found to be a very informative practice. In many cases, bone crush, articular defects and bone loss, were only apparent after a puzzle solution was obtained.

### Surrogate Developmental Work

Due to the novelty of the 3D puzzle solving approach, its successful development benefited from an ordered progression in puzzle complexity. The creation of representative comminuted fracture geometries in a suitable surrogate material provided clinically realistic data in a well-ordered developmental platform that bypassed the many unnecessarily confounding difficulties inherent to *in vivo* tissues. Particularly, it allowed for research to progress without having addressed the difficult CT segmentation problem. This was essential for discovering that matching native surfaces to an intact template was an effective means for virtual fracture reduction. Before that discovery, it was expected that puzzle solving would need to rely upon aligning fracture surfaces. However, complications arise with such a methodology for two main reasons: (1) fracture surface segmentations are susceptible to error, and (2) fracture surfaces may be plastically deformed. Aligning fracture surfaces in such a case would distort the joint's shape. On the other hand, if apposing fracture surfaces are not in contact, the resultant construct would be mechanically unstable and the formation of new bone could be impaired. From the output of the native-template alignment algorithm, one can pre-operatively identify the problematic inter-fragmentary gaps, and intervene with alternative fixation or grafting. Although a template matching methodology is arguably a better approach than aligning fracture surfaces, there needs to be a balance between restoring original anatomy and achieve mechanical stability. Future puzzle solving algorithms will likely use a hybrid approach that takes into account both components. Restoring original anatomy will primarily be achieved by a native-template alignment method, but fine adjustments should be made for bringing fragments into physical contact.

While puzzle solving methods have matured to the point of being used to reconstruct *in vivo* fractures, the surrogate developmental platform may continue to be a useful platform for investigating other aspects puzzle solving. Currently, a pre-operative virtual reconstruction provides only “end-stage” fragment placement instructions. Surrogate fractures provide well-controlled data for exploring intra-operative technologies that link computational models to real-time spatial data. Also, surrogate specimens may be the ideal platform for investigating custom fixation constructs. Once a fracture is precisely reduced, maintaining that configuration is absolutely vital for preserving the joint’s long-term function. In addition to recreating *in vivo* fracture patterns, the polyetherurethane surrogate material has similar mechanical properties to human bone. Therefore, surrogates can be used to test computationally derived fixation constructs that are predicted to promote bone healing. By providing intermediate stability, the objective of fixation in this fracture is to promote secondary bone healing. The amount of strain that is permitted by the fixation construct is a primary determinant for determining the biologic response. Controlling this variable with customized fixation would be a valuable tool for preventing complications such as non-union.

#### Image Analysis Technique

New image analysis methods for virtually reconstructing comminuted joint fractures were developed. The watershed-based CT segmentation approach expedited what was previously a clinically impractical process. In order for puzzle solving to be clinically applicable, accurate fragment geometries have to be extracted from CT with minimal user intervention. The watershed-based approach is a promising technique for performing that task. It not only drastically reduced the processing time from 8-10 hours to less than 20 minutes per case, but it also produced reliably accurate geometries. Although whole-fragment segmentations agreed well with those done manually by an experienced user, greater disagreement was observed along the fracture surfaces. Even

though fracture surfaces are currently not factored into the alignment algorithm, it is important to accurately recover those boundaries so that bone crush and/or gaps are detectable.

Most of the segmentation error occurred on cancellous fracture boundaries. Compared to cortical bone, cancellous boundaries are typically not as well defined on CT. When cancellous bone has a similar radiographic appearance to other tissues, or what it contacts other fracture surfaces, there is no visual cue or image gradient to indicate that there is a fracture boundary. When conceptualized topographically, the region between two non-displaced fragments corresponds to a single “floodplain”. Even in those problematic instance, however, the watershed-based approach produced relatively accurate segmentations. By using the previous iteration’s segmentation as a marker to define image minima in the next watershed operation, the floodplain’s topography was changed incrementally and the flooding process was better controlled. If a single iteration was performed instead of a series of watershed operations, the ridgeline separating two adjacent fragments would often be convoluted and unreliable.

Although fracture surfaces are not currently factored into the puzzle solving algorithms, they are expected to be incorporated into future applications. It is therefore necessary to examine likely causes and possible solutions. Unfortunately, some fracture surface segmentation errors are largely unavoidable due to CT limitations, especially for non-displaced and low-density bone fragments. Such fracture edges are extremely difficult to perceive both subjectively and computationally. As demonstrated by one of the cadaver specimens, fracture edges along some porous cancellous boundaries are undetectable on CT. As a result, physically accurate segmentations are not probable (Figure 64). It is unlikely that the true boundary for these problematic fracture surfaces will be determined solely from CT data. Without any image intensity variation along that border, future post-processing methods may rely upon empirical knowledge of bone fracture behavior and fragment morphology.

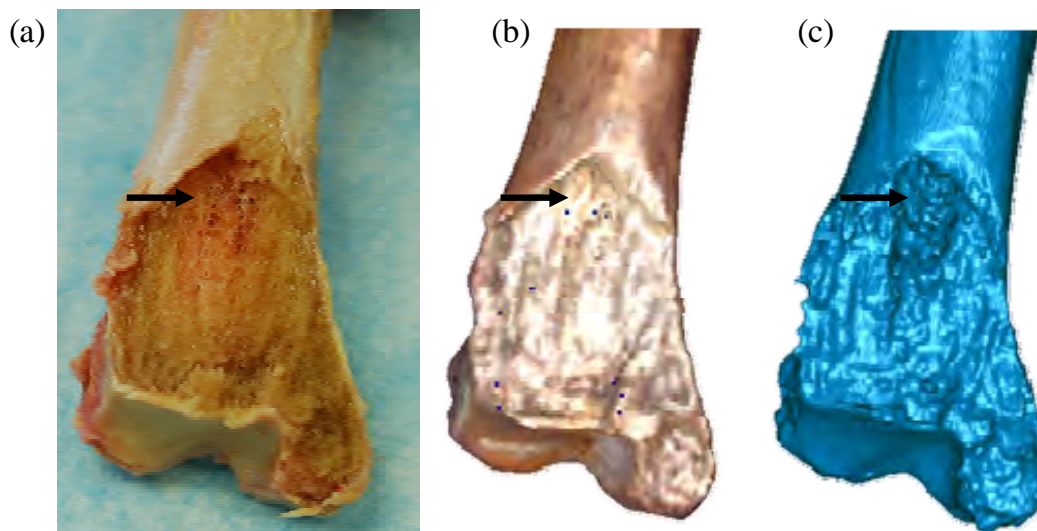


Figure 64 The base fragment from a cadaveric impact is shown (a). A segment of the cancellous fracture surface (arrow) that was detected visually and on the laser scan (b), but was not discernable on CT --causing there to be a cavity in CT iso-surface (low threshold, 100 HU).

For the majority of fracture surfaces, there was only a one or two pixel offset between manual and computer-segmented boundaries. Generally, the contour produced by the computer better followed the irregularities of the cancellous bone. In contrast to the homogenous cortical bone, cancellous bone has a coarse appearance with local concavities and convexities along exposed surfaces (Figure 23). Whereas the human typically traced those edges with mostly smooth lines, the computer followed the contour exactly. Although the manual results were in close proximity to the computer's output, the human did not replicate the rippled-like appearance of the fracture surface (Figure 65). But these are relatively minor deviations, approximately 1mm or less. Considering that CT resolution was between 0.3 and 0.5mm, those results support the accuracy of the watershed technique. However, defining certain cancellous boundaries will continue to be problematic in the immediate future. While this has implications for future puzzle

solving applications such as fixation planning, template-based virtual pre-operative planning is mostly unaffected.

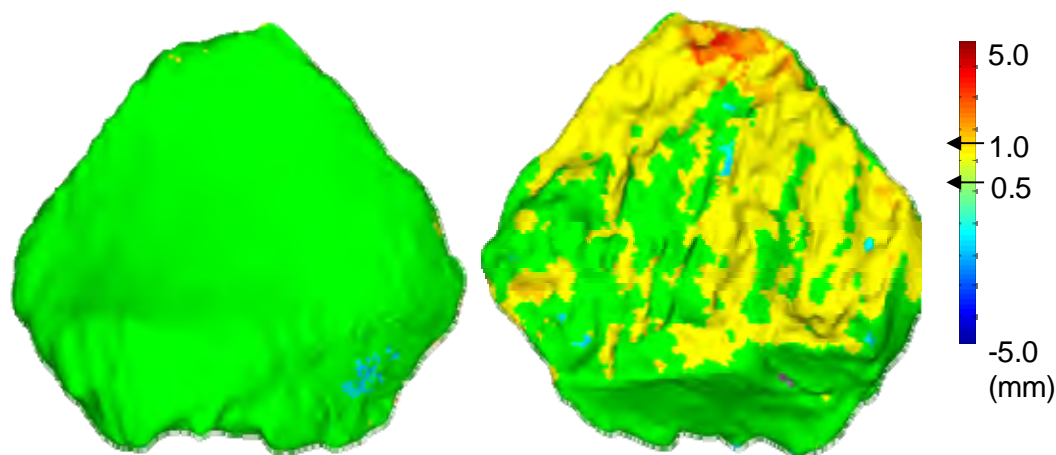


Figure 65 A color map of the surface deviation between manual and watershed segmentation geometries for Case 6 is shown. The majority of the native surface (left) differs by only 0.5mm, whereas there is greater disagreement on the fracture surface (right).

### Pre-Operative Utility

Clinical evidence suggests that anatomic fracture reduction is very important, especially for the joint surface. Displaced articular fragments may elevate cartilage contact stresses and predispose the joint to degeneration. Some joints tolerate incongruity better than others. While the tibial plateau may be more forgiving, some joints such as the hip have been shown to poorly tolerate as little as 1 mm of residual displacement after fracture [8]-[9]. Even without preferential weighting for articular surface alignment, the puzzle solution achieved sub-millimeter accuracies for non-deformed articular fragments. However, it would be useful to have the capability to weight articular surfaces in future puzzle solvers, whether it is weighting the articular

alignment error more heavily during optimization, or allowing for some flexibility in the native surface's alignment.

When bones fracture as a brittle solid, fragment native surfaces match precisely to the intact template in most cases. However, if fragments are plastically deformed, larger surface deviations will be observed. Since joint incongruities are particularly deleterious to the joint's long-term outcome, articular alignment errors were separately quantified, and compared to acute fracture severity. With a clear relationship between the puzzle solution's alignment error and fracture severity, the results from this work suggest that the likelihood for plastically deforming the joint surface increases with fracture energy and articular comminution (Figure 66 left). Since surgical reduction is greatly complicated when fragments are deformed, fracture severity may be a helpful tool for identifying which patients demand a puzzle solution.

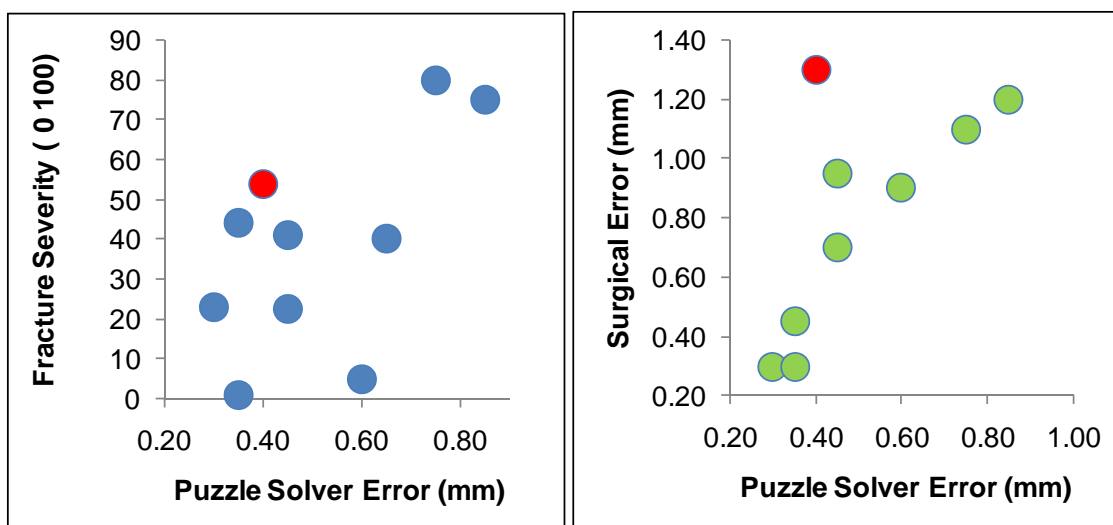


Figure 66 The puzzle solution's articular alignment error was associated with fracture severity (left), and with the actual incongruities after surgical reduction (right). Theoretically, a single case (red marker, Case ID: 9) could have been reconstructed to substantially greater accuracy than what was physically achieved.

Since plastic deformation explains much of the puzzle solution's error, it was not surprising that the surgeon was unable to completely restore the original anatomy. In order to measure how well the articular surface was surgically reduced, immediate post-operative CT scans were segmented and registered to the intact template (Figure 38). Surface deviations between the physical reconstruction and the template were calculated. The results from that analysis showed that surgical error was linearly related to puzzle solution error, but at a greater magnitude (Figure 66, right). Given that the puzzle solver works in an ideal virtual environment, unconstrained by physical realities (e.g. fragment collision), errors would be expected to be less than the surgeon's. However, the increase in error suggests that there is room for improving physical reconstructions.

While executing the perfect reduction may be physically impossible in some cases, puzzle solving can still be used to improve reduction outcomes, particularly by identifying difficult-to-appreciate bone defects. A frequent consideration in that regard arises from crushed/deformed fragments. A more in-depth comparison of the puzzle solution to what was actually achieved surgically further illustrates point (Figure 67). The surgically reduced tibia in Case 4 ended up shortened by more than 2.5 cm, an outcome with likely adverse biomechanical effects. By providing precise limb length and fragment displacement information, the puzzle solution could have enabled the surgeon to better restore the original anatomy. In Case 1, the puzzle solution showed an obvious articular defect. While perfectly repairing that defect would have been difficult if not impossible due to fragment plastic deformation, the defect was not detected intra-operatively. Had this unavoidable defect been appreciated in advance, biological intervention or engineered tissues might have been used to mitigate the associated incongruity. For Case 9, a metaphyseal void in the puzzle solution highlights a loss of bone. Had a puzzle solution been available, this structural deficiency could likely have been recognized in advance, giving the surgeon the opportunity to have either planned an alternate fragment configuration, a different fixation technique, or a bone grafting solution. Unfortunately,

the physical reconstruction was less than ideal, with the joint surface angulated approximately  $30^\circ$  anteriorly (Figure 67) and substantial incongruities (Figure 66 red). Lastly, Case 8's original anatomy was restored both computationally and surgically. These cases illustrate that useful information can be gained from puzzle solutions where fragments do, and do not align perfectly. Whereas fewer complications would be expected in cases with perfect computational reductions, those where defects can be identified preoperatively deserve attention.

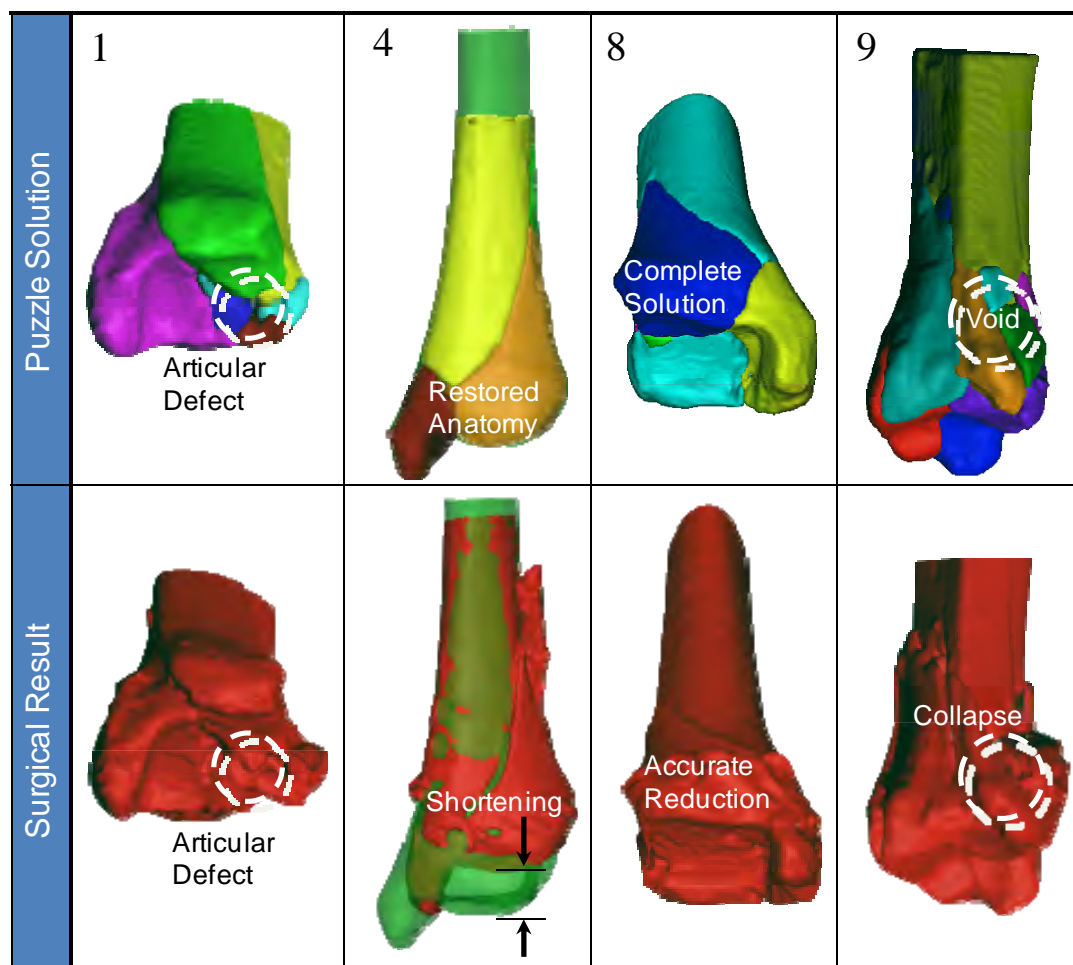


Figure 67 Four puzzle solutions are compared to what was achieved surgically. Inspection of the virtual solution provides prognostic information.

Besides severely comminuted fractures, puzzle-solving methods also hold attraction for more moderate fractures where the decision between operative and non-operative management is borderline. Key features that influence decision-making are often vague or difficult to assess from standard radiographic information [99]. Although the surgeon may have a general idea of how fragments fit together, a puzzle solution provides precise displacement, angulation, and depression data important for making well-informed decisions. For instance, one may not be able to appreciate the magnitude of depression in a tibial plateau fracture simply from traditional imaging, whereas puzzle solving could exactly quantify it in 3D.

### Clinical Translation

To further illustrate clinical practicality, a severe articular fracture case was puzzle solved prospectively (Figure 68). A 19 year old male presented with an open distal tibia fracture, sustained after jumping from a moving train. In addition to substantial articular fragmentation, the diaphysis was severely comminuted. For initial treatment, the fracture was spanned with an external fixator and antibiotic beads were implanted, followed by a CT scan. A complete puzzle solution was obtained within four hours and was provided to the surgeon one week prior to definitive surgery. Execution of the entire puzzle solving process in such a brief time period affords ample time for its integration into surgical planning. It is important to recognize that the comminuted diaphyseal fragments would likely not be reduced clinically. These types of fragments are often devitalized and contaminated, and if left inside the body, would likely cause a severe infection that would jeopardize the limb. Virtual reconstruction was performed to provide evidence that puzzle solving algorithms are effective even in the most challenging of cases.

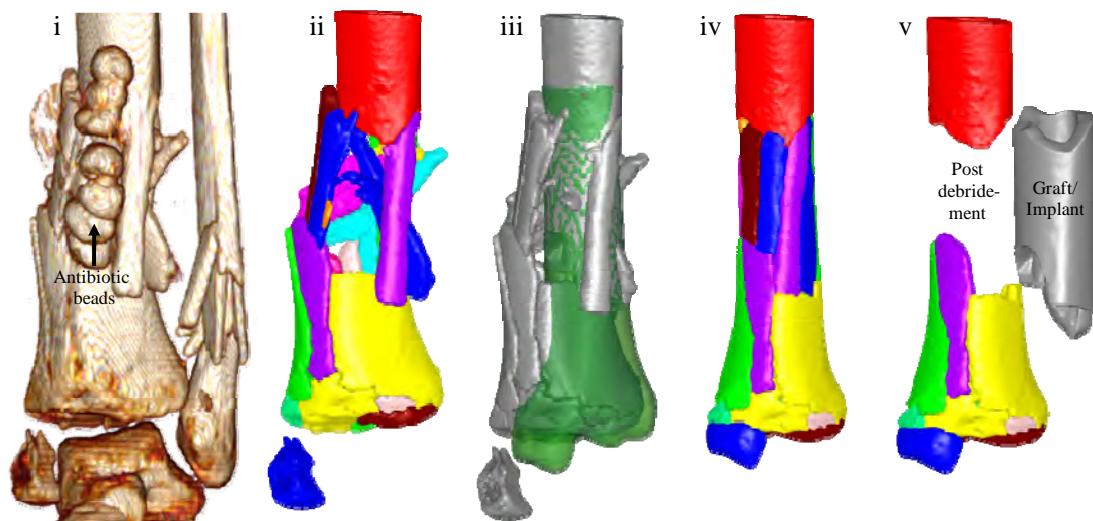


Figure 68 Application of puzzle solving technology to a prospective case. CT data (i) is segmented (ii) and fragment native surfaces are aligned to an intact template (iii-iv). Custom implants can be designed to fill segmental bone defects (v).

The presence of highly comminuted and compromised fragments illustrates another aspect of puzzle solving's clinical application. Puzzle solving may be used to pre-operatively distinguish between those fragments that are biologically functional and those that are likely devitalized fragments. Problematic fragments would be flagged for debridement and the chances for infection might be correspondingly reduced. Furthermore, this case demonstrates how puzzle solving can be used to design custom implants for segmental bone defects. Since bone is often missing or has to be surgically removed, allograft bone is typically used to fill the void and promote bone healing. However, the construct may be initially unstable. An implant with immediate load bearing capabilities, such as trabecular metal, may offer a solution to this difficult problem. From the puzzle solution, the bone defect's geometry can be precisely modeled, and an implant can be manufactured with rapid prototyping.

In future clinical practice, it is crucial that puzzle solving be applicable to joint injuries besides the tibial plafond fracture. The train jumper case provided the impetus to

investigate alternative anatomic applications. Before surgery, virtual reconstructions for the fibula and tibia were requested. The clinician performed a multi-stage treatment approach: once soft-tissue swelling had subsided, the fibula was fixed first, and then the tibia was reduced days later. In the first non-tibial puzzle solving application, the fibula was successfully reduced using the native to template alignment method. In addition to providing useful visualization, precise displacement and re-positioning information was provided days prior to surgery (Figure 69). Considering the fibula's cylindrical shape, new alignment challenges were expected. However, current puzzle solving methods were able to accurately reduce displaced fibular fragments. Although the fibula was not comminuted, it was greatly displaced. If mal-reduced, the tibia's subsequent alignment would be negatively affected. Therefore, it was essential that the fibula was aligned correctly. Unfortunately, assessment of the surgical results cannot be made since post-op CTs were not obtained. While surgically reducing the fibula is possible without assistance, puzzle solving, coupled with a navigation system or with additional surgical guides, could ensure that proper alignment is achieved. Similarly, less complex injuries such as displaced femoral neck fractures could benefit from puzzle solving with future advancements. Alignment and length deformities could be avoided by linking pre-operative models to intra-operative data. As for other high-energy joint fractures, the more frequent tibial plateau fracture is an excellent injury in which to investigate alternative puzzle solving applications.

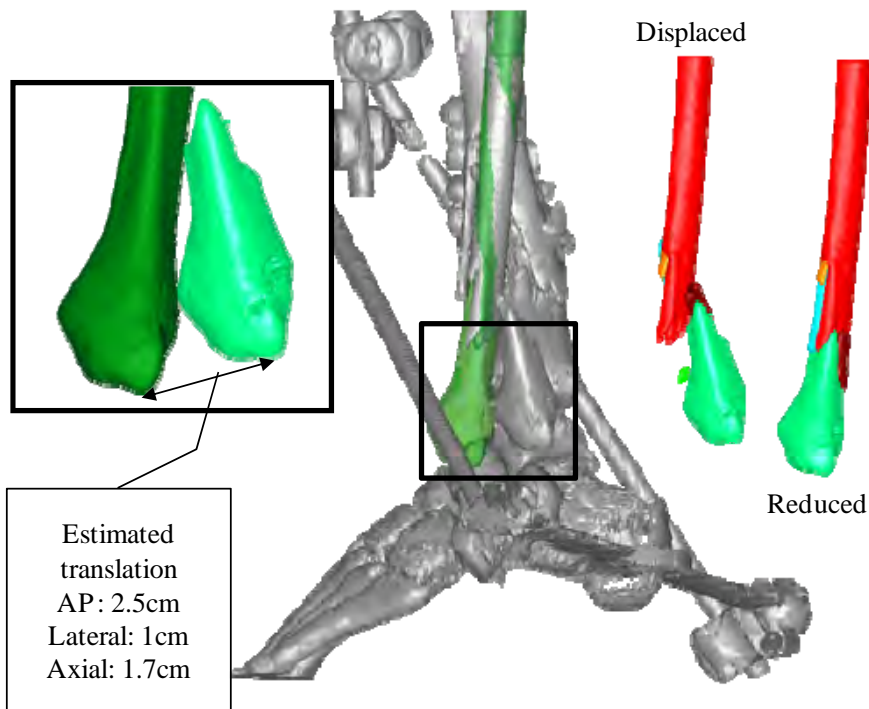


Figure 69 Puzzle solving methods successfully reconstructed a comminuted fibula. Detailed information was provided to the surgeon prior to surgery.

In addition to civilian trauma, puzzle solving and its derivative technologies could aid treatment of combat-related injuries. Wounds sustained from ballistic impacts and explosions are especially susceptible to contamination, infection, and bone loss. As of 2006, 5684 soldiers experienced severe limb injuries in Iraq and Afghanistan, and of those injuries, 7.4% underwent amputation of the lower wrist or ankle joint [100]. While many of those limbs could not be salvaged, it is likely that some could have been surgically repaired if more advanced technologies had been available. In order to investigate whether or not current puzzle solving methods are capable of reconstructing those complicated injuries, cadaver ballistic testing was performed on two fresh frozen ankles. The specimens were shot at 5m range, with a 45 caliber hollow-point round. Afterward, the specimen was CT scanned, segmented, and virtually reconstructed (Figure 70). From inspection of the CT volume rendering and the specimen itself, it can be

appreciated that the distal tibia was severely comminuted, with considerable dusting. In an actual injury, the small bone particles and fragments would likely be surgically excised to prevent infection. Therefore, those fragments were subjectively identified and removed in the virtual environment. The remaining bone fragments were then aligned to the pre-fractured geometry, using previously established puzzle solving methods. Compared to the civilian injuries, a greater degree of manual intervention was required, mostly due to the small size and planar shape of some fragments. However, the puzzle solving methods were able to accurately align the larger articular and metaphyseal fragments automatically. In addition to valuable fragment positioning instructions, the pre-operative CT segmentation and virtual reconstruction data would be very helpful for guiding the debridement and stabilization process. Although this injury challenged current capabilities, these results demonstrate puzzle solving's utility in the most severe of trauma cases where limb salvage would still be contemplated.

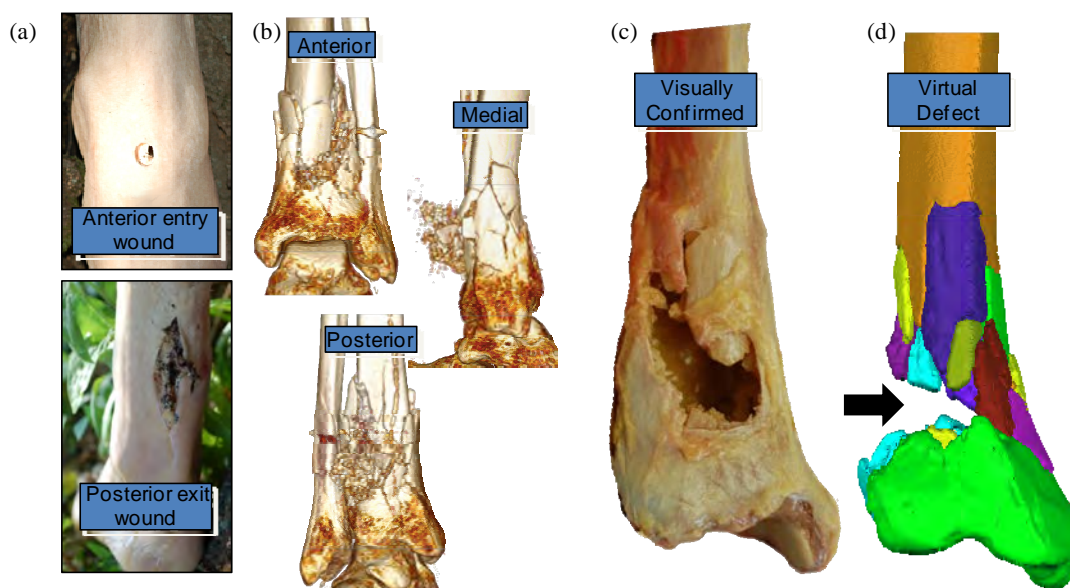


Figure 70 A cadaver ankle was shot with a 45 caliber round to produce a typical ballistic injury encountered in combat (a). CT data (b) and physical inspection (c) reveal a severely comminuted fracture with a large posterior defect.

### Fracture Energy and Injury Severity Assessment

The algorithms developed for puzzle solving also improve fracture severity assessments. Puzzle solving based fracture energy and 3D articular comminution metrics are not subject to the theoretic limitations of previous methods. Since bone density measures along fracture edges are altered by partial volume effects, derivation of local energy release rates is unreliable. For that reason, a heuristic classification scheme was previously developed to label fragment surfaces as dense cortical, less dense cortical and cancellous bone. Energy release rates for each tissue type were derived from bone density approximations. Fracture energy was then quantified by scaling fragment surface areas by those rates. With puzzle solving, reconstructed fracture surfaces were registered to the intact CT data where partial volume effects were negligible, thus enabling the derivation of more dependable voxel-by-voxel energy release rates. In addition to possible rate misestimates, previous fracture energy measures may have been confounded by inaccurate intact surface energies. Rather than calculating the cumulative energy difference between fractured and intact limbs, puzzle solving only quantifies fracture surface energies, thereby making it a more direct measurement method. Given the limitations of previous methods, it was surprising to discover that puzzle solving based fracture energies agreed well with those less sophisticated methods (concordance = 93%).

With a concordance of 83%, acute severity scores (combined fracture energy and articular comminution) also agreed well with previous reports. Both previous and current severity assessment methods demonstrate a strong capacity for predicting joint degeneration. For eight of the nine patients with two year follow-ups, both severity measures accurately identified PTOA prone patients from a severity threshold -- the single outlier is discussed later (Figure 71). Knowing pre-operatively the probability for degeneration could have implications for customizing treatments and interventions. For instance, those severely injured joints that have a high probability for rapid PTOA

development may be better treated with arthrodesis, or a reduction approach that prioritizes complication prevention, rather than precise anatomical reduction. But in cases with a severity score near the PTOA threshold, there should be greater effort to reduce the articular surface more precisely.

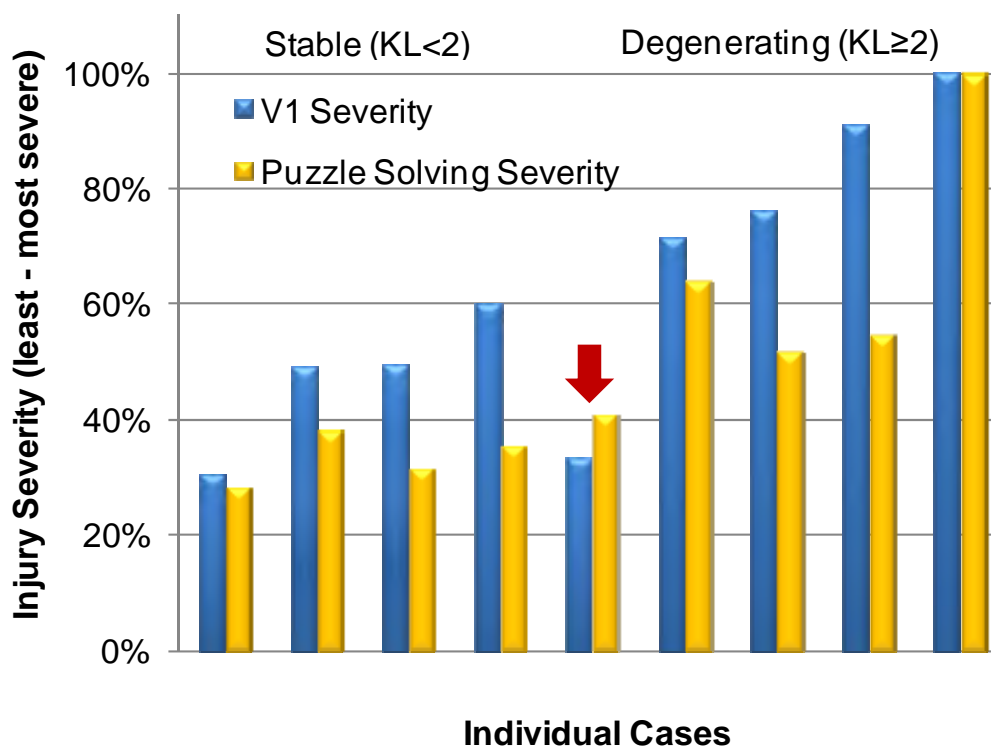


Figure 71 Puzzle solving derived injury severity metrics are compared to those established in earlier work. Although the magnitudes differ, each derivation accurately separates stable and arthritic joints by injury severity – except for one outlier. Both measured one case (red arrow, case ID 6) as having a relatively low severity injury, however that joint developed moderate PTOA after two years.

While fracture severity correlated with PTOA propensity for most patients, there was one outlier. The least severe fracture case (6) developed moderate PTOA after 2 years (Figure 71). There were either additional factors affecting the development of

PTOA, or these fracture severity metrics did not adequately capture the damage to the joint. With only two fragments, gross inspection of the CT volume rendering would suggest that this indeed a low severity (Figure 57). Upon closer inspection, there was substantial comminution within the joint's load bearing region (Figure 72 a). Since the fracture surfaces of these fragments were relatively small, this localized comminution did not significantly elevate the fracture energy measurement. Although minor in relation to other cases, the new 3D articular comminution metric did indicate there to be a more severe injury (Figure 59 right). The virtual puzzle solution confirms that these small fragments are articular and originated in the weight bearing region of the joint (Figure 72c).

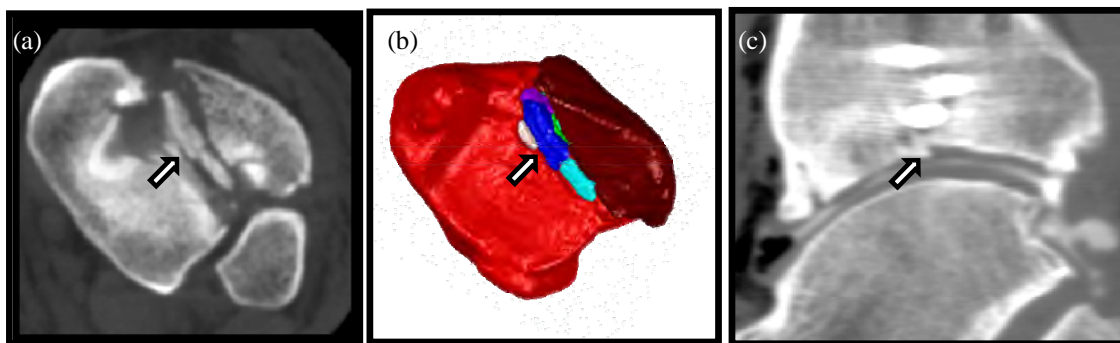


Figure 72 Localized articular comminution is evident on Case 6's injury CT (a) and on the virtually reconstructed plafond (b). Cartilage thinning is apparent in that region after two years with a dual contrast MDCT scan.

Case 6 also highlights a limitation to previous methods. A number of articular fragments in this case were relatively small and may have been displaced outside the 1.5mm measurement window. However, displacement does not affect the new puzzle solving method. Articular fracture edges are quantified regardless of spatial location. In addition to follow-up radiographs, this patient was also imaged two years after injury with dual contrast MDCT. This modality enables the demarcation of both osseous and

cartilage surfaces. Inspection of these data (Figure 72c) confirms that cartilage thinning is occurring in the anterior region (left side of image). It is also important to note that there is a residual incongruity (approximately 1mm) that likely elevated the cartilage contact stresses. It is probable that both articular comminution and residual incongruity contributed to the onset of PTOA in this joint. In order to better understand how articular comminution independently factors into cartilage degeneration, more discriminating measures are needed. Studies have shown that cartilage cells are injured and killed near fracture edges after impact [101]. Since loading these injured cartilage cells causes further damage, comminution within the weight bearing region would be especially deleterious. With the virtual reconstruction, cartilage fracture edges can be demarcated and registered to the pre-fracture state where loading conditions can be estimated. By deriving the location of articular comminution, puzzle solving offers new capabilities for investigating the key factors involved in PTOA propensity.

Articular deformation not only damages cartilage cells at the time of injury, but causes persistent damage by altering the joint's loading environment. As observed in surrogate testing, articular surfaces would have minimal alignment errors if the material fractured as a brittle solid and its native surface retained its pre-fracture shape. Since much of the error in articular alignment can be attributed to subchondral distortions, articular deformation can be estimated from puzzle solution assessments, and be used as another informative severity metric. While the amount of deformation is obviously linked to comminution for many cases, they can be considered separate factors. There may be some instances of severe deformation without substantial bony fragmentation, especially for patients with poorer bone quality. The results from this work suggest that there is some association between articular alignment error and PTOA severity (Figure 73). Although Case 3 did not follow that trend, its degeneration may be explained by the substantial amount of fracture energy (30.0J) that it absorbed. That patient was a young man who had excellent bone density. Without observable deformations, it can be

assumed that his tibia fractured as a brittle solid –another example of comminution and deformation being separate entities.

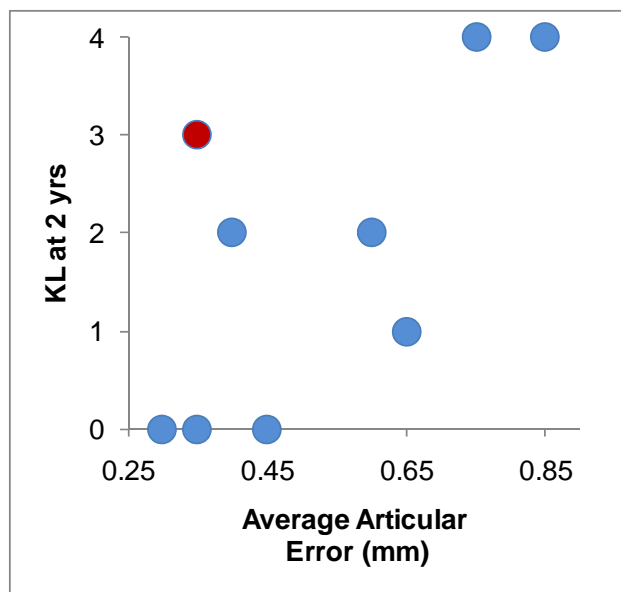


Figure 73 The average articular error in the virtual reconstructions was associated with the severity of PTOA as measured by KL at 2 years. One outlier (Red marker - Case 3) developed PTOA with minimal deformation, but that case also had the second greatest fracture energy (30J).

Numerous injury characteristics can now be precisely measured with puzzle solving. After the virtual reconstruction is obtained, fracture energy, deformation, the location and severity of articular comminution can be measured. In addition to severity metrics, measures of post-operative residual incongruities can now be made with minimal effort, thus enabling an investigation into the relative mechanical effects of acute fracture severity and chronic increased contact stress. As more cases are processed and analyzed, we can begin to identify which fracture features are most relevant to PTOA propensity and clinical outcomes.

### Surgical Simulation

This study was designed to objectively explore the utility of 3D puzzle solving in a simulated surgical setting. Along with fluoroscopic imaging, the surrogate foot and fracture models imitated many of the components encountered in the operating room (Figure 74). Key variables that reflected surgical complexity and surgeon skill were quantified for evaluating the utility of 3D puzzle solving. Even though this setup simplified some intra-operative components, the fundamentals were simulated: a 3D puzzle is reassembled without direct visualization.

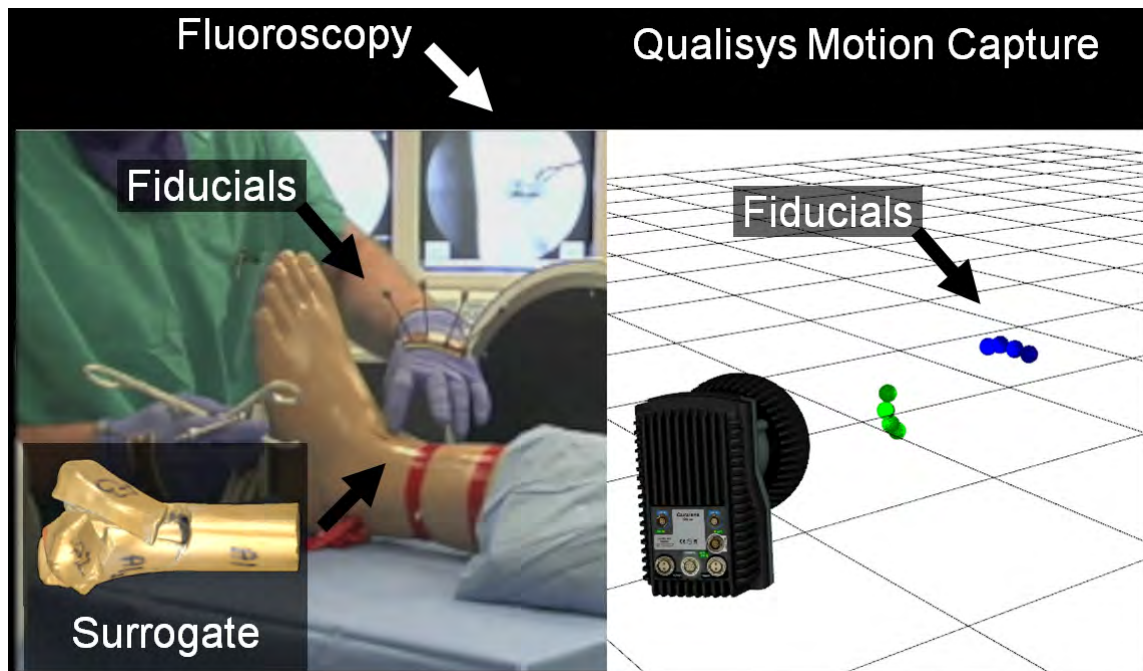


Figure 74 Surgical simulation was successfully completed in five sessions. Fractured surrogate tibias were percutaneously reduced under the guidance of fluoroscopy. Meanwhile, surgeon hand motions were tracked with a Qualisys motion capture system, and synchronized to the video recording.

The puzzle solving software presented a clear illustration of the fracture pattern and displacement in 3D. Versus inspection of 2D CT slices, that imaging information

was particularly helpful for identifying the instability of Pattern A's posterior-lateral fragment. Although puzzle solving allowed for individual fragments and other anatomy to be hidden, CT volume renderings would likely have provided similar utility for these specific fracture configurations. While puzzle solving is more suited for highly comminuted fractures, such cases are expected to be too challenging for this study. The large inter- and intra-surgeon variability in performance would likely confound any meaningful analysis. It is for that reason why fracture patterns A and B were chosen for this study. In future simulations, the 3 segment fracture could be configured differently to better demonstrate the value of puzzle solving. For instance, inverting an articular fragment could provide the added complexity that would exaggerate the differences in performance between groups. Even though such an occurrence might be clinically rare, a configuration where the puzzle solution is not immediately intuitive would better suit the objective of this specific study.

Due to the limited number of completed trials, conclusive statements about puzzle solving's clinical utility cannot yet be made. However, the preliminary results from this work suggest that puzzle solving was helpful in reducing fracture pattern A. Considering that pattern A was more complex than B, it would be expected that A's quality of reduction would be inferior. However, the alignment error between A and B were very similar (Table 4). Since four of the five sessions had the surgeon reduce pattern A with puzzle solving, it can be argued that puzzle solving at least partially compensates for the difference in complexity between the two. Of course this is presently only speculation. Once those five residents are tested a second time, the effects of having a puzzle solution can be better assessed.

Independent of puzzle solving's contribution, the particular reduction technique appeared to have an effect on success or failure of reduction. Some surgeons chose to use tenaculums to manipulate and position fragments, a claw like device that pierces the skin and grasps upon the fragment. For specimen A, it seemed that the most effective

approach was to drill a k-wire through the poster-lateral fragment, and use the k-wire as a joystick to precisely position it. In addition to quantifying utility, this surgical simulation protocol may be quite effective for investigating optimal surgical approaches and reduction techniques for specific fracture patterns.

In retrospect, the fracture pattern of specimen A may have been too difficult for these early stages of testing. The highly unstable posterior-lateral fragment was particularly difficult to reduce due to its size, location, and ability to move freely (no soft-tissue attachments) (Figure 75). While *in vivo* fragments can have the same problematic characteristic, that added complexity may have confounded the already difficult to quantify outcome variables. Some surgeons also noted that in the operating room, a posterior incision would have been made in order to gain access and directly reduce that fragment. However, the experimental protocol prohibited additional nicks or incisions. It was believed reduction would be simplified with puzzle solving in that situation, thereby exaggerating differences between trials with versus without assistance. Although the surgeon was able to better appreciate the fracture pattern and the shape of the fragment with puzzle solving's visualization platform, the virtual model no longer represented the fragment's configuration after reduction started. Although difficult, it was possible to reduce pattern A, and 4 of the 5 surgeons did so. Furthermore, the surgeon who failed had had the specimen reduced and verbally stated that the reduction was acceptable. However, in order to perfect the articular surface's congruity, further manipulations were made that resulted in the deterioration and eventual failure of the reduction. Future simulation studies should reconsider specimen A's pattern, and attempt to make all fracture patterns similar in reduction complexity. Adding navigation capabilities to puzzle solving is a possible approach to improving intra-operative performance. The failure of Resident 2 to penetrate the posterior fragment with the k-wire is another example of the need to link pre-operative models to intra-operative positioning

information. However, tracking comminuted fragments *in vivo* is a nascent field, even in the research setting.

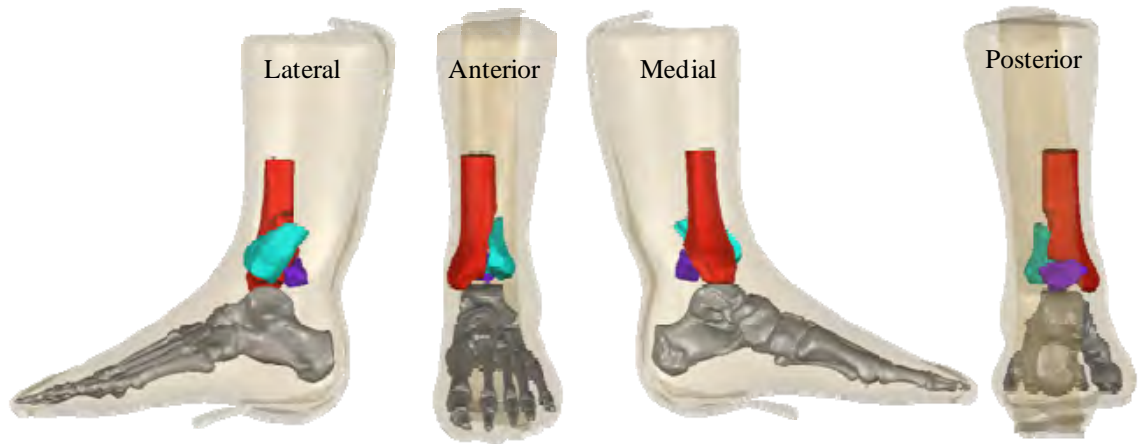


Figure 75. Fracture pattern A is shown with adjacent anatomy. The posterior-lateral fragment (purple) was relatively difficult for all surgeons to reduce due to its not having a lock-and-key fit.

## CHAPTER 6 - LIMITATIONS

Of course there are limitations to the current methods. In the present embodiment, the puzzle solutions are “end stage,” with no account taken as to how to physically achieve that target configuration. The surgical approach and the status of the local neurovascular structures and other surrounding soft tissues will greatly affect how the fragments can move in space. Future embodiments of the algorithm ideally should incorporate such anatomic considerations in calculating feasible/optimal trajectory paths and sequences.

Matching fragments’ native surfaces to an intact template may result in suboptimal consequences, mainly inter-fragmentary gaps. While custom implants may fill large defects, smaller gaps between fracture surfaces present stability concerns. Without fragment contact, the hardware has to bear greater loads and is therefore susceptible to failure. Since bringing fracture surfaces into contact may distort the joint surface, there needs to be some method improving mechanical stability when adjacent fragments are not in compression. A grout like material may be the solution to this problem. Once fragments are reduced such that normal anatomy is restored, some grafting material may be injected into the spaces to not only improve acute stability, but also to promote healing with some biologic agent. A material such as Osteotech’s© Plexur grafting composite could be a potential candidate.

Current puzzle solving methods are limited by their reliance on the contralateral limb being intact. Although rare, bilateral fractures therefore are not amenable to analysis with this methodology. Distal tibia surface area has been shown to be predictable with allometric scaling ([102]). Generic population-based templates could potentially be used in such cases, but the similarity in tibia shapes across patients would need to be documented beforehand. To investigate that possibility, a generic tibia was created from the intact data of these ten patients. Using Geomagic, all intact tibias were made to be

right limbs, and then scaled in three-dimensions to correspond to a 5'8" person (tibia length =  $0.285 \times \text{height}$  (Associates W, 1978)). The ten tibial plafond surfaces were globally registered and then averaged to obtain a generic tibia model. The generic tibia was scaled back for each patient and the surface deviation between the generic and actual intact surfaces was calculated. From the results of this preliminary work, the distal tibia is similar in shape for patients of different ages and sexes when scaled for height. With only an average surface deviation of  $0.69 \pm 0.7\text{mm}$ , these results suggest that generic population based tibias might be used in bilateral fracture cases. If generic tibias were to be used in puzzle solving, further research is warranted for determining how generic tibias could better model specific patients with additional anthropometric parameters.

Although alignment to an intact template offers an effective strategy, it is also important to consider how well the fragments' internal fracture surfaces fit together. If substantial inter-fragmentary gaps would exist clinically after native surface alignment, additional fragment repositioning or supplemental bone grafting might well be needed for adequate stability. While this was not an issue with most fragments in the present cases, the techniques reported for internal fragment alignment accuracy in this study could straightforwardly identify situations of bone loss (either existing, or necessitated by contamination or necrosis requiring fragment removal), and thereby provide the surgeon with a precise description of the void's geometry. To puzzle solve such cases, both native surface and inter-fragmentary alignments need to be taken into account, thus requiring a dual strategy that simultaneously combines both matching to the intact contralateral template and alignment along inter-fragmentary boundaries.

While useful in its current capacity, puzzle solving has the potential to mature into an essential component for use in treating highly comminuted articular fractures. Presently, puzzle solving provides only final destination information from a pre-operative CT. A future step for 3D puzzle solving could be intra-operative integration, to help guide the actual surgical reduction in real time. This would require substantial

developments not only in the puzzle solving algorithms themselves, but also in the imaging modalities that link the virtual and physical worlds. As surgical navigation and imaging systems become more advanced, this long-term vision becomes more feasible. In an intermediate step, it is feasible to track a subset of the total number of fragments with a motion capture system. Similar to the setup in an in-vitro study performed by Khalafi and Citak, reflective markers that are rigidly attached known landmarks could be tracked intra operatively to ensure that at least limb length and alignment was restored [103]. A possible procedure could begin with a full pre-operative virtual reconstruction. During definitive fixation, the articular block would be reconstructed and pinned. Reflective markers would then be attached to a pin fixed to the articular block, and to a pin in the diaphysis. Then intra-operative imaging would be taken and registered to the pre-operative models. Using a motion capture system, real time positioning feedback could be provided. Although this proposed method would not necessarily affect joint congruity, it would improve alignment and length, important factors for restoring joint function. In the short-term, puzzle solving's pre-operative utility is not limited to simply generating the ideal reduction. It also provides input data for computationally modeling possible fixation constructs, and for assessing their initial mechanical stability.



Figure 76 Restoration of normal anatomy is measured with navigation reference markers.

## CHAPTER 7 - CONCLUSION

Currently, surgeons reduce fractures by assessing fragment inter-digitations visually and by touch, typically by trial and error. Unfortunately, each such “error” prolongs the procedure and adds to the surgical trauma to the wound bed. In addition to iatrogenic trauma, patient outcomes are adversely affected by residual incongruities. While fluoroscopy has been useful for advancing the use of limited approaches, the process of solving a three-dimensional puzzle using two-dimensional images remains very challenging. In the distant future, it seems likely that these issues will be resolved by incorporating some type of computer assistance. Although the particulars of that technology can now only be imagined, it is safe to assume that future surgeons will not be manually reducing comminuted articular fractures without guidance. The tools and algorithms developed here provide the groundwork for progressing toward that future.

Much of the clinical practicality of puzzle solving hinges upon the development of an effective CT segmentation method. Extracting accurate bone fragment geometries with minimal user intervention was a major advancement. The laborious slice-by-slice approach in previous methods would have severely hindered the development, and the ultimate relevance of these puzzle solving methods. The ability to process image data in less than one half hour greatly expands the opportunities for research and clinical investigation. While the watershed algorithm has proven to be effective in the distal tibia, it remains to be tested in other anatomy. Even though other joints are expected to present new challenges, their composition and fracture behavior should be similar to the distal tibia. Therefore, the *a priori* knowledge that proved so useful in system development for the ankle should also be applicable to other joints. In addition to supporting puzzle solving, the watershed segmentation approach substantially expedites the objective assessment of fracture severity.

In view of the high rates of both short and long term complications, it is surprising that puzzle solving technology has sometimes encountered only tepid responses by some. It is true that many two or three segment fractures can be accurately reconstructed without assistance. However, the surgical simulation trials are demonstrating that presumably simple fractures can present considerable difficulties. Troubles in reducing Pattern A's problematic fragment led to extensive puncturing of the fragment and soft tissues. Even though four of those reductions were performed with 3D puzzle solving assistance, it is likely that the degree of iatrogenic trauma would have been even greater without puzzle solving -- a pre-operative plan can provide only so much benefit. It is imperative that future reduction procedures incorporate better intra-operative feedback.

Moreover, more precise knowledge of where a fragment is in space, and where it needs to be positioned, will require future significant technological advancements. Potentially, shape matching methods could be used to register pre-operative models to intra-operative fluoroscopic information. The surrogate model and simulation setup are an ideal platform for piloting that investigation. Computational and logistical feasibility could be established without confounding *in vivo* complexities. Regardless of modality, the future of puzzle solving likely will involve real-time guidance. The development of pre- and intra-operative guidance systems will enable new and exciting fracture reconstruction breakthroughs. For example, the frequency of non-union and hardware failure could be greatly reduced with fixation constructs designed and implanted with technologies based upon puzzle solving. While there are limitations that need attention before broad clinical application, results from this work suggest that 3D puzzle solving offers a powerful new tool for enhancing surgical reconstruction of complex peri-articular fractures.

## APPENDIX

A. CLASSIFICATION RESULTS

Table A1 Classification results with patient-specific vs. compiled training models are provided.

| Patient Specific Training |                     |          |            |  |          |            |  |            |
|---------------------------|---------------------|----------|------------|--|----------|------------|--|------------|
| Case                      | Average Probability |          |            | % Area Correctly Classified with Certainty |          |            | % Area Incorrectly Classified with Certainty |            |
|                           | Articular           | Fracture | Periosteal | Articular                                  | Fracture | Periosteal | Articular                                    | Periosteal |
| 1                         | 92%                 | 96%      | 96%        | 56%  | 14%      | 70%        | 19%  | 17%        |
| 2                         | 97%                 | 96%      | 98%        | 87%  | 14%      | 87%        | 6%   | 5%         |
| 3                         | 91%                 | 98%      | 96%        | 58%  | 6%       | 77%        | 11%  | 12%        |
| 4                         | 97%                 | 95%      | 97%        | 78%  | 14%      | 84%        | 11%  | 8%         |
| 5                         | 98%                 | 88%      | 95%        | 90%  | 39%      | 77%        | 3%   | 6%         |
| 6                         | 96%                 | 97%      | 90%        | 76%  | 11%      | 52%        | 10%  | 18%        |
| 7                         | 98%                 | 94%      | 97%        | 91%  | 19%      | 83%        | 3%   | 6%         |
| 8                         | 98%                 | 96%      | 96%        | 88%  | 13%      | 79%        | 7%   | 9%         |
| 9                         | 96%                 | 96%      | 97%        | 59%  | 14%      | 88%        | 28%  | 1%         |
| 10                        | 95%                 | 87%      | 91%        | 74%  | 38%      | 69%        | 11%  | 2%         |
| Average                   | 96%                 | 94%      | 95%        | 76%  | 18%      | 77%        | 11%  | 9%         |
| Compiled Training         |                     |          |            |  |          |            |  |            |
| Case                      | Average Probability |          |            | % Area Correctly Classified with Certainty |          |            | % Area Incorrectly Classified with Certainty |            |
|                           | Articular           | Fracture | Periosteal | Articular                                  | Fracture | Periosteal | Articular                                    | Periosteal |
| 1                         | 91%                 | 89%      | 88%        | 71%  | 36%      | 42%        | 2%   | 20%        |
| 2                         | 84%                 | 92%      | 93%        | 44%  | 25%      | 69%        | 4%   | 9%         |
| 3                         | 94%                 | 94%      | 95%        | 79%  | 18%      | 53%        | 3%   | 30%        |
| 4                         | 84%                 | 93%      | 92%        | 41%  | 19%      | 60%        | 5%   | 7%         |
| 5                         | 86%                 | 88%      | 92%        | 51%  | 39%      | 72%        | 6%   | 3%         |
| 6                         | 89%                 | 91%      | 88%        | 36%  | 30%      | 57%        | 31%  | 6%         |
| 7                         | 87%                 | 92%      | 93%        | 55%  | 26%      | 70%        | 3%   | 8%         |
| 8                         | 95%                 | 89%      | 89%        | 80%  | 35%      | 58%        | 6%   | 8%         |
| 9                         | 93%                 | 87%      | 92%        | 76%  | 41%      | 63%        | 1%   | 13%        |
| 10                        | 91%                 | 90%      | 88%        | 69%  | 32%      | 50%        | 3%   | 10%        |
| Average                   | 89%                 | 91%      | 91%        | 60%  | 30%      | 59%        | 6%   | 11%        |

B. OSTATS

Table B1 Detailed global 5 point rating scale and pass/failure score for Objective Structured Assessment of Technical Skill.

|   |   |          |  |          |  |
|---|---|----------|--|----------|--|
| <b>Respect for tissue</b>                     | Often used unnecessary force on tissue or caused damage by inappropriate use of instruments<br><b>1</b> | <b>2</b> | Careful handling of tissue but occasionally caused inadvertent damage<br><b>3</b>                    | <b>4</b> | Consistently handled tissues appropriately, with minimal damage<br><b>5</b>                      |
| <b>Time and motion</b>                        | Many unnecessary moves<br><b>1</b>  | <b>2</b> | Efficient time and motion, but some unnecessary moves<br><b>3</b>                                    | <b>4</b> | Economy of movement and maximum efficiency<br><b>5</b>   |
| <b>Instrument handling</b>                    | Repeatedly makes tentative or awkward moves with instruments<br><b>1</b>                                | <b>2</b> | Competent use of instruments, although occasionally appeared stiff or awkward<br><b>3</b>            | <b>4</b> | Fluid moves with instruments and no awkwardness<br><b>5</b>                                      |
| <b>Knowledge of instruments</b>               | Frequently asked for the wrong instrument or used an inappropriate instrument<br><b>1</b>               | <b>2</b> | Knew the names of most instruments and used appropriate instrument for the task<br><b>3</b>          | <b>4</b> | Obviously familiar with the instruments required and their names<br><b>5</b>                     |
| <b>Flow of operation and forward planning</b> | Frequently stopped operating or needed to discuss next move<br><b>1</b>                                 | <b>2</b> | Demonstrated ability for forward planning with steady progression of operative procedure<br><b>3</b> | <b>4</b> | Obviously planned course of operation with effortless flow from one move to the next<br><b>5</b> |
| <b>Knowledge of specific procedure</b>        | Deficient knowledge. Needed specific instruction at most operative steps<br><b>1</b>                    | <b>2</b> | Knew all important aspects of the operation<br><b>3</b>  | <b>4</b> | Demonstrated familiarity with all aspects of the operation<br><b>5</b>                           |
| <b>Overall, Pass or Fail</b>                  | Pass  |          | Fail   |          |  |

**C. SURGICAL SKILLS RUBRIC**

Table C1 Grading for surgeon performance.

| <b>Surgical Simulation Grading</b> |                            |                       |
|------------------------------------|----------------------------|-----------------------|
| <b>Weighting</b>                   | <b>Criteria</b>            | <b>Points (1 - 5)</b> |
| 1                                  | Duration (minutes)         |                       |
|                                    | 0 - 15                     | 5                     |
|                                    | 16-20                      | 4                     |
|                                    | 21-25                      | 3                     |
|                                    | 26-30                      | 2                     |
|                                    | >30                        | 1                     |
| 1                                  | Average error (mm)         |                       |
|                                    | 0.0 - 0.5                  | 5                     |
|                                    | 0.51 - 1.0                 | 4                     |
|                                    | 1.01 - 1.5                 | 3                     |
|                                    | 1.51 - 2.0                 | 2                     |
|                                    | >2.0                       | 1                     |
| 1                                  | Max Step-Off (mm)          |                       |
|                                    | 0.0 - 1.0                  | 5                     |
|                                    | 1.01 - 2.0                 | 4                     |
|                                    | 2.01 - 3.0                 | 3                     |
|                                    | 3.01 - 4.0                 | 2                     |
|                                    | >4.0                       | 1                     |
| 1                                  | Observer Rating<br>(OSATS) |                       |
|                                    | 24 - 30                    | 5                     |
|                                    | 18 - 23                    | 4                     |
|                                    | 12 - 17                    | 3                     |
|                                    | 6 - 11                     | 2                     |
|                                    | < 5                        | 1                     |
| 1                                  | Motion (Percentile)        |                       |
|                                    | 80th                       | 5                     |
|                                    | 60th                       | 4                     |
|                                    | 40th                       | 3                     |
|                                    | 20th                       | 2                     |
|                                    | 10th                       | 1                     |
|                                    | Total                      | _____                 |
|                                    |                            | 25                    |

## REFERENCES

1. Brown, T.D., et al., *Posttraumatic osteoarthritis: a first estimate of incidence, prevalence, and burden of disease*. J Orthop Trauma, 2006. **20**(10): p. 739-44.
2. Anderson, D.D., et al., *Is elevated contact stress predictive of post-traumatic osteoarthritis for imprecisely reduced tibial plafond fractures?* Journal of Orthopaedic Research, 2010: p. n/a-n/a.
3. Heim, U., *The Pilon Tibial Fracture*. 1995, Berlin: Springer-Verlag.
4. Schmidt, A., C. Finkemeier, and P. Tornetta III, *Treatment of closed tibial fractures*. The Journal of Bone and Joint Surgery, 2003. **85**(2): p. 352.
5. Ruedi, T. and M. Allgower, *The operative treatment of intra-articular fractures of the lower end of the tibia*. Clinical Orthopaedics & Related Research, 1979. **138**: p. 105.
6. Dirschl, D., et al., *Articular fractures*. Journal of the American Academy of Orthopaedic Surgeons, 2004. **12**(6): p. 416.
7. Watson, J.T., et al., *Pilon fractures. Treatment protocol based on severity of soft tissue injury*. Clin Orthop Relat Res, 2000(375): p. 78-90.
8. Marsh, J.L., et al., *Articular Fractures: Does an Anatomic Reduction Really Change the Result?* The Journal of Bone and Joint Surgery, 2002. **84-A**(7): p. 1259-71.
9. Matta, J.M., *Fractures of the acetabulum: accuracy of reduction and clinical results in patients managed operatively within three weeks after the injury*. J Bone Joint Surg Am, 1996. **78**(11): p. 1632-1645.
10. Brown, T., et al., *Contact stress aberrations following imprecise reduction of simple tibial plateau fractures*. Journal of Orthopaedic Research, 1988. **6**(6): p. 851-862.
11. Li, W., et al., *Patient-specific finite element analysis of chronic contact stress exposure after intraarticular fracture of the tibial plafond*. Journal of Orthopaedic Research, 2008. **26**(8): p. 1039-1045.
12. Jones, S., et al., *Triplane fractures of the distal tibia requiring open reduction and internal fixation:: Pre-operative planning using computed tomography*. Injury, 2003. **34**(4): p. 293-298.
13. Thomas, T., et al., *A Computational/Experimental Platform for Investigating Three-Dimensional Puzzle Solving of Comminuted Articular Fractures* Comput. Methods Biomech. Biomed. Engin., 2010: p. In Press.
14. Sands, A., et al., *Clinical and functional outcomes of internal fixation of displaced pilon fractures*. Clin Orthop Relat Res, 1998(347): p. 131-7.
15. Bone, L.B., *Fractures of the tibial plafond. The pilon fracture*. Orthop Clin North Am, 1987. **18**(1): p. 95-104.

16. Seggl, W., R Szyszkowitz, W Grechenig *Tibial pilon fractures* CURRENT ORTHOPAEDICS, 1999. **13**: p. 42 - 52.
17. Bonar, S.K. and J.L. Marsh, *Tibial Plafond Fractures: Changing Principles of Treatment*. Journal of the American Academy of Orthopaedic Surgeons, 1994. **2**(6): p. 297-305.
18. Germann, C.A., et al., *Orthopedic pitfalls in the ED: tibial plafond fractures*. Am J Emerg Med, 2005. **23**(3): p. 357-62.
19. Blauth, M., et al., *Surgical options for the treatment of severe tibial pilon fractures: a study of three techniques*. Journal of Orthopaedic Trauma, 2001. **15**(3): p. 153.
20. Gustilo, R.B., *Prevention of infection in the treatment of one thousand and twenty-five open fractures of long bones: retrospective and prospective analyses*, in *The Journal of Bone and Joint Surgery*. 1976, JBJS. p. 453-458.
21. Tscherne, H. and L. Gotzen, *Fractures with soft tissue injuries*. 1984: Springer.
22. Marsh, J., et al., *Use of an articulated external fixator for fractures of the tibial plafond*. The Journal of Bone and Joint Surgery, 1995. **77**(10): p. 1498.
23. Ruff, C.B. and F.P. Leo, *Use of computed tomography in skeletal structure research*. Yearbook of Physical Anthropology, 1986. **29**: p. 181-196.
24. Hopper, K.D., M.P. Wang, and A.R. Kunselman, *The use of clinical CT for baseline bone density assessment*. J Comput Assist Tomogr, 2000. **24**(6): p. 896-9.
25. Lai, Y.M., et al., *Regional differences in cortical bone mineral density in the weight-bearing long bone shaft--a pQCT study*. Bone, 2005. **36**(3): p. 465-71.
26. Ciarelli, M.J., et al., *Evaluation of orthogonal mechanical properties and density of human trabecular bone from the major metaphyseal regions with materials testing and computed tomography*. J Orthop Res, 1991. **9**(5): p. 674-82.
27. Rho, J.Y., M.C. Hobatho, and R.B. Ashman, *Relations of mechanical properties to density and CT numbers in human bone*. Med Eng Phys, 1995. **17**(5): p. 347-55.
28. Snyder, S.M. and E. Schneider, *Estimation of mechanical properties of cortical bone by computed tomography*. J Orthop Res, 1991. **9**(3): p. 422-31.
29. McFerran, M.A., et al., *Complications encountered in the treatment of pilon fractures*. J Orthop Trauma, 1992. **6**(2): p. 195-200.
30. Ovadia, D.N., *Fractures of the tibial plafond*, in *The Journal of Bone and Joint Surgery*. 1986, JBJS. p. 543-551.
31. Buckwalter, J.A. and T.D. Brown, *Joint injury, repair, and remodeling: roles in post-traumatic osteoarthritis*. Clin Orthop Relat Res., 2004(423): p. 7-16.

32. Anderson, D.D., et al., *Quantifying tibial plafond fracture severity: Absorbed energy and fragment displacement agree with clinical rank ordering*. Journal of Orthopaedic Research, 2008. **26**(8): p. 1046-52.
33. Gibson, L.J., *Biomechanics of cellular solids*. J Biomech, 2005. **38**(3): p. 377-99.
34. Thordarson, D.B., *Complications After Treatment of Tibial Pilon Fractures: Prevention and Management Strategies*. Journal of the American Academy of Orthopaedic Surgeons, 2000. **8**(4): p. 253-265.
35. Bhattacharyya, T., et al., *Complications associated with the posterolateral approach for pilon fractures*. J Orthop Trauma, 2006. **20**(2): p. 104-7.
36. Options, T., *Combined Percutaneous Internal and External Fixation of Type-C Tibial Plafond Fractures*. The Journal of Bone and Joint Surgery, 2002. **84**: p. 109-115.
37. Rüedi, T., et al., *AO Principles of Fracture Management: Principles/Specific Fractures*. 2007: Thieme Publishing Group.
38. Fractures, I., K. Koval, and R. Cantu, *Rockwood & Green's Fractures in Adults 6th Edition*.
39. Etter, C. and R. Ganz, *Long-term results of tibial plafond fractures treated with open reduction and internal fixation*. Archives of Orthopaedic and Trauma Surgery, 1991. **110**(6): p. 277-283.
40. Bonar, S. and J. Marsh, *Tibial plafond fractures: changing principles of treatment*. Journal of the American Academy of Orthopaedic Surgeons, 1994. **2**(6): p. 297.
41. Pugh, K., et al., *Tibial pilon fractures: a comparison of treatment methods*. The Journal of trauma, 1999. **47**(5): p. 937.
42. Teeny, S. and D. Wrs, *Open reduction and internal fixation of tibial plafond fractures: variables contributing to poor results and complications*. Clinical orthopaedics and related research, 1993. **292**: p. 108.
43. Borrelli, J. and E. Ellis, *Pilon Fractures : Assessment and Treatment*. Orthopedic Clinics of North America, 2002. **33**(1): p. 231-245.
44. Hahn, D.M., *Current Principles of Treatment in the Clinical Practice of Articular Fractures*. CLINICAL ORTHOPAEDICS AND RELATED RESEARCH, 2004. **423**: p. 27-32.
45. Pollak, A.N., et al., *Outcomes after treatment of high-energy tibial plafond fractures*. J Bone Joint Surg Am, 2003. **85-A**(10): p. 1893-900.
46. Teeny, S.M. and D.A. Wiss, *Open Reduction and Internal Fixation of Tibial Plafond Fractures: Variables Contributing to Poor Results and Complications*. SECTION I. Clinical orthopaedics and related research, 1993: p. 108-117.
47. Moskowitz, R.W., *Osteoarthritis Diagnosis and Medical/Surgical Management*. 4th ed. 2007, Philadelphia: Wolters kluwer, Lippincott Williams & Wilkins.

48. Saltzman, C.L., et al., *Impact of Comorbidities on the Measurement of Health in Patients with Ankle Osteoarthritis*. The Journal of Bone and Joint Surgery, 2006. **88**(11): p. 2366.
49. Borrelli Jr, J. and W.M. Ricci, *Acute Effects of Cartilage Impact*. Clinical Orthopaedics & Related Research, 2004. **1**(423): p. 33-39.
50. Duda, G.N., et al., *Chondrocyte death precedes structural damage in blunt impact trauma*. Clin Orthop Relat Res, 2001(393): p. 302-9.
51. Dirschl, D.R. and P.A. Dawson, *Injury severity assessment in tibial plateau fractures*. Clin Orthop Relat Res, 2004(423): p. 85-92.
52. Olson, S.A. and F. Guilak, *From articular fracture to posttraumatic arthritis: a black box that needs to be opened*. Journal of Orthopaedic Trauma, 2006. **20**(10): p. 661-662.
53. Crutchfield, E.H., et al., *Tibial pilon fractures: a comparative clinical study of management techniques and results*. Orthopedics, 1995. **18**(7): p. 613-7.
54. Macko, V.W., *The joint-contact area of the ankle. The contribution of the posterior malleolus*, in *The Journal of Bone and Joint Surgery*. 1991, JBJS. p. 347-351.
55. Carter, D.R., et al., *The mechanobiology of articular cartilage development and degeneration*. Clin Orthop Relat Res, 2004. **427**(suppl 427): p. S69-S77.
56. McKinley, T.O., et al., *Incongruity versus instability in the etiology of posttraumatic arthritis*. Clin Orthop Relat Res, 2004(423): p. 44-51.
57. Jeffrey, C., R., et al., *Radiographic evaluation of osseous displacement following intra-articular fractures of the distal radius: Reliability of plain radiography versus computed tomography*. The Journal of Hand Surgery, 1997. **22**(5): p. 792-800.
58. Pardo, X., et al., *A snake for CT image segmentation integrating region and edge information*. Image and vision computing, 2001. **19**(7): p. 461-475.
59. Yao, W., et al., *An estimation/correction algorithm for detecting bone edges in CT images*. IEEE transactions on medical imaging, 2005. **24**(8): p. 997.
60. Impoco, G., *Level Set Segmentation of Knee Bones Using Normal Profile Models*. Computer Vision/Computer Graphics Collaboration Techniques, 2009: p. 195-206.
61. Sebastian, T., et al., *Segmentation of carpal bones from CT images using skeletally coupled deformable models*. Medical Image Analysis, 2003. **7**(1): p. 21-45.
62. Fornaro, J., G. Székely, and M. Harders, *Semi-automatic Segmentation of Fractured Pelvic Bones for Surgical Planning*, in *Biomedical Simulation*, F. Bello and S. Cotin, Editors. 2010, Springer Berlin / Heidelberg. p. 82-89.

63. Tomazevic, M., et al., *Preoperative Planning Program Tool in Treatment of Articular Fractures: Process of Segmentation Procedure*, in *XII Mediterranean Conference on Medical and Biological Engineering and Computing 2010*, P.D. Bamidis and N. Pallikarakis, Editors. 2010, Springer Berlin Heidelberg. p. 430-433.
64. Freeman, H. and L. Garder, *Apictorial jigsaw puzzles: The computer solution of a problem in pattern recognition*. IEEE Transactions on Electronic Computers, 1964: p. 118-127.
65. da Gama Leitão, H. and J. Stolfi, *A multiscale method for the reassembly of two-dimensional fragmented objects*. IEEE Transactions on Pattern Analysis and Machine Intelligence, 2002: p. 1239-1251.
66. Wolfson, H., et al., *Solving jigsaw puzzles by computer*. Annals of Operations Research, 1988. **12**(1): p. 51-64.
67. McBride, J. and B. Kimia, *Archaeological Fragment Reconstruction Using Curve-Matching*, in *IEEE Workshop on Applications of Computer Vision in Archaeology; 2003*. 2003.
68. Cao, Y. and D. Mumford, *Geometric structure estimation of axially symmetric pots from small fragments*, in *Proceedings of the International Conference on Signal Processing, Pattern Recognition, and Applications*. 2002.
69. Üçoluk, G. and I. Hakk Toroslu, *Automatic reconstruction of broken 3-D surface objects*. Computers & Graphics, 1999. **23**(4): p. 573-582.
70. Willis, A., *Stochastic 3d geometric models for classification, deformation, and estimation*. 2004, Brown University: Providence, RI.
71. Willis, A., X. Orriols, and D. Cooper, *Accurately estimating sherd 3D surface geometry with application to pot reconstruction*, in *Conference on Computer Vision and Pattern Recognition (CVPR) Workshop*. 2003.
72. Willis, A. and D. Cooper, *Bayesian assembly of 3D axially symmetric shapes from fragments*. 2004, IEEE Computer Society; 1999.
73. Kong, W. and B. Kimia, *On solving 2D and 3D puzzles using curve matching*. 2001, IEEE Computer Society; 1999.
74. Papaioannou, G., E. Karabassi, and T. Theoharis, *Virtual archaeologist: Assembling the past*. IEEE Computer Graphics and Applications, 2001: p. 53-59.
75. Cooper, D., et al., *Bayesian virtual pot-assembly from fragments as problems in perceptual-grouping and geometric-learning*, in *International Conference on Pattern Recognition (ICPR)*. 2002. p. 297-302.
76. Plochocki, J., *Bilateral variation in limb articular surface dimensions*. American Journal of Human Biology, 2004. **16**(3).
77. Auerbach, B.M. and C.B. Ruff, *Limb bone bilateral asymmetry: variability and commonality among modern humans*. Journal of Human Evolution, 2006. **50**(2): p. 203-218.

78. Ron, O., et al., *Computer-based periaxial rotation measurement for aligning fractured femur fragments*. International Congress Series, 2001. **1230**: p. 307-313.
79. Scheuering, M., et al., *Interactive Repositioning of bone fracture segments*. 2001, Aka GmbH. p. 499-506.
80. Winkelbach, S. and F. Wahl, *Pairwise Matching of 3D Fragments Using Cluster Trees*. International Journal of Computer Vision, 2008. **78**(1): p. 1-13.
81. Harders, M., et al., *An Optimized Surgical Planning Environment for Complex Proximal Humerus Fractures*, in *MICCAI Workshop on Interaction in Medical Image Analysis and Visualisierung*. 2007.
82. Cimerman, M. and A. Kristan, *Preoperative planning in pelvic and acetabular surgery: The value of advanced computerised planning modules*. Injury, 2007. **38**(4): p. 442-449.
83. Citak, M., et al., *Virtual 3D planning of acetabular fracture reduction*. Journal of Orthopaedic Research, 2008. **26**(4): p. 547-552.
84. Suero, E.M., et al., *Use of a virtual 3D software for planning of tibial plateau fracture reconstruction*. Injury, 2010. **41**(6): p. 589-591.
85. Chowdhury, A., et al., *Virtual multi-fracture craniofacial reconstruction using computer vision and graph matching*. Computerized Medical Imaging and Graphics, 2009.
86. Roser, S.M., et al., *The Accuracy of Virtual Surgical Planning in Free Fibula Mandibular Reconstruction: Comparison of Planned and Final Results*. Journal of Oral and Maxillofacial Surgery, 2010. **In Press, Corrected Proof**.
87. Willis, A., et al., *3D reconstruction of highly fragmented bone fractures*. Medical Imaging 2007: Image Processing. Edited by Pluim, Josien PW; Reinhardt, Joseph M.. Proceedings of the SPIE, 2007. **6512**: p. 65121P.
88. Zhou, B., et al. *Improving Inter-fragmentary Alignment for Virtual 3D Reconstruction of Highly Fragmented Bone Fractures*. in *SPIE Medical Imaging*. 2009. Lake Buena Vista, Florida.
89. Beardsley, C., et al., *High density polyetherurethane foam as a fragmentation and radiographic surrogate for cortical bone*. The Iowa Orthopaedic Journal, 2000. **20**: p. 24.
90. Frank, M., R. Wysk, and S. Joshi, *Rapid planning for CNC milling—A new approach for rapid prototyping*. Journal of Manufacturing Systems, 2004. **23**(3): p. 242-255.
91. Besl, P. and H. McKay, *A method for registration of 3-D shapes*. IEEE Transactions on Pattern Analysis and Machine Intelligence, 1992. **14**(2): p. 239-256.
92. Yushkevich, P., et al., *User-guided 3D active contour segmentation of anatomical structures: significantly improved efficiency and reliability*. Neuroimage, 2006. **31**(3): p. 1116-1128.

93. Kellgren, J.H. and J.S. Lawrence, *Radiological assessment of osteo-arthritis*. *Ann Rheum Dis*, 1957. **16**(4): p. 494-502.
94. Meyer, F., *Topographic distance and watershed lines*. *Signal Processing*, 1994. **38**(1): p. 113-125.
95. Anderson, D.D., et al., *Quantifying tibial plafond fracture severity: absorbed energy and fragment displacement agree with clinical rank ordering*. *J Orthop Res*, 2008. **26**(8): p. 1046-52.
96. Beardsley, C.L., *Development of Quantitative Measures For Bone Comminution*, in *Biomedical Engineering*. 2002, Univ of Iowa Iowa City.
97. Martin, J., et al., *Objective structured assessment of technical skill (OSATS) for surgical residents*. *British Journal of Surgery*, 1997. **84**(2): p. 273-278.
98. Citak, M., et al., *Virtual 3D planning of acetabular fracture reduction*. *Journal of Orthopaedic Research*, 2007. **26**(4): p. 547-552.
99. Martin, J., et al., *Radiographic fracture assessments: which ones can we reliably make?* *Journal of Orthopaedic Trauma*, 2000. **14**(6): p. 379.
100. Stansbury, L., et al., *Amputations in US military personnel in the current conflicts in Afghanistan and Iraq*. *Journal of Orthopaedic Trauma*, 2008. **22**(1): p. 43.
101. Lewis, J., et al., *Cell death after cartilage impact occurs around matrix cracks*. *Journal of Orthopaedic Research*, 2003. **21**(5): p. 881-887.
102. Thomas, T., et al., *A Method for the Estimation of Normative Bone Surface Area to Aid in Objective CT-Based Fracture Severity Assessment*. *The Iowa Orthopaedic Journal*, 2008. **28**: p. 9.
103. Khalafi, A., et al., *The accuracy and precision of computer assisted surgery in the assessment of frontal plane deviations of the lower extremity: a femoral fracture model*. *Archives of Orthopaedic and Trauma Surgery*, 2009. **129**(9): p. 1183-1187.